ESCOLA SUPERIOR DE SAÚDE
POLITÉCNICO DO PORTO

M

MESTRADO
BIOESTATÍSTICA E BIOINFORMÁTICA APLICADAS À SAÚDE

Assessing Functional Activity of Astrocytes by Calcium Imaging: How do Astrocytes Respond to the Electrophysiological Microenvironment?

Sara Cristina da Costa e Silva

09/**2019**

ESCOLA
SUPERIOR
DE SAÚDE

Assessing Functional Activity of Astrocytes by Calcium Imaging: How do Astrocytes Respond to the Electrophysiological Microenvironment?

Autor

Sara Cristina da Costa e Silva

Orientadores

Doutor Miguel Aroso, INEB/i3S

Professor Doutor Paulo de Castro Aguiar, INEB/i3S

Professora Doutora Brígida Mónica Faria, ESS-P.Porto

Dissertação apresentada para cumprimento dos requisitos necessários à obtenção do grau de Mestre em Bioestatística e Bioinformática Aplicadas à Saúde pela Escola Superior de Saúde do Instituto Politécnico do Porto.

09/**2019**

À minha família

Apoio Financeiro

Este trabalho recebeu apoio da FCT – Fundação para a Ciência e a Tecnologia/Ministério da Ciência, Tecnologia e Ensino Superior, no contexto do projeto PTDC/EMD-EMD/31540/2017 (POCI-01-0145-FEDER-031540).

Os autores agradecem o apoio da Plataforna Científica do i3S, Advanced Light Microscopy, membro da infrastructura nacional PPBI – Plataforma Portuguesa de Bioimagem (PPBI-POCI-01-0145-FEDER-022122).

Agradecimentos

Primeiramente gostaria de agradecer ao Doutor Miguel Aroso, não só pelo seu papel como orientador deste projecto, mas também pelo incansável apoio e compreensão ao longo deste ano. Por todo o tempo que dedicou a ensinar-me, pelo prazer que foi poder trabalhar ao seu lado e pela motivação que me deu, incessantemente, quando tudo ficou mais difícil, o meu sincero obrigado. Nada disto teria sido possível sem ele.

Ao Professor Doutor Paulo de Castro Aguiar, co-orientador deste projecto, gostaria de agradecer todos os momentos em que me transmitiu o seu conhecimento e, especialmente, por ter acreditado em mim e me ter aceite no seu grupo apesar das circunstâncias, tendo-me dado a oportunidade de realizar um sonho ao fazer parte de um projecto tão interessante.

À minha co-orientadora, Professora Doutora Brígida Mónica Faria, agradeço toda a disponibilidade e preocupação que demonstrou desde o início deste projecto.

Aos restantes membros do NCN, muito obrigada por me terem recebido desde o primeiro momento como sendo uma de vós. Foi um prazer muito grande conhecer-vos a todos, certamente levarei comigo esta experiência para o resto da minha vida.

Aos meus avós, aos meus pais, ao meu irmão e à Celine, um enorme obrigado por sempre, sempre me apoiarem na busca pelos meus sonhos, mesmo que por vezes significasse deixá-los para segundo plano. Todos vós são um verdadeiro exemplo a seguir de preserverança, superação e empenho. Espero continuar a deixar-vos orgulhosos.

Ao Nuno, agradeço por ter sido sempre o meu porto de abrigo, o meu ouvinte mais atento e o apaziguador das minhas inquietações... enfim, o meu melhor amigo.

Às minhas amigas, Cláudia, Joana, Liliana e Raquel, por terem entrado na minha vida há 8 anos e terem escolhido ficar, obrigada por tornarem os momentos duros mais suportáveis. Em especial à Cláudia, a nós, companheiras desta aventura, por mais uma meta atravessada lado a lado!

Por último, aos meus colegas de trabalho, por toda a paciência que demonstraram ao longo deste ano, em especial à Raquel, Miriam e Márcia, pelo apoio constante.

Resumo

Apesar de não serem capazes de produzir potenciais de acção, é sabido que os astrócitos integram as sinapses, sendo capazes de detectar e responder a estímulos externos com dinâmicas de cálcio espaciotemporalmente complexas, podendo modelar a transmissão sináptica.

O objectivo deste projecto é avaliar as dinâmincas de cálcio dos astrócitos através da modelação do seu microambiente electrofisiológico. Para tal, culturas de astrócitos foram estimuladas recorrendo a ThinMEAs©, monitorizando a actividade de cálcio.

Os resultados obtidos demonstraram que os astrócitos respondem a estímulos de ±600mV ou ±800mV, gerando uma onda de cálcio que se propaga para células vizinhas. A amplitude, tempo de subida e velocidade de propagação da onda de cálcio está dependente do estímulo, sendo que um estímulo de maior amplitude resulta numa resposta de maior amplitude, demorando mais tempo a atingir o seu pico máximo mas atingindo distâncias mais longas.

Apesar de preliminares, estes resultados indicam que os astrócitos são capazes de detectar e responder a mudanças eléctricas externas. Desta forma, os astrócitos são células electricamente excitáveis, possivelmente através do seguinte mecanismo: a estimulação leva à abertura dos canais de cálcio voltagem-dependentes de maneira dependente da voltagem, que irá sensibilizar o retículo endoplasmático resultando numa cascata de libertação de cálcio, gerando uma onda de cálcio que se irá propagar através de junções comunicantes ou gliotransmissão vesicular.

Palavras-chave: Ondas de cálcio dos astrócitos; imagem de cálcio ; estimulação eléctrica; arrays de microeléctrodos; análise de bioimagem.

Abstract

Although not able to generate action potentials, it is known that astrocytes integrate synapses, being able to sense and respond to external stimuli with complex calcium dynamics, having the ability to shape synaptic transmission.

The aim of this project is to assess astrocytic calcium dynamics upon the modulation of their eletrophysiological microenvironment. To accomplish this, astrocyte cultures were electrically stimulated using ThinMEAs© while monitoring their calcium activity.

Obtained data showed that astocytes respond to a ±600mV or ±800mV stimulus by generating a calcium wave which propagates to neighboring cells. The amplitude, rise time and propagation velocity of the calcium wave is dependent on the stimulus, with a higher stimulation amplitude leading to a higher response amplitude, wich takes longer to reach its maximum peak but reach a larger distance.

Although preliminary, these results indicate that astrocytes are able to sense and respond to changes of the electrical environment. In this way, astrocytes are electrically excitable cells, possibly due to the following mechanism: electrical stimulation causes voltage-gated calcium channels to open in a voltage-dependent manner, which will sensitize the endoplasmic reticulum leading to a cascade of calcium releases, generating a calcium wave, which will propagate through gap junctions or vesicular gliotransmission.

Keywords: Astrocytes calcium waves; calcium imaging; electrical stimulation; microelectrode arrays; bioimage analysis.

Index

1. Introduction

The human central nervous system (CNS) is the most complex structure known to man, housing billions of neurons and glial cells, including macroglia (astrocytes, oligodendrocytes, and NG2-glia) and microglia (1,2).

Although glial cells and neurons were first described simultaneously by Dutrochet in 1824, the majority of our knowledge in neuroscience still arises from the study of neurons (3,4). For over a century, glial cells were thought to have a secondary, supportive role in the CNS (3–5). Limitations in the study of brain cells, which in the 19th century was purely morphological, resulted in the description of non-nervous cells as forming part of the "connective tissue" surrounding neurons, being proposed the hypothesis of the existence of "active" (neurons) and "passive" (glia) elements in the CNS (Gabriel Valentin, 1836) (3,4). For that reason, glial cells remained silent throughout the years whereas neuron electrophysiology was already progressing (3).

Defined as a particular type of cells in 1893 by Michael von Lenhossék, astrocytes were merely attributed a supportive role in the nervous system (3,4). Nevertheless, with the development of histological techniques, new hypothesis on glial cells' functions were proposed, namely in neurotransmission and other specific brain functions (3).

Despite astrocytes are the most abundant glial cells in the CNS, the astrocyte-to-neuron ratio is still not consensual, with a lot of different ratios being indicated in the literature (2,6). Although usually presenting a stellate morphology resembling their name (star-like cells) with several processes extending from the soma, astrocytes may exhibit different shapes accordingly to their location and function in the CNS (7,8). This great structural and functional heterogeneity, both within and between brain regions, is partially due to the existence of several subtypes of astrocytes, with the majority of them being protoplasmic and fibrous astrocytes of the grey and white matter respectively. The first exhibit many and elaborated fine processes (of on average 50 μm) contacting with both blood vessels (forming the perivascular endfeet) and neurons, while the latter are very long (up to 300 μm), having a less complex structure and establishing perivascular and subpial endfeet, contacting also axons at the nodes of Ranvier (8–10).

Astrocytes do present an increased complexity closely related to the evolution of the brain(6,8). In fact, comparison of mammalian species revealed an increment in glia-to-neuron ratio as the brain size has increased; yet, what stands out the most is the difference in the morphology of astrocytes by species: human astrocytes are about 2 to 2.5 times larger in diameter than rodent's and for instance protoplasmic astrocytes have about 10 times more primary processes (and multiple more fine processes), contacting with around two million synapses, compared to one hundred thousand in rodents (6). Interestingly, although human neurons are definitely larger, their linear dimensions are only approximately 1.5 times

greater than in rodents, presenting similar shapes and a very close number of synapses per neuron and density of synaptic contacts (6).

The most exciting finding is the presence of distinct populations of astrocytes in primates which have not been seen in other mammals: interlaminar astrocytes, which have processes that go through the cortex, ending in the third and fourth layers, and polarized astrocytes, found in the fifth and sixth layers (6,8). Curiously, terminal processes of the interlaminar astrocytes were particularly large in Albert Einstein's brain, however whether this was responsible for his genius is not known (8).

Besides regulating brain homeostasis and managing regional blood flow by forming part of the brain–blood–barrier, astrocytes also play a major part in synaptic transmission, being able to sense and respond to external signals, thus modulating neuronal activity(11–13) . Unlike neurons, astrocytes are not capable of generating action potentials, however they increase cytosolic calcium (Ca^{2+}) levels in response to synaptic activity (6). Because of this, there are a lot of divergent opinions in the literature on whether astrocytes are electrically excitable cells or not(14–18).

Astrocytic Ca^{2+} events can last for seconds and be confined to a single cell or propagated by intercellular Ca^{2+} waves through gap junctions, presenting characteristic spatial and temporal properties. The duration and frequency of Ca^{2+} transients could be dependent on different responses to intra or extracellular events, which might determine their downstream effect (11,19,20).

Although recent advancements in imaging techniques like Ca^{2+} imaging allowed the study and characterization of the astrocytic activity, many aspects of Ca^{2+} oscillation dynamics remain poorly understood (21,22). Moreover, alterations in astrocytic Ca^{2+} events have been described in neurodegenerative disorders (for instance in Alzheimer's disease and Parkinson's disease) and other pathologies like Down syndrome and epilepsy(23–28). Therefore, assessing Ca^{2+} dynamics in both normal and pathological conditions is essential to better understand the role of astrocytes.

1.1. Physiology of Astrocytes

In the 1960s, microelectrode recordings of invertebrate glial cells were first accomplished by Stephen Kuffler and his colleagues (29–31). Similarly to other recordings performed during the next decade, voltage-gated ion conductance was not evidenced, contributing to the general appreciation of glial cells as electrically non-excitable cells(29). It was only when glial cell cultures and patch clamp became available worldwide that this panorama changed: in the 1980s and 1990s several experiments have been performed on glial cells and have proven their ability to express a wide variety of ion channels and neurotransmitter receptors, in a similar way neurons do(32).

1.1.1. Ion Concentrations and Membrane Potential

Cytosolic ion concentrations are dependent on the cell membrane permeability, the energy-dependent active transport and, in case of Ca^{2+}, on cytosolic specific buffers. Astrocytic cytosolic concentration of potassium (K^+) ranges from 120 and 140mM, whereas in the cerebrospinal fluid (CSF) and in the interstitial fluid its concentration is approximately 3mM, setting the equilibrium potential for K^+ at -98mV (32,33). Astrocytic cytosolic sodium (Na^+) concentration ranges from 15 to 20 mM, being generally higher than in neurons (32,34). The equilibrium potential for Na^+ lies between +55 and +60mV, as the CSF concentration of this ion is about 145 to 155mM. In its turn, the concentration of Ca^{2+} in the cytoplasm of astrocytes varies from 50 to 150nM, with Ca^{2+} equilibrium potential ranging from +120 to +140mV, since the concentration of this ion in adult rodents is approximately 1.4mM. Astrocytes also possess a high concentration of chloride (Cl^-) ions (around 30 to 60mM) when comparing to neurons, setting the equilibrium potential for chloride at -35mV (32,35).

Despite their already described morphological heterogeneity, astrocytes display remarkable electrophysiological properties: a hyperpolarized resting potential ranging from -75 to -90mV (close to the equilibrium potential of K^+) together with low input resistance, which determines a high resting membrane permeability to K^+ (32,36,37), reflected by almost linear current to voltage proportion. This stable negative resting membrane potential (V_{rest}) influences astrocytic homeostatic abilities by defining the electric driving force for numerous membrane transporters (32,37).

1.1.2. Ion Channels

Ion channels are pore-forming proteins that allow the flow of ions across membranes, either plasma membranes or the membranes of intracellular organelles (38). Astrocytes exhibit a great diversity of ion channels, which is dependent on the state of development and the brain region, probably reflecting regional specialization (35).

1.1.2.1 Potassium Channels

Astrocytes possess a high K^+ conductance thanks to the high number of K^+ ion channels, responsible for their V_{rest}. K^+ channels exhibit a great diversity, being grouped accordingly to their biophysical properties (2).

The establishment of the V_{rest} mainly relies on the activity of inward rectifying K^+ channels which are related to the extracellular K^+ buffering function of astrocytes, removing excessive extracellular K^+ ions and with that assisting neuronal excitability. When the membrane is depolarized they tend to be

closed, opening when the membrane is hyperpolarized to levels around or more negative than the membrane resting potential, favoring K^+ influx (35).

Other astrocytic K^+ channels are outward rectifying K^+ channels, Ca^{2+}-dependent K^+ channels and passive K^+ channels. The first is a surprising finding, since it is generalized that the role of outward K^+ currents is the repolarization of action potentials; electrical depolarization of astrocytes does result in electrotonic changes of the membrane potential, however it does not produce regenerative action potentials under physiological conditions. As referred, astrocytes also express Ca^{2+}-dependent K^+ channels, which can be both strongly voltage-dependent and sensitive to micromolar Ca^{2+} concentrations, or weakly voltage-dependent and sensitive to nanomolar Ca^{2+} concentrations. They remain closed at membrane resting potential and their activation requires depolarization of the cell membrane at values more positive than -40mV, with consequent K^+ influx (2,35,37).

The functional relevance of these voltage-gated K^+ channels is still not clear, although it is thought to be involved with the regulation of astrocytic proliferative activity. Passive K^+ channels are not time or voltage dependent, and are thought to be upregulated in astrocytes during their postnatal maturation (2).

1.1.2.2 Sodium Channels

Voltage-dependent sodium (Na^+) channels are considered the basis of cellular excitability and for that reason their discovery in astrocytes was unexpected. However, the main difference when comparing to neurons is the Na^+ channel density, which is one hundred to ten thousand times lower in glial cells (2,32). The low amount of these channels, together with the already referred high K^+ conductance prevents the generation of regenerative action potentials. Patch clamp recordings demonstrated the presence of neuron-like Na^+ channels in protoplasmic astrocytes, having a voltage-dependency similar to neurons and being sensitive to blockage, whether fibrous astrocytes were resistant to Na^+ channels blockage (8). The expression of different Na^+ channels between astrocyte subpopulations is still not clarified (34).

Na^+ channels in astrocytes are probably related to homeostasis maintenance; besides this, intracellular Na^+ regulates the activity of several transporters.

1.1.2.3 Calcium Channels

Ca^{2+} channels serve as transporters of Ca^{2+} into the cell and comprise high-voltage activated Ca^{2+} channels and low-voltage activated Ca^{2+} channels. These channels have great diversity, rising from a variety of genes encoding the principal subunit of the channel, which forms a voltage-gated pore. The expression of these channels in astrocytes is also quite heterogeneous, most certainly differing between brain regions. It has been shown that activation of Ca^{2+} channels in astrocytes leads to high amplitude Ca^{2+} elevations inside the cell, demonstrating their involvement in the generation of Ca^{2+} signals (2,32,35,38).

Astrocytic Ca^{2+} signaling will be further approached in chapter 1.1.5.

1.1.2.4 Chloride Channels

Chloride (Cl^-) channels are related to plasmalemmal ion transport in astrocytes, representing counter-ions for various ion exchanges producing outward rectifying currents. This ion is particularly highly concentrated in astrocytes, resulting in a membrane equilibrium potential of Cl^- of around -35 to -40mV. A link between the cytoskeleton and Cl^- channels has been described, showing that astrocytes respond to volume changes by opening anion channels, thus suggesting that these might be involved in astrocyte swelling by accumulating K^+ and changes in volume plasticity (2,8,35).

1.1.3. Receptors to Neurotransmitters and Neuromodulators

The expression of receptors to neurotransmitters and neuromodulators by glial cells endowed them with the ability of sensing information released from neurons during synaptic transmission (2,8,35). This interaction includes uptake processes with activation of receptor-mediated transmembrane currents (through ionotropic receptors) and second-messenger pathways (through metabotropic receptors) (35).

It is known that astrocytes from different locations in the brain express a distinct and limited set of receptors, specific for the neurotransmitters released in their proximity (2,14,39), with the major types being glutamate receptors, GABA receptors and purinoreceptors. They also express numerous receptors to neuropeptides, cytokines and chemokines, important for the regulation of growth and differentiation (2).

1.1.3.1 Glutamate Receptors

Glutamate is the main excitatory aminoacid neurotransmitter in the CNS, also important in the regulation of neuronal circuitry (40). Ionotropic glutamate receptors are abundantly expressed in astrocytes and can be subdivided into three main families, accordingly to their electrophysiological and pharmacological properties: AMPA, kainate and NMDA receptors. AMPA and kainate receptors are nonselective cation channels permeable to Na^+ and K^+ and occasionally to Ca^{2+}. Nonetheless, while the former generate quite fast membrane responses, fully inactivating within around 100ms, the later generates slower and longer responses. In its turn, NMDA receptors, which like the first two correspond to cation channels, are highly permeable to Ca^{2+} and generate long lasting membrane responses (2,35).

Astrocytic metabotropic glutamate receptors (mGluR) are positively coupled either to phospholipase C ($mGluR_1$ and $mGluR_5$, which activation and conversion of phosphatidylinositol bisphosphate leads to an increase in inositol triphosphate (IP_3) intracellular concentration (41),

subsequently triggering Ca^{2+} release from the endoplasmic reticulum (ER)), or to adenylate cyclase ($mGluR_3$, which regulates intracellular levels of cAMP). Thus, glutamate triggers glial Ca^{2+} signals and regulates cAMP-dependent reactions such as inhibition of K^+ currents, swelling, proliferation and regulation of expression of glutamate transporters (35).

1.1.3.2 GABA Receptors

γ-aminobutyric acid (GABA) is the most prevalent inhibitory neurotransmitter in the CNS. In astrocytes, GABA and related compounds usually cause depolarization of the membrane due to the opening of Cl^- channels and its efflux (35). In this way, $GABA_A$ receptors, a subtype of GABA receptors, were proposed to regulate extracellular Cl^- concentration. Furthermore, they were shown to play a role in shaping astrocyte morphology, since GABA released from neurons led to the formation of more complex processes in neighboring astrocytes (2). This type of neuron-astrocyte signaling also works the other way around, since it upregulates branching of neuronal dendrites. It was also shown that activation of $GABA_A$ receptors in hippocampal astrocytes resulted in Ca^{2+} influx through voltage-gated Ca^{2+} channels, evoking Ca^{2+} signaling (2,42,43).

On the other hand, activation of astrocytic $GABA_B$ receptors, which are mainly clustered in perisynaptic processes (2,44) leads to ER Ca^{2+} release (2,45), triggering intracellular Ca^{2+} oscillations (46).

1.1.3.3 Purinoreceptors and Glycine Receptors

Purinoreceptors, or nucleotide receptors, are expressed by astrocytes and can be grouped as ionotropic receptors (P2X), ligand-gated nonselective cationic channels activated by extracellular adenosine triphosphate (ATP) or metabotropic receptors (P2Y) (2,35,47,48).

ATP and related P2X agonists evoke membrane depolarization due to the activation of non-selective cation channels, resulting in the influx of Na^+, K^+ and Ca^{2+} ions. In addition, activation of P2Y channels by ATP has been shown to trigger Ca^{2+} influx, lasting from seconds to minutes. Furthermore, ATP has also been shown to initiate intercellular Ca^{2+} waves both in vitro and in vivo, and a specific subtype of purinoreceptor, P2Y1, has been pointed as the responsible for the propagation of Ca^{2+} waves (49).

Inhibitory glycine-gated channels mediate Cl^- efflux and thus membrane depolarization, sometimes resulting in the influx of Ca^{2+} through voltage-gated Ca^{2+} channels (35,50).

1.1.3.4 Other Receptors

Additionally to the receptors reviewed above, astrocytes express many more receptors, related to their interactions with the immune and vascular systems. Cytokine and chemokine receptors are also expressed in astrocytes, as well as immune complement receptors and endothelin and thrombin receptors, among others (2).

1.1.4. Gap Junctions and Glial Syncytium

Unlike neurons whose network is formed by synaptic contacts, macroglial cells in the brain are physically connected by gap junctions, thus forming a functional network called the glial syncytium (51).

Gap junctions are composed of hundreds of intercellular channels of specialized proteins known as connexins, forming an intercellular channel connecting the cytoplasm of both adjacent cells. Each connexon is composed of six symmetrical subunits, the connexins, with Cx_{43} being the most abundant in astrocytes. In its turn, connexins have four transmembrane domains which form the channel pore and gating mechanism. When hundreds of connexons are joined to form a cluster they give rise to a functional gap junction. Gap junctions are permeable to relatively large molecules, allowing the intercellular diffusion of many cytoplasmic second messengers, nucleotides and ions, providing effective electrical coupling. These intercellular channels behave like membrane ion channels, undergoing rapid transitions from open to closed states (52–54).

Astrocytes present a high intercellular coupling in the CNS, having the highest density of gap junctions – on average two astrocytes from the grey matter are connected by approximately 230 gap junctions (8). Nevertheless, coupling between them varies considerably across brain regions, and so does the network (51,55,56).

1.1.5. Calcium Signaling in Astrocytes

Ca^{2+} ions are a ubiquitous inorganic signaling species, being the most versatile intracellular messengers described so far involved in the regulation of the majority of cellular functions (22). Ca^{2+} regulates a wide variety of intracellular processes with tremendously different temporal domain including secretion, fertilization, gene transcription and apoptosis. In a physiological system, intracellular and extracellular Ca^{2+} concentrations are often not in equilibrium and the concentration gradient is regulated by the cell with a very complex system of ion channels and transporters (22,57).

Physiological effects of Ca^{2+} ions are produced by enzymatic intracellular Ca^{2+} sensors, which are located in different parts of the cell and modify their activity upon Ca^{2+} binding. That said, local Ca^{2+} gradients might specifically regulate particular sets of Ca^{2+}–dependent processes. These peculiarities of

intracellular Ca^{2+} effector systems allow for amplitude and space encoding of Ca^{2+} signals and solve the problem of specificity of such an intrinsically promiscuous system (24,58). Ca^{2+} channels and transporters represent the molecular systems responsible for controlling intracellular Ca^{2+} homeostasis and producing Ca^{2+} signaling events. These systems are very much conserved and ubiquitously expressed within species. Most importantly, all these systems are regulated by Ca^{2+} itself, thus making a very robust, although versatile and adaptable piece of molecular machinery (8,22,58,59).

1.1.5.1 Calcium Release from Intracellular Stores

The predominant source of cytosolic Ca^{2+} ions is associated with release from the ER, which serves as storage of intracellular Ca^{2+}, being the main responsible for the generation and shaping of cytoplasmic Ca^{2+} signals (58).

From there, Ca^{2+} is delivered to the cytosol through two ligand-gated Ca^{2+} channels of the endomembrane, namely ryanodine receptors (RyRs), activated by Ca^{2+} ions in the cytosol and acting as an amplifier of Ca^{2+} signals, IP_3 receptors (IP_3R) (60).

IP_3R Ca^{2+} channels are activated by the intracellular second messenger IP_3, which in turn triggers IP_3-induced Ca^{2+} release. IP_3Rs are also regulated by cytosolic free Ca^{2+}, so the elevation of the latter increases the sensitivity of receptors to IP_3 (58,61), creating a positive feed-back loop termed as Ca^{2+}-induced Ca^{2+}-release (CICR) (62). When several local events take place, intracellular Ca^{2+} increases globally in the cell. ER consists of a continuous, inter-connecting network of tubules and cisterns (63), extending throughout the cell soma, forming the nuclear envelope and spreading towards more distant processes (64). Thus, release of Ca^{2+} from several ER channels activates neighboring RyRs and IP_3Rs (40,58,65), resulting in a propagating ER excitation wave, allowing Ca^{2+} signals to travel intracellularly for long distances within cells.

Three isoforms of IP_3R (IP_3R_{1-3}) have been described in vertebrates (59); in astrocytes, although a dominance of IP_3R_2 is clear, roles for IP_3R_1 and IP_3R_3 in mediating residual Ca^{2+} signals have been suggested, since knockout mice for IP_3R_2 still presented physiological residual Ca^{2+} signaling within astrocyte branches (59,66). Results have confirmed the presence of these spatially and restricted Ca^{2+} transients, showing that they occurred in the fine extensive processes of astrocytes and were not due to IP_3-mediated release from the ER (66–68). It has been demonstrated that at least some of the Ca^{2+} signals of fine processes' microdomains occur via efflux from the mitochondrial permeability transition pore and showed that the distribution of Ca^{2+} microdomains overlapped with the distribution of mitochondria (69), with this organelle being until then, an unappreciated large Ca^{2+} store in cells that sequester and release Ca^{2+} (70).

Recently, an IP_3R_2-independent Ca^{2+} release was also described by Okubo et al. (71), whose results suggested Ca^{2+} transfer from the ER to the mitochondria through nanodomains formed by ER-mitochondria contact sites. Interestingly, crucial roles for IP_3R_1 and IP_3R_3 in ER-mitochondrial coupling have been described: the first participates in the physically linkage of the ER to the mitochondria, whereas the latter has been identified as a major subtype which mediates Ca^{2+} transfer from the ER to the mitochondria (71). It has been demonstrated that mitochondria slowly release Ca^{2+} into the cytosol via NCXs and by the formation of the mitochondrial permeability transition pore (58,69,70). In fact, mitochondrial inner membrane is very electronegative (up to –200 mV), and elevations of cytosolic Ca^{2+} drive Ca^{2+} ions into the mitochondria, where they activate ATP synthesis, providing a mechanism for coupling cell stimulation with energy production (69,72).

The ER and plasmalemma are functionally connected by a specific signaling system known as Store-Operated Ca^{2+} Channels (SOCCs), allowing additional Ca^{2+} influx when the ER is depleted from Ca^{2+} (58,73). Ca^{2+} entry pathways in mature astrocytes are represented by several types of Ca^{2+} permeable ligand-gated channels (most notably by ionotropic glutamate and P2X purinoreceptors) and SOCCs, being that the main source for astrocytic Ca^{2+} signaling is associated with the ER Ca^{2+} store (73). The intra-ER Ca^{2+} concentration in glial cells is lower than in neurons, ranging from 100 to 300 M (2). Astrocytes express numerous metabotropic receptors and their activation causes an increase in cytosolic concentration of IP_3, which binds to the IP_3Rs causing rapid Ca^{2+} release. Although both astrocytes and microglia express RyRs, they play a relatively minor role in shaping Ca^{2+} signals in these cells, with IP_3-induced Ca^{2+} release representing the leading mechanism of Ca^{2+} signaling in astrocytes. The release of Ca^{2+} from intracellular stores lowers intra-ER Ca^{2+} concentration, which in turn triggers the opening of SOCCs, resulting in prolonged Ca^{2+} signals that may significantly outlast the duration of stimulation (58).

When Ca^{2+} ions enter the cytoplasm, many of them are immediately bound by Ca^{2+}-binding proteins (which determine Ca^{2+}-buffering capacity of the cytoplasm); however, some Ca^{2+} ions escape binding, generating an intracellular Ca^{2+} signaling event. The cytoplasmic Ca^{2+} buffering capacity varies considerably among different cells and brain regions (22).

If excessive Ca^{2+} ions enter the cytoplasm during stimulation, several plasmalemmal and intracellular transporters – sarcoplasmic/endoplasmic reticulum Ca^{2+}-ATPase (SERCA) pumps, which use the energy of ATP hydrolysis to transport Ca^{2+}, and Na^+/Ca^{2+} exchangers (NCXs), which uses the electrochemical gradient of Na^+ ions as the driving force for Ca^{2+} efflux) remove Ca^{2+} from the cytosol against a concentration gradient, preventing the system from overloading. A part of the Ca^{2+} is removed by active uptake into the lumen of the ER, a mechanism strongly regulated by the free Ca^{2+} concentration within the ER (58). Excessive Ca^{2+} influx into the cytosol has a damaging effect, being the main cause of so-called 'Ca^{2+} excitotoxicity' which occurs during long-lasting excessive stimulation of Ca^{2+} entry, for

instance by pathological release of glutamate during brain ischemia, or failure of Ca^{2+} extrusion systems (52).

The interplay between Ca^{2+} release, Ca^{2+} reuptake into the ER and SOCC-related Ca^{2+} entry determines the shape of the resulting Ca^{2+} signal, which may vary from a rapid and transient peak-like response, through intracellular Ca^{2+} elevations lasting up to hundreds of seconds with a clear plateau, to multiple transient Ca^{2+} oscillations. These kinetically different intracellular Ca^{2+} changes underlie the temporal coding of the Ca^{2+} signal, whereas Ca^{2+} oscillations are responsible for frequency coding of the Ca^{2+} signal (8,19,20).

1.1.5.2 Free Intracellular Calcium Ions

Free intracellular Ca^{2+} represents only a small fraction of total cellular Ca^{2+}, being unevenly distributed between intracellular compartments, serving as sources and/or sinks for this ion (58). In contrast, Ca^{2+} concentration within the ER is much higher, being similar to the extracellular Ca^{2+} concentration. These concentration differences result in an extremely large electrochemical force, maintaining the cytosol under continuous Ca^{2+} pressure as Ca^{2+} ions try to diffuse from high concentration regions to low free Ca^{2+} compartments through specific transmembrane Ca^{2+}-permeable channels, ATP-driven Ca^{2+} pumps and electrochemically-driven Ca^{2+} exchangers (members of the transient receptor potential (TRP) family, that include transient TRPA1) (57).

Voltage-gated, ligand-gated and nonspecific channels provide major paths for plasmalemmal Ca^{2+} entry, having distinct activation mechanisms and differing in their Ca^{2+} permeability. The most selective for Ca^{2+} ions are plasmalemmal voltage-gated Ca^{2+} channels (VGCCs), which are relativity scarce in the majority of mature astrocytes. Ca^{2+} entry through VGCCs in astrocytes has been hypothesized to sensitize IP_3 receptors for activation via CICR or by refilling luminal Ca^{2+} stores. Nonetheless, voltage-gated Ca^{2+} currents are present in immature astroglial cells and their expression is down-regulated during development, suggesting their involvement in growth and differentiation (41).

Besides the ones discussed above, other channels allow the passage not only of Ca^{2+}, but also other cations. It is the case of the already referred AMPA type glutamate receptors, which are mainly ligand-gated Na^+/K^+ channels, but are also permeable to Ca^{2+}. Due to the very abrupt concentration gradient of Ca^{2+} between the extracellular space and the cytosol, the opening of a low amount of plasmalemmal Ca^{2+} channels results in a relatively large Ca^{2+} influx, changing cytosolic free Ca^{2+} (32,58).

Taken together, there are several Ca^{2+} delivery/retrieval pathways involved in regulating cytosolic Ca^{2+} levels, which are sufficient and necessary for triggering exocytotic release of glutamate and/or other gliotransmitters from astrocytes (58,74).

1.1.5.3 Propagation of Calcium Signals

Astrocytes are stimulated in physiological conditions by local and transitory exposure to various neurotransmitters, leading to the localized Ca^{2+} release through IP_3R. Despite being highly confined events, these may result in a propagating signal throughout the cell, having the possibility of traveling through the astrocytic syncytium (21,58), thus representing a unique type of intercellular communication in astrocyte networks intercalating neuronal circuitries and vasculature (56). These signals (Ca^{2+} waves) can travel for approximately 300 to 400 μm, at a velocity of 15 to 20 μm/s (8) and are considered responsible for the transmission of physiologic and pathologic signals within the brain, since they are able to influence the activity of neurons, microglia and endothelial cells (56).

Intracellular propagation of Ca^{2+} signals is dependent on the ER membrane, which has the ability to detect and convert a local response above a certain threshold into a propagating wave, being an excitable medium thanks to RyR and IP_3R sensibility to Ca^{2+}. The local Ca^{2+} release induced by a localized elevation of IP_3 recruits neighbouring channels, not only amplifying the initial Ca^{2+} release event, but also creating a propagating wave of Ca^{2+} release along the ER membrane by a CICR mechanism (75). Noteworthy, a Ca^{2+} wave is not a propagating wave of Ca^{2+} ions, but it results from a propagating wave of elementary Ca^{2+} release events throughout the ER endomembrane, as the movement of Ca^{2+} ions is severely controlled by cytoplasmic Ca^{2+} buffering (67,75).

Intercellular propagation of Ca^{2+} signals in astrocytes is fundamentally different from that in neurons, where the substrate for excitability is the plasma membrane, generating a swift propagating wave of openings and closures of Na^+/K^+ channels (propagating action potential). In contrast, the substrate for excitability in astrocytes is the intracellular ER membrane, which generates a much slower propagating wave (lasting from seconds to minutes) of openings and closures of Ca^{2+} channels (56,75).

This type of propagation relies mainly on two routes: the direct and fast intercellular diffusion of IP_3 via gap junctions and the extracellular diffusion of ATP, which triggers metabotropic receptor-mediated Ca^{2+} release in neighboring cells regulating, by its turn, IP_3 (56,75,76). Even though both mechanisms can coexist, intracellular propagation through gap junctions is likely the predominant signaling mechanism in many astrocytes (75). More recently, Fujii et al. demonstrated, using mechanically stimulated cells, that the fast propagation of persistent Ca^{2+} increases in the proximal region is mediated by gap junctions, travelling at approximately 20 μm/s and sustaining for several minutes, whereas slow propagation of transient Ca^{2+} increases (approximately 13.9 μm/s) in the distal region is mediated by extracellular ATP, within a 201 μm radii (56). However, transported IP_3 has to reach a minimum threshold concentration to trigger CICR in neighboring cells, ceasing propagation whenever this condition is not verified. Therefore, a mechanism has been suggested as being responsible for at least partial regeneration of IP_3 levels (PLCδ-mediated IP_3 production), which plays an important role in Ca^{2+} wave propagation

inducing local IP_3 concentrations large enough to trigger CICR (75). This mechanism likely underlies persistent Ca^{2+} increases and gap junction-mediated propagation, whereas the lack of a regenerative process probably accounts for the lower propagation velocity in the distal region (56). Computational modelling by Goldberg et. al showed that nonlinear coupling between astrocytes favors IP_3 partial regeneration thus promoting large-distance intercellular Ca^{2+} wave propagation, and that long-distance wave propagation critically depends both on the nature of intracellular Ca^{2+} encoding (whether Ca^{2+} signals display frequency modulation (FM) or amplitude modulation (AM)) and the spatial arrangement of the cells (75). Experimental data suggest that a stimulus arriving on an astrocyte is preferentially encoded in FM of Ca^{2+} oscillations, being often characterized by pulsating waves with smaller width than period. Although the possibility of AM or even coexisting AM and FM (AFM) encoding have also been inferred, both frequency and amplitude of astrocytic Ca^{2+} oscillations are highly variable, depending on cell-specific properties such as Ca^{2+} content of the intracellular stores, or the spatial distribution, density and activity of SERCA pumps (75). Yet, the propagation of wave-like signaling in the context of such great variability is yet not fully understood. They also demonstrated that regenerative Ca^{2+} wave propagation is possible when the gap junctions are rendered by nonlinear permeability but only when most of the model astrocytes are tuned to encode the strength of incoming IP_3 signal into FM Ca^{2+} oscillations (75).

Yet, it should also be noted that astroglial networks of different areas in the brain can have distinct mechanisms of intercellular Ca^{2+} wave propagation; for instance, genetic deletion of Cx_{43}, which forms gap junctions between astrocytes, results in the complete absence of astroglial Ca^{2+} waves in the neocortex (53,75,77), but not in the corpus callosum or in the CA1 hippocampus area where Ca^{2+} wave propagation relies predominantly on ATP release (56).

Furthermore, Ca^{2+} waves can be propagated outside of the astroglial syncytium through the release of different extracellular messengers (gliotransmitters) to act on neighbouring neurons, modulating the excitability of neurons and controlling the flow of information at synaptic terminals (74,75,78,79), oligodendrocytes and microglia.

1.2. Pathophysiology of Astrocytes

As discussed before, astrocytes play an important role, maintaining the homeostasis in the CNS and being part of the synaptic transmission together with neurons. Hence, astrocytic dysfunction can be responsible for alterations in neuronal function, contributing to the complex pathogenesis of a variety of neurologic disorders (80). Conceptually, astrogliopathological changes are classified into reactive gliosis, astrodegeneration with astroglial atrophy and loss of function and pathological remodeling of astrocytes. (24,52). Degenerative alterations and death in astrocytes are manifested by the decrease in number of astrocytes and impairment in their homeostatic abilities (for instance in glutamate clearance), contributing

to the development of psychiatric disorders (23,24) through aberrant synaptic connectivity and transmission. In neurodegenerative diseases, astrodegeneration with astroglial atrophy and loss of astrocytic homeostatic mechanisms is common: in amyotrophic lateral sclerosis, reduced astroglial glutamate clearance is responsible for excitotoxic neuronal death; in Alzheimer's disease (AD), astroglial atrophy leads to a reduced synaptic coverage and overall decrease in homeostatic support contributing to neuronal death and brain atrophy (28); astroglial pathological remodeling occurs in Alexander disease and infectious encephalopathies, where astrocytes acquire a pathological phenotype, affecting their function and driving neuropathology (52).

Some of the most prevalent neurological pathologies, where astrocytic dysfunction is a key aspect, are further discussed below.

1.2.1. Reactive Gliosis

Reactive gliosis, a graded continuum of molecular, cellular and functional changes in astrocytes is considered the hallmark of several pathologies in the CNS, with these alterations varying accordingly to the disease severity and being regulated through signaling molecules in a context-specific manner (23). Astroglial reactivity is an evolutionary conserved astroglial response activated by a variety of signals associated with polyaetiological insults to the CNS, as in ischemia and stroke, among others (52).

Astrocytic proliferation is not always present in astrogliosis, however increased expression of glial fibrillary acidic protein (GFAP) has been reported, together with cell body and process hypertrophy, in mild to moderate astrogliosis. Copper-zinc superoxide dismutase, glutathione peroxidase and metallothionein have also been described to be up-regulated in this condition, as well as the expression of inducible nitric oxide synthase and release of trophic factors, cytokines, interleukins and interferons in the moderate form. Both mild and moderate forms present potential for resolution if the trigger is removed, contrary to severe diffuse astrogliosis where enhanced astrocytic proliferation takes place, causing the overlapping of neighboring astrocytic processes disturbing their individual domains, sometimes leading to the formation of a glial scar. Molecular factors behind proliferation of astrocytes involve epidermal growth and fibroblast growth factors, endothelin 1, ATP, nitric oxide and lipopolysaccharide. Glial scars are formed in the periphery of damaged tissue, inflammatory infiltration, necrosis, tumors, infection and neurodegeneration areas, acting as barriers to inflammatory cells thus protecting surrounding healthy tissue from nearby inflammation areas. Reactive astrocytes also protect CNS cells by regulating inflammation, uptaking excitotoxic glutamate, producing glutathione against oxidative stress, degrading β-amyloid peptides, and balancing extracellular ion concentration. Nevertheless, astrogliosis appears to have opposite effects, preventing axon regeneration and contributing to the development of Alexander's disease and amyotrophic lateral sclerosis through the acquisition of genetic mutations (23,24,52).

1.2.2. Brain Tumors

The majority of primary brain tumors have their origin in glial cells (gliomas), being that astrocytomas represent the most common subtype, where several structural and morphological changes in astrocytes take place, affecting extracellular glutamate levels and membrane channel functions. Altered expression of cytoskeleton elements – increased expression of GFAP and presence of the vimentin-binding 300-kDa intermediate filament associated protein (usually absent in the normal adult brain) – may be responsible for the modified structure of astrocytic glioma cells, which present only up to two to three thick processes, nuclear atypia scant cytoplasm and high nucleus-to-cytoplasm ratio. An impaired expression of glutamate transporters on glioma cells have been identified contributing to an elevated extracellular glutamate concentration, as well as a reduced expression of Cx_{43} and gap-junction mediated coupling, critical for cell-to-cell communication. This favors malignant transformation via reduction of inhibitory signals controlling cell division and proliferation received from neighbouring cells. Besides these, changes in the expression of Na^+ and K^+ channels also occur: astrocytoma cells display almost exclusively delayed rectifying K^+ currents, while no transient A-type and inward rectifying K^+ channels were detected, resulting in a depolarized membrane potential and a round swollen cell body (24,52).

1.2.3. Major Depression Disorder

Major depression disorder (MDD) is a condition with prominent pathological astrocytic alterations affecting density, morphology, protein expression and membrane channel functions. However, unlike what is observed in other neurological and neurodegenerative disorders, astrogliosis and prominent neuronal pathology is absent in MDD. Changes in glial density may affect specific brain regions differently, in an age-dependent manner, as well as glial nuclei size and GFAP expression. Moreover, dysfunction of astrocytic-mediated regulation of GABA and glutamate homeostasis have been demonstrated on depressed subjects, which may be related to the reduced astrocytic packing density, depending also on patient age and chronicity of depression. Impairment in glutamate-related gene expression is specific to astrocytes in MDD, not occurring in neurons, thus underlying the astrocytic basis of the pathology. Besides these, several astrocytic-specific membrane channels have also been shown to be altered in particular brain regions, and the Ca^{2+}-binding protein S100 is also affected, with reduced mRNA levels in astrocytes but increased levels of the protein in the cerebrospinal fluid (CSF) and plasma of patients (24,52).

1.2.4. Epilepsy

An astrocytic basis for epilepsy has been proposed since changes in astrocytic channels and receptors have been identified in epilepsy patients, suggesting that astrocyte dysfunction can lead to

hyper-excitation, neurotoxicity and seizure spreading, in addition to established neurogenic mechanisms. Reactive astrogliosis is present in almost all forms of epilepsy leading to the increase in GFAP and vimentin, associated with the decrease of the enzyme glutamine synthetase which converts glutamate to glutamine, a GABA precursor. It has been hypothesized that this results in a lack of inhibitory synaptic transmission in neighboring neurons, therefore leading to the accumulation of glutamate in astrocytic cytoplasm and decreased synaptic glutamate clearance. Reactive astrogliosis is also related to an increased amount of adenosine kinase (ADK), an enzyme which converts adenosine (which in its turn plays a neuroprotective role in seizure regulation) in adenosine monophosphate, potentially reducing adenosine levels, thus aggravating seizure (80). Modifications in glutamate and GABA transporters have also been shown, with reduced levels of glutamate transporters GLT-1 and GLAST found in the more severe form of the disease, whereas increased expression of GABA transporter GAT_3, leading to reduced extracellular levels of the neurotransmitter during seizure (81).

Also reported in some studies was the alteration in expression, localization and function of several membrane proteins: reduced to complete lack of glial gap junctions coupling was demonstrated in epilepsy patients and the kainate mouse model; $Kir_{4.1}$ channels have been shown to be decreased in epilepsy patients, impairing K^+ buffering by astrocytes and enhancing seizure susceptibility; water transportation through the membrane was found to be abnormal, since the main water transporter in astrocytes, AQP_4, can be decreased along the perivascular membrane domain of astrocytes, in its turn affecting extracellular K+ buffering; the metabotropic glutamatergic receptors $mGluR_{2/3}$, $mGluR_4$ and $mGluR_8$ were highly expressed; astrocytic voltage-gated channels (expressed at low levels in astrocytes of healthy brains) showed an altered expression, increasing intensely Na^+ currents in cultured mesial temporal lobe epilepsy astrocytes, which displayed a depolarized membrane potential and action potential like responses when stimulated; a significant up-regulation of the α1c subunit of voltage-gated Ca^{2+} channels was also observed, suggesting an increased Ca^{2+} uptake (23,81). Noteworthy, different manifestations and states of the disease may be dependent on different molecular dysfunctions, as well as the affected brain regions.

1.2.5. Alzheimer's Disease and Other Dementias

Although astrocytes have been shown to be closely associated with damaged neurons, they were initially considered to have a secondary non-specific role in the pathological process, with a neurocentric view predominating in neurodegeneration research (82). Nevertheless, astrocytes have a deterministic role in the pathogenesis of neurodegenerative diseases (23).

Reactive astrogliosis is considered a hallmark of Alzheimer's disease, with eight out of the ten GFAP isoforms are up-regulated and hypertrophy of astrocytes occur nearby amyloid plaques. In

advanced stages of the disease, these are accompanied by a dysregulation in the expression of cytoskeleton proteins and tight junctions and adherens junctions (23).

Astrocytes were shown to uptake and degrade beta-amyloid (Aβ), which accumulates in the brain of AD patients, giving rise to secondary plaques by the death of Aβ-loaded astrocytes (82). This accounts, in part, for the variety of plaque morphology identified in AD brains (23). Low-density lipoprotein receptor-related protein 1 (LRP1) has been identified as being involved in Aβ uptake and clearance in astrocytes, but whether their response is a protective mechanism or results in further damage it is not known; however, age might affect the ability of astrocytes to uptake and degrade Aβ efficiently: it was demonstrated in cultures of primary neurons with a small density of astrocytes that toxic properties of Aβ are enhanced and changes in tau phosphorylation and cleavage are only seen in the presence of astrocytes associated with a specific astrocytic inflammatory profile (82).

Astrocytic glutamatergic function is also impaired in AD, with reduced GLT-1 immunoreactivity described in the frontal cortex of patients, and decreased hippocampal expression of GLT-1 and GLAST nearby amyloid plaques in early stages of the disease. Although glutamate transporter expression is highly variable among AD patients, the results described above suggest a deficient glutamate clearance ability of astrocytes which might drive the neurotoxic effect. GABA homeostasis was also shown to be affected in AD, with an increased production of GABA in astrocytes related to an increase in the expression of GAT_3. Other astrocyte-specific functions were described as being altered in AD, such as gap junction communication (because of increased expression and immunoreactivity of Cx_{43} both within and outside plaque-containing regions) and K+ buffering. Expression of $Kir_{4.1}$ and AQP_4 is also decreased, with the latter also being misallocated in severe cases of the pathology (23,24).

Dysregulated cellular Ca^{2+} levels were proposed as initial contributors to AD progression due to the long-lasting overload in the cytoplasm and endoplasmic reticulum, triggering cell death. Basal Ca^{2+} levels are elevated in the astrocytic network and Ca^{2+} transients have increased frequency, being coordinated across long distances and independent from neuronal activity as shown in the cortex AD mice. An altered expression of metabotropic glutamate receptor 5 ($mGlu_5$) might be in the origin of the enhanced Ca^{2+} response. It is possible that astrocytic Ca^{2+} signals have a protective role in the early stage of the disease, as the disruption of IP_3R_2-mediated Ca^{2+} signaling in astrocytes resulted in the progression of Aβ deposition and dysfunction of the synaptic plasticity. Boosted glutamatergic gliotransmission is present as well in AD since increased frequency in resting conditions of the slow inward currents mediated by activation of NMDA receptors in neurons was detected (23).

1.3. Astrocyte–Neuron Interaction

Astrocytes play a role in metabolic support, buffering extracellular K^+ and controlling neurotransmitter extracellular levels and diffusion, being essential for proper synaptic development and homeostasis. Moreover, astrocytes are found near synaptic structures and respond to sensory input and exhibit neurotransmitter–induced Ca^{2+} oscillations and subsequent gliotransmitter release engaging in a bidirectional communication with neurons (13,83), demonstrating their close involvement in synaptic transmission.

1.3.1. The tripartite synapse

Until the 1990's the chemical synapse was considered to involve merely a presynaptic and a postsynaptic neuron. However, there is strong evidence that synapses are built from three equally important parts, the presynaptic terminal, the postsynaptic neuronal membrane and the surrounding astrocyte, known as the 'tripartite synapse' (84). In fact, imaging techniques have confirmed that astrocytic membranes are closely associated with neuronal membranes and specifically with synaptic regions, partially or completely enwrapping both presynaptic terminals and postsynaptic structures, being organized non–homogeneously into microdomains with fine structures which can contact synaptic clefts (13). Astrocytic membranes ensheathe about 80 per cent of large perforated synapses (the most functionally active), whereas only about half of macular (smaller) synapses are covered by astrocytic membranes. However, studies focusing on astrocyte contact with excitatory synapses have reported that the amount of synapses contacted by astrocytes varies between brain regions and that these contacts are dynamic and can be altered by neuronal activity: an increase in neuronal activity results in an increase in the extent of astrocyte coverage of dendritic spines, as well as in the number of spines contacted by astrocytic processes (13,84).

1.3.2. Gliotransmission

The close apposition with synaptic structures allow the exposure of astrocytes to neurotransmitters released during synapse. As referred in chapter 1.1.3, astrocytes express neurotransmitter receptors, which are specific to neurotransmitters released at the synapses they contact. Therefore, neurotransmitters released from the presynaptic terminal activate receptors in both the postsynaptic neuronal membrane and perisynaptic astrocytic membrane, resulting in the generation of a postsynaptic potential in the neuron and a Ca^{2+} signal in the astrocyte. This signal might propagate intracellularly through the astrocyte or intercellularly throughout the astrocytic syncytium, being able to

trigger the release of gliotransmitters from astrocytes onto both pre- and postsynaptic neuronal membranes (74,79).

For a chemical to be classified as a gliotransmitter, it has to meet the following criteria: be synthesized by and/or stored in glial cells; its regulated release has to be triggered by a stimulus (physiological and/or pathological); it has to generate rapid responses either on itself or in neighbouring cells; and play a role in pathophysiological processes. Gliotransmitters comprise excitatory aminoacids, nucleotides, prostaglandins, neurotrophins, cytokines and taurine, released from astrocytes via several pathways: through plasma membrane channels or transporters (nonvesicular gliotransmission), or Ca^{2+}-dependent exocytosis (vesicular gliotransmission) (58).

Astrocytes are capable of responding to neuronal input through G-protein-coupled receptors (GPCRs) and other intracellular pathways, often through an increase in frequency encoded intracellular Ca^{2+}. Interestingly, astrocytes can discriminate not only between different neurotransmitters and synaptic inputs but also the intensity of neuronal activity. For instance, increasing concentrations of GPCR agonists lead to increases in the frequency of Ca^{2+} oscillations and the traveling distance by intracellular Ca^{2+} waves without a marked effect on the amplitude of Ca^{2+} responses (22). Moreover, high frequency stimulation of neurons evokes repetitive Ca^{2+} signals in astrocytes, and the frequency of intracellular Ca^{2+} elevations is directly dependent on the frequency or intensity of the stimulation. Ca^{2+} responses in astrocytic processes were also asynchronous because of the existence of isolated compartments (microdomains), following activation of individual synapses surrounded by a specific process. In astrocytes, periods of intense synaptic stimulation induce a long-lasting potentiation of the frequency of the later responses, resembling the long-term potentiation of synaptic activity in neurons. However, in the later, synaptic stimulation induces an increase in the amplitude of post-synaptic potentials, whereas in astrocytes the increase occurs at the frequency level (11,14,19).

Taken together, astrocytes respond to neurons with feedback signals with a nonlinear response, thus controlling neuronal output through the modulation of synaptic transmission, control of synaptic efficiency, or regulation of synaptic scaling. Computational modeling has predicted that astrocytes may modulate the probability of vesicle release(85), optimize neural network performance(85,86), control the threshold value of transition from synchronous to asynchronous behavior among neurons(87), and lead to spike-timing-dependent plasticity at remote synaptic sites(88).

Moreover, chemical signaling is now known to underlie bidirectional communication between astrocytes and neurons(40,89), since the release of neurotransmitters is not exclusive of neurons and neuro-endocrine cells, but can also be performed by astrocytes – the so called gliotransmission.

1.3.2.1 Nonvesicular Gliotransmission

Nonvesicular gliotransmission involves reversed activity of transporters, volume-activated anion and hemichannels (uncoupled gap junctions) and $P2X_7$ purinoreceptors (39).

Once glutamate and Na^+ accumulate in astrocytes increasing intracellular concentrations, together with increased extracellular concentration of K^+ leading to cell depolarization, release of glutamate from astrocytes may happen due to activation of reverse activity transporters. It can occur in ischemia and other pathological conditions, which are accompanied by neuronal damage and massive release of glutamate and K^+ into the extracellular space (90).

Volume-activated anion channels provide a route for the release of glutamate and other negatively charged aminoacids. These volume-activated anion channels are opened by a decrease in extracellular osmotic pressure, leading to rapid swelling of astroglial cells. This is physiologically relevant in the supraoptic nerve of the hypothalamus, where minor changes of extracellular osmotic pressure stimulate or inhibit taurine release from pituicytes in the hypophysis, which in turn interacts with glycine receptors in the terminals of vasopressin/oxytocin neurons, thus regulating the secretion of these two neuro-hormones, important in the regulation of overall body osmotic homeostasis (58).

Hemichannels that do not form gap junctions provide a further route for neurotransmitter release from astroglial cells (for instance glutamate, aspartate and ATP), a pathway that might be regulated by physiological changes in intra- or extracellular Ca^{2+} concentration (53,91).

$P2X_7$ purinoreceptors are large enough to be permeable to aminoacid molecules and may also constitute a pathway by which neurotransmitters can be released from astrocytes, although $P2X_7$ receptors are most likely activated under pathological conditions when extracellular ATP rises (78).

1.3.3. Vesicular Gliotransmission

Vesicular release, or exocytosis, is the main mechanism for regulated secretion of neurochemicals by neurons which underlies Ca^{2+}-dependent secretion of neurotransmitters, comprising both fast – at neuronal synapses – and slower processes of secretion of various neuromodulators and neuro-hormones. Local elevations in cytosolic Ca^{2+} concentration, either by plasmalemmal Ca^{2+} entry or receptor-stimulated Ca^{2+} release from intracellular stores, have the ability of triggering the exocytotic mechanism, resulting in neurotransmitter release coupled to stimulation which underlies the synchronized activity of neural cells. Although this is an important triggering event, neurosecretion depends also on the production and maturation of vesicle containing neurochemicals in the Golgi apparatus and its transportation to the targeted site of release, where they are prepared for exocytosis by docking and priming. When the Ca^{2+} concentration in the vicinity of the vesicle is increased, the Ca^{2+}-sensor synaptotagmin I is activated, which in turn stimulates the formation of a complex between synaptobrevin

II, or vesicle-associated membrane protein 2 (VAMP2), in the vesicular side and syntaxin and synaptosome-associated protein (SNAP25), in the plasma membrane side. This complex represents the main core of the fusion mechanism, known as soluble N-ethylmaleimide-sensitive factor-associated protein receptors, or SNARE proteins, being responsible for the fusion of the vesicle with the plasma membrane, together with other assisting proteins like sectetogranin, synapsin I and Rab3 (58,74,78,92).

To reach the plasma membrane vesicles are transported along the cytoskeleton; besides microtubules and actin filaments, astrocytes express intermediate filament proteins (GFAP, vimentin, nestin and synemin, which also play a role in directional vesicle mobility in these cells, in addition to the maintenance of cell shape (58).

While neuronal exocytosis is mainly dependent on Ca^{2+} entry through plasmalemmal channels, astrocytic vesicular glutamate release is predominantly derived from Ca^{2+} release from intracellular stores, thus developing considerably slower when compared to neurons. Astrocytes have intracellular structures similar to synaptic microvesicles, occupied by synaptobrevin II and a particularly high concentration of glutamate, due to the expression of vesicular glutamate transporters (VGLUT) which accumulate glutamate therein. Glutamate is synthesized within astrocytes via the tricarboxylic acid cycle. Due to the expression of the enzyme pyruvate carboxylase, astrocytes can synthesize glutamate de novo. Astroglial release of glutamate in response to increased intracellular Ca^{2+}, stimulated by activation of astroglial metabotropic receptors, is sensitive to the intracellular Ca^{2+} elevation, as chelation of Ca^{2+} through membrane-permeable Ca^{2+}-binding agents effectively inhibits the release (58,74).

ATP is produced in cells by glycolysis and oxidative phosphorylation. Extracellularly released ATP can directly act on purinergic receptors, or indirectly, upon its hydrolysis by membrane-bound ectonucleotidases to ADP and adenosine, can activate various plasma membrane receptors. Diffusion of glutamate and/or ATP is limited due to the action of glutamate transporters and degradation of ATP, thus defining spatiotemporal range for the local effect of astrocytes on neurons and synapses (75). V-ATPase (vacuolar type of proton ATPase) is responsible for sequestering ATP into vesicles, which drives protons into the vesicular lumen creating the proton concentration gradient necessary for glutamate/ATP transport into vesicles via VGLUTs (vesicular glutamate transporters) 1, 2 and 3 and VNUT (vesicular nucleotide transporter) respectively (58). Besides glutamate and ATP, astrocytes also secrete d-serine through vesicular exocytosis, which activates the glycine site of NMDA receptors, playing an important role in astrocyte-to-neuron signaling (93).

Studies of vesicle trafficking in astrocytes revealed complex properties of glutamatergic and peptidergic vesicle mobility and their specific responses to extracellular stimuli. It appears that all vesicle types in astrocytes do not respond to altered physiological and pathological conditions in the same pattern. This may represent a new cellular paradigm of how astrocytes contribute to the phenotype of brain function in physiological and pathological conditions (58).

1.4. Calcium Imaging in Astrocytes

Ca^{2+} is a ubiquitous second messenger that regulates a handful of different physiological and pathological pathways. Astrocytes exhibit an intricate toolkit of countless Ca^{2+} channels, pumps, exchangers and buffering proteins that enable a great variation of the Ca^{2+} concentration with a high spatiotemporal precision (94).

A great part of our current knowledge in astrocytic Ca^{2+} signals resulted from the progressive development in fluorescent Ca^{2+} indicator probes, allied to advances in optical imaging technology. Using Ca^{2+} imaging, it is now possible to monitor Ca^{2+} flux through individual channels in living cells with millisecond temporal accuracy and sub-micrometer spatial resolution (95).

1.4.1. Calcium Indicators

Ca^{2+} indicators are dyes or engineered proteins that bind to Ca^{2+}, evidenciating its location in the cell. The signal intensity of these molecules increases when Ca^{2+} binds to the probe, providing information about relative or absolute Ca^{2+} concentrations in targeted cell structures(94). An ideal Ca^{2+} indicator would have low basal fluorescence together with a large variation in fluorescence upon small changes in Ca^{2+} concentration, resulting in a good signal-to-noise ratio (SNR) – or how well a given Ca^{2+} signal is detected above baseline noise. Moreover, it should have fast kinetics (good Ca^{2+} binding and dissociation rates) to report brief, transient changes in Ca^{2+} concentration in a reliable manner. Ca^{2+} indicators show a broad range of excitation/emission spectra (varying from ultraviolet to red wavelengths) and thus the choice of a Ca^{2+} indicator is dependent not only on the sample, but also on the detection method used (94).

1.4.1.1 Calcium Indicator Dyes

Imaging cellular Ca^{2+} signals was first made possible by Tsien, who developed small molecule fluorescent Ca^{2+} indicator dyes (94). These fluorescent Ca^{2+} indicators and sensors consist of a Ca^{2+} chelating moiety conjugated with a fluorescent reporter, which in absence of Ca^{2+} ions the photo-induced electron transfer from the Ca^{2+} chelator quenches fluorescence of the conjugated fluorophore. When bound to Ca^{2+} this process is inhibited, leading to the formation of multiple coordination bonds with the metal ion and the sequestration of the latter (chelation) , resulting in a change in the fluorescence intensity or a shift in spectral properties (95,96).

Ca^{2+} chelators comprise EDTA (Ethylenediaminetetraacetic acid), EGTA (ethylene glycol-bis(β-aminoethyl ether)-N,N,N',N'-tetraacetic acid) and BAPTA (1,2-bis(o-aminophenoxy)ethane-N,N,N′,N′-tetraacetic acid), which are widely used. Although classical Ca^{2+} indicators are mainly based in the first two

chelators, they are somewhat slow in binding $Ca^{2+}$and releasing it. Chelators with enhanced Ca^{2+} ion specificity or pH stability represent a better alternative since they show higher affinity for Ca^{2+}, faster kinetics of binding and release, and higher specificity for Ca^{2+} over unwanted magnesium (94).

Ca^{2+} indicator dyes can be categorized by their loading mechanism: cell-impermeable dyes are typically microinjected or added via patch-pipet, restricting the dye to one or a few cells (when coupled by gap junctions). Cell-permeant dyes, on the other hand, are modified with acetoxymethyl esters (AM) in order to render the molecule lipophilic, in a way that they can cross the lipid bilayer of the plasma membrane. Once inside the cell, the ester group is cleaved by esterases freeing carboxyl groups, allowing the indicator to bind Ca^{2+} ions, resulting either in an significant increase of fluorescence or in an emission/excitation wavelength shift (94).

The dynamic range of the dye, which refers to its brightness at baseline and increase in the signal intensity upon binding, should also be taken into consideration since subtle changes in Ca^{2+} concentration may not be detected when using a low range dye, if the sample has a high background or auto-fluorescence (94).

There are two classes of fluorescent Ca^{2+} indicator dyes, non-ratiometric and ratiometric, which trigger two different processes upon Ca^{2+} binding.

1.4.1.1.1 Non-ratiometric Calcium Indicator Dyes

Non-ratiometric or single-wavelength dyes show a large increase in fluorescence intensity upon binding to Ca^{2+}, with the relative change in fluorescence intensity being suggestive of an alteration in Ca^{2+} concentration. Therefore, obtaining an accurate Ca^{2+} concentration using these indicators is challenging, being mainly used for qualitative imaging where the relative obtained signal is then converted into a roughly quantitative signal, with an uncertainty degree (97).

Noteworthy, acquisition conditions, probe concentration and optical path length can contribute to fluorescence intensity although not related to a change in the Ca^{2+} concentration, and non-ratiometric dyes do not account for these (22).

Nevertheless, Ca^{2+} dyes have suffered numerous improvements over the years, resulting in the emergent next-generation fluorescent Ca^{2+} indicators with enhanced brightness, sensitivity and SNR, contrary to the first generation dyes, which although very much used (e.g. Fluo-3 AM and Fluo-4 AM), still present drawbacks like high background fluorescence (98).

One example of the former is CAL-520® AM, a non-ratiometric dye with an excitation/emission spectrum of 492/514nm and high Ca^{2+} affinity and specificity, allied to fast kinetics (dissociation constant, k_d = 320nM), capable of detecting small changes in Ca^{2+} concentration. Moreover, this Ca^{2+} indicator also showed a complete dye retention after incubation thus being stable and suitable for long-lasting

experiments (99,100). Using human neuroblastoma SH-SY5Y cells, Lock et. al demonstrated that CAL-520® AM is the optimal indicator for accurately detecting and tracking local Ca^{2+} puffs, in a comparison made between nine different Ca^{2+} indicator dyes, comprising both green and red emitting wavelengths, and three variants of genetically encoded Ca^{2+} indicators (GECIs) (94).

Other example of next-generation Ca^{2+} indicators is FLUOFORTE® Calcium Assay Kit, a commercially available kit with enhanced brightness and superior cell permeability and retention, presenting an excitation/emission spectrum of 490/525nm and an expected k_d = 389nM, being comparable to CAL-520® AM (99,101).

1.4.1.1.2 Ratiometric Calcium Indicator Dyes

Ratiometric or dual-wavelength indicators undergo a shift in their optimum absorption or emission wavelength intensities upon Ca^{2+} binding, possessing unique spectral properties. Their spectrum presents two excitation peaks depending on whether they are bound to or free of Ca^{2+} (94,100).

An increase in Ca^{2+} concentration initiates both an increase and decrease in the fluorescence emission intensities of the indicator when excited at the Ca^{2+}-bound and Ca^{2+}-free peak excitation wavelengths, respectively. Data is obtained by alternating excitation between the two peaks, acquiring results from both and attaining the ratio of the measurements, which can then be backcalculated using a calibration curve produced by several known Ca^{2+} concentrations. By doing so, these Ca^{2+} indicators have the advantage of accurately determine intracellular Ca^{2+} concentrations with higher (SNR), while reducing the effects caused by uneven probe loading, poor dye retention and photobleaching (94).

However, besides these dyes cannot be targeted to specific cell types or subcellular locations (102), the majority of ratiometric probes are also excited at phototoxic ultraviolet (UV) wavelengths (94), which can lead to the production of reactive oxygen species and induce cell apoptosis. For this reason, red-shifted indicators have become increasingly popular, since longer wavelengths (red and near infrared) show reduced phototoxicity and scattering (94).

1.4.1.2 Genetically Encoded Calcium Indicators

Genetically Encoded Ca^{2+} Indicators (GECIs) are protein-based fluorescent Ca^{2+} probes that can be incorporated in the genome of the target cells or tissues by transfection or transduction. While transfection consists of introducing exogenous genetic material into cells by either physical or chemical methods (e.g. by electroporation or formation of cationic lipid complexes, respectively), transduction requires the infection of cells with exogenous genetic material by a virus or a viral vector (94,95). In

addition, GECIs can be integrated in the genome of transgenic mice (94,95), contouring the need for loading with exogenous indicators, and can be targeted and tethered to different populations of cells and/or subcellular locations using specific promoters and targeting sequences, enabling the detection of local Ca^{2+} increases. In fact, many transgenic mouse lines have been generated for tamoxifen-inducible Cre-mediated recombination of target genes in astrocytes (95), however none of them achieves sufficient recombination in the majority of cortical astrocytes. In 2016, two labs have reported the generation of new transgenic mouse lines for selectively targeting astrocytes, Aldh1l1-Cre/ERT2, resultant from tamoxifen-inducible Cre-mediated recombination of the aldehyde dehydrogenase 1 family member L1 (Aldh1l1) (59,103), which has been shown to be specifically expressed in astrocytes. Most importantly, using the GECI GCaMP6, Srinivasan and colleagues have developed double transgenic mice for the study of Ca^{2+} signals by Ca^{2+} imaging in astrocytic processes and in the cytosol, Lck-GCaMP6fflox × Aldh1l1-Cre/ERT2 and cyto-GCaMP6f × Aldh1l1-Cre/ERT2, respectively (104,105). In this way, GECIs can be used as in vivo sensors of brain activity (94).

GCaMP is the most used single-fluorophore sensor GECI, which consists of the circularly permuted green fluorescent protein (GFP) fused to the calmodulin (CaM) binding region of chicken myosin light kinase (M13) at its N terminus and to a vertebrate CaM at its C terminus. When bound to Ca^{2+}, M13 and CaM domains interact with each other, resulting in an increase of fluorescence. To date, many variants of the GCaMP sensor (94)have been developed, yet GCaMP6 variants (slow, medium and fast) have been reported to outcompete synthetic indicator dyes in terms of their sensitivity and dynamic range for the detection of somatic Ca^{2+} signals (94,106). However, controversially, in the previously referred comparison by Lock et. al, they did not perform well when imaging more localized, subcellular Ca^{2+} signals in comparison to the Ca^{2+} indicator dyes CAL-520 and Rhod-4 (94).

Besides being technically harder to use, these genetic Ca^{2+} indicators also present lower SNR in comparison to Ca^{2+} indicator dyes.

1.4.2. Calcium Imaging Analysis

Analyzing data obtained from Ca^{2+} imaging performed in astrocytes can be quite complex (107,108). One limitation is the generation of big data, an ongoing and much needed trend in neuroscience: from these large datasets, it is possible to obtain unprecedented levels of information on space and time coordinates and interactions between key cellular components. In this way, manual identification and analysis of functionally meaningful regions of interest (ROIs) is very time-consuming and since it might be difficult to identify a clear compartmentalization in astrocytic processes and the identification of proximal and distal processes is, at times, somewhat subjective, segmentation of functional units is often

challenging (95,107). Therefore, there is a need for automated detection and analysis of both functional units and signals (109).

Over the years, plentiful of softwares became available to analyze Ca^{2+} signals in neurons, being that the majority of them rely on a number of fundamental assumptions that are true for neurons, but cannot be transposed to astrocytes. The former usually consider that: a single functional unit likewise the soma (which can be constrained in terms of its size and/or shape) carries most of the relevant information (due to the generation of action potentials); each pixel of the unit has the same time-course as the unit and stereotyped kinetics dependent on the dye used; and the defined ROI is activated multiple times during the recording in a reproducible manner. Conversely, astrocytes present a vast spatiotemporal diversity in Ca^{2+} responses as well as the already mentioned lack of distinct morpho-functional specialization, making the use of these analysis tools unsuitable for astrocytic Ca^{2+} elevations (109).

More recently, significant progress has been made with several tools developed for the study of Ca^{2+} signals of astrocytes(107,108,110–116). Various comprehensive frameworks allow for the treatment of these datasets, as is the case of Fiji/ImageJ© and Matlab© image processing toolbox. Fiji/ImageJ© is an open-source, user-friendly, customizable, continuously updated and expandable software with hundreds of available plugins, thus being an attractive option for analyzing astrocytic Ca^{2+} imaging data (109).

1.5. Recording and Stimulation of Astrocytes

The use of patch-clamp in the late 1980s has brought new prospects to the study of astrocyte electrophysiology. Although, according to patch-clamp measurements, astrocytes are not electrically excitable cells due to their lack of action potentials, their membranes do display slow ion fluctuations and a variety of functional channels (2,58,117) (see 1.1. Physiology of Astrocytes). More recently, extracellular planar electrodes, known as microelectrode arrays (MEAs) (117,118) have also been used to measure electrical fluctuations in astrocytes (48,117,119).

These electrophysiological devices represent the most relevant methods within the neuroscience community.

1.5.1. Intracellular Electrophysiology Devices

Patch-clamp, together with sharp-intracellular microelectrodes are powerful tools to record neuronal action potentials, subthreshold and synaptic potentials with a high SNR, having a very good electrical coupling with the cell. These intracellular devices enable the study of a single cell and its functions through direct measurement of intracellular voltage. Patch-clamp is also used to measure the ionic currents of single ion channels (120).

Tips used with both devices are pushed through the cell's plasma membrane, directly contacting with the cytosol. In the case of patch electrode tips, when introduced in the cell break the plasma membrane making direct contact between the cytosol and the interior solution of the patch electrode (121). Current injections through these electrodes are able to intracellularly stimulate cells, which is useful to study biophysical parameters such as membrane capacitance, input resistance and, in neuronal cells, synaptic properties. However, the use of this technique is limited to a few cells per experiment being impossible to record and stimulate hundreds of individual cells simultaneously. Moreover, intracellular recordings and stimulation progressively damage the plasma membrane, representing a limitation in long-lasting studies. In addition, perfusion of the cytoplasm by patch electrodes has been shown to cause alterations in the intracellular composition of the neurons (121).

1.5.2. Extracellular Electrophysiology Devices

Planar MEAs systems are being increasingly used in neuroscience, since they offer simultaneous, parallel, multisite and long-term recordings of the electrical activity from large populations of excitable cells at millisecond time scale (118). Furthermore, they represent a non-invasive technique, as no mechanical damage occurs on the plasma membrane of cells, thus allowing multiple recordings over a large time course of an experiment. Nevertheless, extracellular recording technologies also have disadvantages when compared to intracellular ones: they display relative low SNR and a less efficient coupling between cells and the extracellular electrodes (118,122). Noteworthy, membrane events from single neurons that can affect cell's excitability (such as excitatory or inhibitory subthreshold synaptic potentials or membrane voltage oscillations) but do not result in an action potential cannot be detected by the standard MEAs, limiting the study of neuronal networks (118,122).

Besides allowing the recording of excitable cells, MEAs systems can also be used to influence and control neuronal cells and network activity through electrical stimulation. In order to reduce the number of electrodes and to achieve a high spatial coupling for input and output mapping of neuronal networks, it possible to use the same electrode to both stimulate and record. Stimulation pulses can be delivered to cells in voltage or current-mode stimulation, being that voltage-mode is set precisely as a function of time but the current can vary freely, whereas in current-mode roles are inverted . It is important that the applied stimulus do not damage cells, which is not always straightforward contrary to intracellular stimulation where there is already a variety of well-defined protocols. Charge transfer to the plasma membrane should be accounted for since it can cause damage to the cells by irreversible electroporation or electrochemical reaction, being advisable the delivery of weak capacity stimuli trains to cells (118,122).

Although very much used for recording and stimulating neurons, there are only a few studies regarding the use of MEAs for recording (117,123–125) and even fewer for the stimulation of astrocytes (48,119).

1.5.3. Recording and Stimulation of Astrocytes using Microelectrode Arrays

High-frequency voltage oscillations (250–400 Hz) have been observed in cortical and hippocampal cell cultures upon electrical stimulation on microelectrode arrays (MEAs), but were not assigned to a cell type (126).

The fact that MEAs are optimized to detect and measure action potentials and that the associated thermal noise of commercially available electrodes in MEA systems can easily reach 10mV makes it a less attractive technology for studying astrocytes' electrophysiology. Thermal noise is directly proportional to electrodes' impedance (in opposition to current flow when voltage is applied), which in its turn is inversely proportional to the size of the electrodes.

In comparison with an action potential, ionic fluctuations generated by astrocytes are approximately one thousand times weaker and slower, lasting for several seconds with a few microvolt amplitudes. To record these ultra-weak signals electrodes with low intrinsic thermal noise are required (117). One way of reducing thermal noise is by increasing effective surface area of electrodes, which can be achieved by using conductive materials with porous in the electrode's surface. Recording of ultra-weak signals in populations of glioma cells was demonstrated using large capacitive electrodes with a low thermal noise (127), being that extracellular signals were recorded with amplitudes below 1mV (128). In 2017, Mestre et al. have shown the potential of this ultra-sensitive electrical method to measure extracellular ionic fluctuations in primary cultures of astrocytes (117). The authors reported spontaneous electrical signals with striking similarities as the ones from optical imaging methods in astrocytes, supporting the idea that the obtained electrophysiological measurements were correlated with the features of some of the well-known astrocytes oscillations, namely on signal width, shape and frequency. For instance, Kuga et al. reported repetitive signals with 1 minute of periodicity, lasting for approximately 10–20s (129); Nieden et al. showed spontaneous Ca^{2+} transients with a frequency of approximately 1.3 signals per minute, each lasting for 10–20s (90); and Srinivasan et al. demonstrated that astrocytic Ca^{2+} fluctuations lasted for approximately 14s (66). Likewise what was observed by Mestre et al., reported signals were also characterized by a fast rise time, followed by a slower decay to the baseline, presenting signal patterns with both frequency and amplitude modulation that repeated in an nearly periodic trend (117).

Although electrical signals are not selective to ionic species, extracellular electrophysiological measurements do show a richness of detail difficult to obtain when using imaging methods. Astrocytic

signals start by increasing gently in amplitude and rate, showing that an increasing number of cells become synchronized or somehow correlated. The temporal properties of the synchronization can be followed in real time, which is not entirely perceived using fluorescence techniques (117).

High frequency voltage oscillations have already been reported in astrocytes in 2015, when Fleischer et al. demonstrated that, when electrically stimulated with MEAs, astrocytes displayed very fast and long-lasting extracellular voltage oscillations, which covered a broad frequency spectrum up to 600Hz with decreasing frequencies over time (48). It is worth noting that frequencies between 200 and 600Hz are considered pathological and might relate to some sort of epileptiform activity (48). It is also known that astrocytic Ca^{2+} signaling can lead to neuronal depolarization and spontaneous epileptiform discharges (20). Furthermore, low levels of extracellular Ca^{2+} in hippocampal slices efficiently evoked Ca^{2+} oscillations in astrocytes followed by simultaneous Ca^{2+} elevations in adjacent neurons, thus facilitating neuronal synchrony and epileptiform activity. However, whether astrocytes are key players in brain oscillatory activity was still not clear, due to the lack of a prominent frequency band (100-200Hz) in astrocytic oscillations. Nevertheless, while the involvement of voltage-gated ion channels in the generation of HFOs was clear, this work still raised doubt since astrocytes were thought to be electrically passive cells, showing a rather linear voltage/current relationship due to the lack of voltage-gated ion currents (48), although the expression of voltage-activated channels has already been reported (70). In addition, these HFOs were shown to be: (1) highly susceptible to changes in extracellular Ca^{2+}, possibly representing the early steps in a signaling cascade that may result in propagating Ca^{2+} waves; (2) not dependent on synaptic release or volume-regulated anionic channels; (3) strengthened by hyperpolarization and increase in extracellular Na^{+}, as it increases the driving force for ions with equilibrium potentials in the positive range (influx of Na^{+} and Ca^{2+}, as well as efflux of anions like ATP^{3-} and $glutamate^{-}$ are facilitated); and (4) dependent on purinergic ATP receptors, as ATP induces ion currents through P2X receptors, which are increased with low extracellular Ca^{2+} concentration, corroborating the observations that low Ca^{2+} resulted in powerful HFOs (48).

It has been proposed that the electrical stimulus leads to Ca^{2+} influx through voltage-gated Ca^{2+} channels, mediating ATP release and subsequent activation of P2X receptors, which causes the opening of membrane pores facilitating influx of Na^{+} and Ca^{2+}. (48)

More recently, in order to better understand the interaction between astrocytes and neurons and the effect of the neuromodulator norepinephrine in their communication, Bar El et al. performed both electrical stimulation with MEAs (to activate the neuron-astrocyte glutamate-mediated pathway) and Ca^{2+} imaging in neuron-astrocyte (mixed) co-cultures and astrocyte (isolated) cultures (119). Interestingly, the authors reported different astrocyte behaviors based on their coupling to neurons: besides morphological changes in astrocytes, norepinephrine caused an increase in Ca^{2+} signaling (in both mixed and isolated cultures), a decrease in neuronal spontaneous activity and, therefore, the communication

between neuron-astrocyte networks was altered. In astrocytes, this neuromodulator activates IP_3-mediated mechanism that leads to Ca^{2+} oscillations between the cytosol and intracellular Ca^{2+} stores (119).

Most importantly, although the application of the proposed electrical stimulation protocol in isolated cultures did not cause astrocytes to respond, by stimulating a mixed culture astrocytic Ca^{2+} elevations were triggered, in astrocytes coupled to activated neurons. Upon treatment with norepinephrine, astrocytes did no longer respond to the electrical stimulation (not even when coupled to neurons), confirming that detected Ca^{2+} oscillations were caused by neuronal activation (119).

1.6. Aim

Although the last decades have been trully revolucionary in the study of astrocytes, there are still a lot of characteristics of their complex Ca^{2+} signaling to unravel. Furthermore, many authors worlwide disagree on astrocytes' electrical excitability, since they do not have the ability of generating action potentials. Having this in mind, the main goal of this project, developed in the Neuroengeneering and Computational Neuroscience group (INEB/i3S), is to assess the response of astrocytes to the modulation of their electrophysiologic microenvironment, by evaluating and characterizing their response to the extracellular electrical stimulation. Therefore, we are interested in addressing the following questions: do astrocytes respond differently to different stimulus? To which stimulation amplitudes are astrocytes sensitive to? Do astrocytes respond differently to the same stimulus' amplitude? What is the effect of the stimulation amplitude in the rise and decay times of Ca^{2+} signals? Is the travelled distance of Ca^{2+} waves dependent on the stimulation amplitude? Does the same happen with the mean velocity propagation of Ca^{2+} waves?

In order to achieve this, electrical stimulation using ThinMEAs© will be used, coupled with Ca^{2+} imaging for the monitorization of astrocytic activity.

1.7. Dissertation Overview

This dissertation is organized into five chapters. Chapter 1 is the introduction, and includes the motivation for the development of this work and a review of the state-of-the-art: the first sections cover themes like the Physiology of Astrocytes (section 1.1), Pathophysiology of Astrocytes (section 1.2) and Astrocyte-Neuron Interaction (1.3), whereas in the next sections are covered the following themes: Calcium Imaging in Astrocytes (section 1.4), where are reviewed the different Ca^{2+} indicator dyes (section 1.4.1) and Ca^{2+} Imaging analysis techniques (section 1.4.2). Still in the introduction, are reviewed the themes Recording and Stimulation of Astrocytes using Microelectrode Arrays (section 1.5), and it is discussed the

Intracellular (section 1.5.1) and Extracellular (section 1.5.2) Electrophysiology Devices, as well as the proposed goals for this project (section 1.6).

Chapter 2 corresponds to Materials and Methods, where it is described the methodology adopted for the development of this work. Sections 2.1 and 2.2 present the followed protocol for the isolation and culture of astrocytes and the immunocytochesmistry for evaluation of the purity of astrocytic cultures, respectively. Section 2.3 Calcium Imaging describes the methodology used for the staining of astrocytes with both CAL-520© AM (section 2.3.1) and FLUOFORTE© (section 2.3.2). In Section 2.4 are described the protocol for the acquisition of images, and Section 2.4.1. Modulation of the Astrocytic Microenvironment. Image analysis is described in detail in the Section 2.5.

Results are presented in chapter 3, from the optimizations implemented in the laboratory (section 3.1) and the assessment of the astrocytic culture purity (section 3.2), to the stimulation of astrocytes (section 3.3), in which are presented the sections 3.4.1. Delivery of Consecutive Stimulu to Astrocytes, 3.4.2. Simultaneous Stimulation on Neighboring Microelectrodes, 3.4.3. Stimulation of Astrocytes with Stimuli of Different Amplitudes, and 3.4.4. Characterization of Astrocytic Ca^{2+} Signals, the latter including the measurement of Ca^{2+} signals' amplitudes (section 3.4.4.1), rise and decay times (section3.4.4.2) and mean propagation velocity (section 3.4.4.3).

In chapter 4 obtained results are discussed taking into consideration previous work done in this field, and conclusions and future perspectives are presented in sections 5 and 5.1, respectively.

2. Materials and Methods

2.1. Isolation and culture of Astrocytes

Astrocytes were isolated from the cortex of Wistar Han rat pups 1 to 2 days after birth. Briefly after decapitation brains were removed, the cortex dissected and the meninges and cerebellum discarded. Cortex tissue was mechanically dissociated and enzymatically digested with 0.01% trypsin and 0.01% DNase I (Sigma-Aldrich) at 37ºC for 15 minutes. Cells were seeded in 75cm^2 flasks coated with 10μg/mL poly-D-lysine (PDL) (Sigma-Aldrich) and kept in culture using DMEM-Glutamine high glucose medium (Corning©) with 10% Fetal Bovine Serum (FBS) (Sigma-Aldrich©) and 1% Penicillin-Streptomycin (Pen-Strep) (Gibco©), at 37ºC, 5% CO_2. Microglia and oligodendrocyte precursor cells were mechanically detached by shaking, primarily after 12 days in culture, then once a week every two weeks, whereas astrocytes remained attached to the surface of the flask(130). After the last shake, cells were trypsinized with 0.05%Trypsin-EDTA (Gibco©) and plated at a 1:2 ratio. Astrocytes were used from the third passage (P), point at which the culture is considered pure, until they reach P8.

All experiments were performed in accordance with institutional and European guidelines for the care and use of laboratory animals.

2.2. Immunocytochemistry

A total of 150000 astrocytes were seeded on a 35 mm μ-dish (Ibidi, Germany). After 1-2 days in culture, cells were fixed with 4% paraformaldehyde in PBS, pH 7.4 for 20 min at RT. The samples were washed 3x with PBS following permeabilization and blocking with 5% FBS, 0.3% Triton X-100 for 1h at RT. Anti-GFAP (Z0334, Dako) diluted 1:2000 in blocking solution was incubated O/N at 4ºC. Cells were washed 3x with PBS and incubated with secondary antibody anti-rabbit Alexa 488 (ThermoFisher). Fluorescence images were acquired using the microscope described in chapter 2.4.

2.3. Calcium Imaging

For Ca^{2+} imaging, astrocytes were trypsinized and seeded (2x10^5 cells) on PDL-coated (10μg/mL) 35mm imaging dish (Ibidi) and ThinMEA (MultiChannel© systems) chips and kept in culture from 2 to 4 days. Contrary to standard chips, ThinMEAs are only 180μm thick, thus being the best option for high-resolution imaging. These chips contain 252 microelectrodes of 30μm each plus four reference microelectrodes, embedded in a very thin glass substrate on a robust ceramic carrier, with a 200μm spacing between electrodes (figure 1).

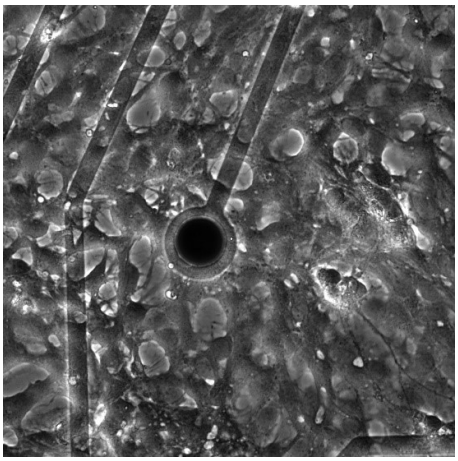

Figure 1 – Bright field image of astrocytes cultured on ThinMEA® chips. In the center of the image is seen the microelectrode, with astrocytes displayed around it (40x).

Both fluorescent organic Ca^{2+} indicator dyes, CAL-520® AM (AAT Bioquest®) and FLUOFORTE® (Enzo Life Sciences®) were used, being that the working concentration of CAL-520® AM was optimized in the laboratory, whereas FLUOFORTE® was prepared accordingly to the manufacturer's instructions. As discussed in chapter 1.4.1.1, these indicators show fast response time to changes in Ca^{2+} having the advantage of not being dependent on the transfection of cells, contrarily to GECIs, thus being technically easier to use(11) and guaranteeing a more homogeneous distribution among cells.

2.3.1. CAL-520® AM Staining

In order to optimize CAL-520® AM staining, two different concentrations were tested, in accordance to the literature(94): 10μM and 20μM. Cell medium was replaced by 1x Hepes-buffered Hanks balanced salt solution (HHBSS) with 0,04% of Kolliphor® P407 (BASF) and CAL-520® AM, and incubated at 37ºC, 5% CO_2 for either 60 or 90 minutes, followed by 30 minutes at room temperature (RT). Kolliphor® P407 is a nonionic detergent used to increase the aqueous solubility of CAL-520® AM esters, facilitating its entrance in cells(131). Previously to microscopy, medium was removed and replaced with 1x HHBSS.

The mean fluorescence of 28 free-hand drawing ROIs defined around cells' soma from 4 untreated images of different fields was quantified for each condition. Statistical analysis was assessed by performing a One-way ANOVA followed by a post hoc for multiple comparisons (Turkey HSD) test using IBM® SPSS® Statistics 25.0 (p-value was considered significant at ≤0.05). Results from the optimization are presented in 3.1.1. Optimization of CAL-520® AM Dye Concentration.

2.3.2. FLUOFORTE® Staining

For FLUOFORTE® staining, cell medium was removed and cells were incubated with 1mL of dye at 37ºC, 5% CO_2 for 45 minutes and then 15 minutes at RT. This Ca^{2+} indicator dye was selected for the staining of cells seeded on ThinMEAs, as FLUOFORTE® requires a shorter period of incubation and does not need any additional washing step.

2.4. Microscopy

For microscopy, a Leica© DMI 6000B FFW microscope adapted for live cell imaging and equipped with a Hamamatsu Orca Flash 4.0 camera, an epi-fluorescence with a metal halide 100W lamp and a L5 (Excitation: 460-500; Beam Splitter: 505; Emission: 512-542) filter set was used.

Image acquisition was performed at 100Hz with 4x4 binning, in a total of 20 seconds, using a 40x objective with 0.6 numeric aperture (NA).

2.4.1. Modulation of the Astrocytic Microenvironment

Modulation of astrocytic microenvironment was assessed by Ca^{2+} imaging and achieved by performing both chemical and electrical stimulation immediately after initiating image acquisition.

2.4.1.1 Chemical Stimulation of Astrocytes

To chemically stimulate astrocytes, neurotransmitters already described in the literature to modulate astrocytic response by inducing Ca^{2+} events (namely Glutamate (Sigma-Aldrich) and ATP (Sigma-Aldrich)) were used. Both chemicals were added individually to cells upon microscopy at a concentration of 100μM(132).

2.4.1.2 Electrical Stimulation of Astrocytes

Extracellular stimulation of astrocytes was performed using the MEA2100 system© (MultiChannel© Systems) with an integrated stimulus generator and temperature control, and was based on the protocol described by Fleischer et al.(48). After a 6s stimulus-free baseline recording, different separate biphasic square stimuli (±200mV, ±400mV, ±600mV and ±800mV), were applied once – unless otherwise stated – with 200μs of duration per phase. Total recording time was 30 seconds.

2.5. Image Analysis

In order to evaluate Ca^{2+} activity at cellular and network level in stimulated astrocytes, Ca^{2+} signal curves and event amplitudes, average travelled distance and average spatial propagation velocity of intercellular Ca^{2+} waves were quantified. Image analysis was accomplished by using custom written Fiji/ImageJ macros, which are attached to this document (see Appendix). Unless otherwise stated, all data treatment was performed using Microsoft Office© Excel 2013 and 2017.

2.5.1. Image Preprocessing

Aiming at the enhancement of acquired images' quality, a non-linear median filter was used to remove noise while preserving edges, thus maintaining cell morphology. With this filter, each pixel value is replaced with the median value in its neighborhood – which is dependent on the selected radius –, eliminating pixels that have a very high or low intensity when compared to their neighbor pixels. To evaluate the effect of the selected radius in the profile of the fluorescence signal, a comparison between the non-filtered and filtered images with two different radius, 1 (1x1 pixels) and 2 (2x2 pixels), was performed. After comparing the filtered images, a radius of 1 was chosen to filter images, since it allowed the removal of noise without losing detail.

To accurately detect changes in the fluorescence and remove background, images were normalized by calculating ΔF/F0. To determine the baseline fluorescence (F0), the first stimulus-free 300 frames (prior to stimulation), corresponding to the first 3 seconds of recording, were duplicated to get a new image and the median intensity Z-projection was computed. This creates an image in which each pixel assumes its median value of the input stack. The resultant image was then subtracted to each frame of the original image (F-F0, or ΔF) and normalized by dividing the output image by the previously estimated background (ΔF/F0).

Moreover, for future spatial distance calculations, images were calibrated using a pixel value of 0,4996μm since images were acquired with 4x4 binning: considering that the imaging system is calibrated, under the acquisition conditions the size of 1 pixel corresponds to 0,1249μm laterally.

The Fiji/ImageJ custom written macro used for preprocessment can be consulted in Appendix A.

2.5.1. Comparison of the Amplitude of Astrocytic Response to Different Stimuli and the Travelled Distance of Ca^{2+} Signals

Both the amplitude of the astrocytic response upon the application of different stimuli with the same amplitude, and the travelled distance of Ca^{2+} signals were addressed initially by calculating the median fluorescence intensity Z-projection of the normalized image (ΔF/F0), in a given ROI. By using the median values, the influence of outliers (e.g. the presence of saturated pixels or of artifacts with high fluorescence values, or the absence of fluorescent cells in the selected ROI) in the overall fluorescence intensity was prevented.

Using a Fiji/ImageJ custom written macro (see Appendix B), the user is able to insert the radius increment and the number of new ROIs, as well as define the electrode by drawing a circular ROI. In our data, we used a radius of 30 pixels (approximately 15μm, since it is the microelectrode radius) and a number of 12 ROIs so that we could reach all field-of-view. By means of calculating the coordinates and centroid of the defined electrode, the algorithm then draws new ROIs radially located around the electrode, having the same centroid and an incremented radius, until it reaches the number of ROIs defined by the user (figure 2).

Afterwards, to each of the new ROI it is subtracted the ROI within its interior, thus creating a new "donut" shaped ROI that is added to the ROI manager.

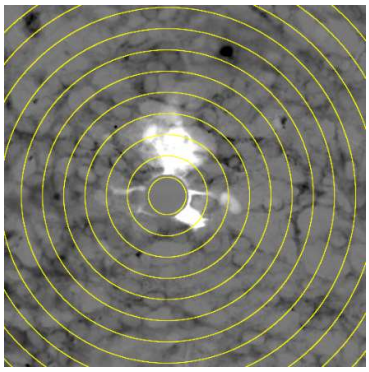

Figure 2 – Semi-automatic definition of radial ROIs around the microelectrode. Upon definition of the microelectrode by the user, the algorithm then draws the remaining ROIs with the inserted parameters (40x).

ROI area, mean, standard deviation and minimum and maximum values were measured, and the maximum values were plotted in order to get the fluorescence profile in function of the distance to the electrode. By doing so, it is possible to evaluate the intensity of Ca^{2+} signals in ROIs closer to or further away from the electrode in an accessible and semi-automatic manner, allowing to gauge the travelled

distance of Ca^{2+} signals. Statistical analysis was assessed by performing a Kruskal–Wallis with a pairwise comparisons test using IBM® SPSS® Statistics 25.0 (p-value was considered significant at ≤0.05).

2.5.2. Measurement of the Amplitude and the Rise and Decay Times of Ca^{2+} Signals

In order to measure the amplitude and rise (T_{20-80}) and decay (T_{80-20}) times of Ca^{2+} signals resultant from electrical stimulation with both ±800mV and ±600mV, the macro used for the preprocessment of images was updated (Appendix A). There, and to facilitate ROI definition, the user is able to insert the number of ROIs, with an already fixed size, in the image resultant from the median intensity projection of the normalized (ΔF/F0) image and place them in the site where they want to measure Ca^{2+} signals. Then, ROIs are restored in the normalized image and the Z-axis profile of Ca^{2+} signals is plotted. Afterwards, the user is asked to draw a rectangle selecting the maximum and the baseline of the Ca^{2+} wave, and resultant values will be saved as a .cvs file. Then, the moving average of the values was calculated so that the signal noise is attenuated and interpretation of values is facilitated (figure 3).

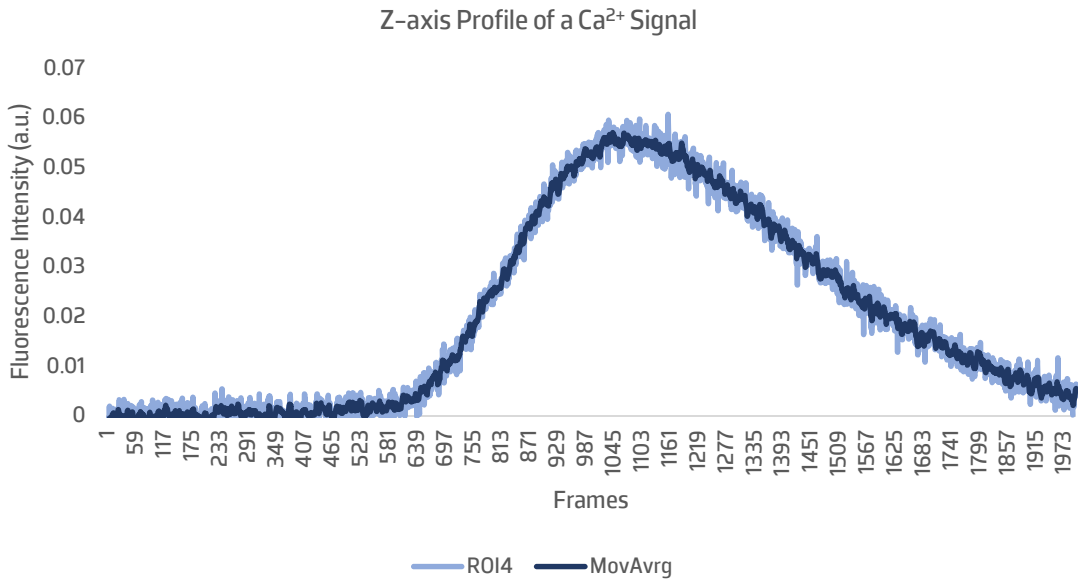

Figure 3 – Representation of a Ca^{2+} signal profile over the course of the experiment. The moving average was used as a means for facilitating the selection of the peak and baseline values, since it soothes the obtained signal.

To each defined ROI, the height of the drawn rectangle will be the amplitude of the Ca^{2+} signals, thus the 20% and 80% amplitudes were calculated by multiplying the amplitude by 0.2 and 0.8, respectively. T_{20-80} and T_{80-20} was achieved by extracting the frames correspondent to the 20% and 80% amplitude and calculating the time. The average and standard deviation of the five measured

microelectrodes were then plotted for comparison between stimuli. Statistical analysis was addressed by performing a T-test for independent samples regarding the amplitude of Ca^{2+} signals and a Mann-Whitney U test regarding the rise time of Ca^{2+} signals, using IBM® SPSS® Statistics 25.0 (p-value was considered significant at ≤0.05).

2.5.3. Measurement of the Average Propagation Velocity of Ca $^{2+}$ Signals

To measure the average propagation velocity of Ca^{2+} signals the normalized (ΔF/F0) stack image was used, where several representative linear ROIs were drawn (figure 4) and the grey values of each ROI were plotted.

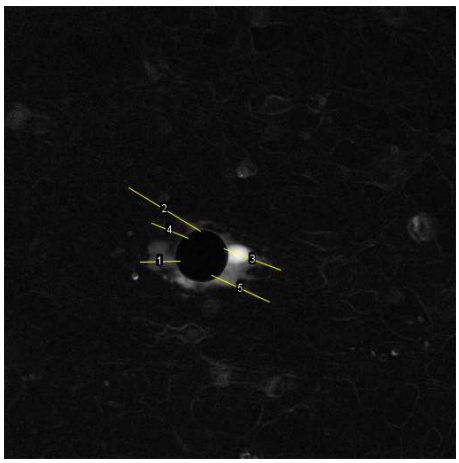

Figure 4 – ROI definition for the mean propagation velocity calculation. Maximum Z-projection image to show the definition of representative linear ROIs for the calculation of the propagation velocity (40x). Our values were extracted from ROIs drawn in the normalized image (ΔF/F0).

The distance of the signal was obtained by getting the mid-high value of the front of the wave in six different frames. These values were used to generate a plot of distance in function of time, in which the slope of the trendline corresponds to the average velocity. Statistical analysis was addressed by performing a Mann-Whitney U test, using IBM® SPSS® Statistics 25.0 (p-value was considered significant at ≤0.05).

3. Results

Astrocytes present complex spatiotemporal Ca^{2+} dynamics in response to diverse external stimuli that are intrinsically related to their function as a third element of synapses. Therefore, understanding their activity upon different electrophysiological conditions is an emergent subject. In order to evaluate the effect of the modulation of the electrophysiological microenvironment of astrocytes, both chemical and electrical stimulation of astrocytic rat primary cultures coupled with Ca^{2+} imaging was performed. Obtained results, from the optimization of Ca^{2+} imaging to the effects of the electrical stimulation on astrocytes, are presented in this chapter.

3.1. Optimization Process

3.1.1. Optimization of the CAL-520 ® AM Dye Concentration

Ca^{2+} imaging was achieved by making use of two organic dyes – CAL-520® AM and FLUOFORTE®. With the purpose of optimizing CAL-520® AM concentration, both 10µM and 20µM of dye were incubated for 60 minutes or 90 minutes at 37ºC followed by 30 minutes at RT and the mean fluorescence for each condition was quantified (figure 5).

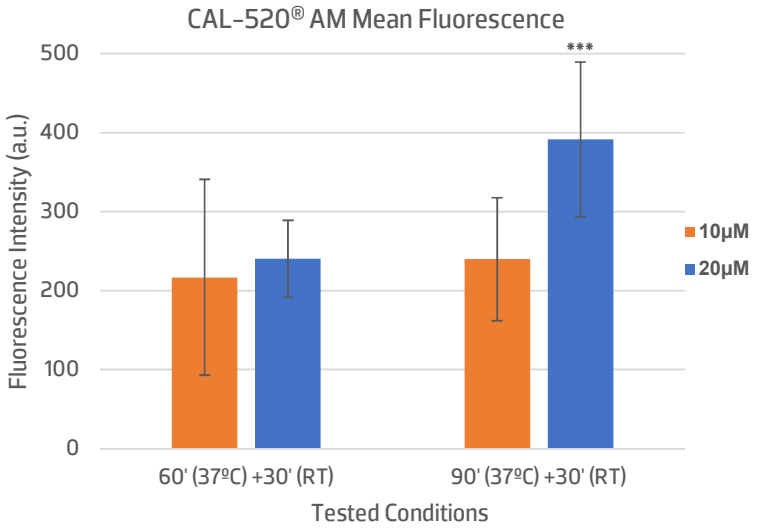

Figure 5 – Optimization of CAL-520® AM staining concentration. Two concentrations of the Ca^{2+} indicator dye were tested and each concentration was incubated for either 60 or 90 minutes at 37ºC, followed by 30 minutes at RT. Fiji/ImageJ was used to quantify the mean fluorescence of at least 28 cells from 4 images of each condition, in a total of 112 quantified cells. 20µM of dye incubated for 90 minutes at 37ºC and 30 minutes at RT showed the higher mean fluorescence ($p<0.001$) when compared to other conditions. *** indicates $p<0.001$.

Astrocytes incubated with 10µM of dye for 60 minutes at 37ºC followed by 30 minutes at RT presented a mean fluorescence of 216.87a.u., which increased for 239.76au when incubated for 90 minutes at 37ºC followed by 30 minutes at RT. When the concentration of CAL-520® AM used was 20µM, incubation for 60 minutes at 37ºC followed by 30 minutes at RT resulted in a mean fluorescence of 240.27a.u., increasing to 391.47a.u. when incubated for 90 minutes at 37ºC followed by 30 minutes at RT. Therefore, incubation with 20µM of dye for 90 minutes at 37ºC and 30 minutes at RT represented the higher mean fluorescence, when compared to all other conditions ($p<0.001$), being selected for further experiments.

3.2. Assessment of the Astrocytic Culture Purity

To ensure that astrocyte cultures, isolated as previously described (see 2.1. Isolation and Culture of Astrocytes), were enriched with astrocytes, staining with an astrocytic specific marker, GFAP, was addressed beforehand (figure 6).

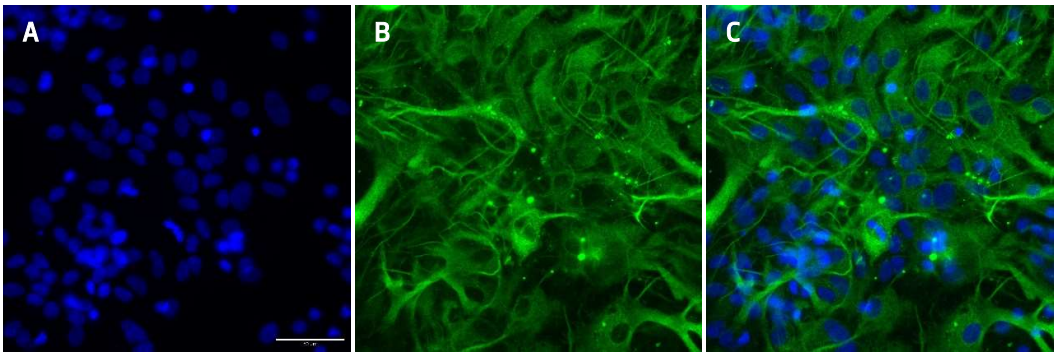

Figure 6 – Immunocytochemistry of astrocytic cultures with GFAP. Isolated primary rat cultures of astrocytes were stained with an astrocyte specific marker (GFAP), where the majority of cells are stained with GFAP, with only a few doubtful nucleus, 40x. **A)** Nucleus stained with DAPI (blue). **B)** GFAP staining in the cytoplasm of astrocytes (green). C) Composite image of cells astrocytes with both DAPI and GFAP. The scale bar represents 50µm.

As showed in figure 6, the majority of cells in the field of view were stained with GFAP, whereas only a few cells did not present any staining for GFAP, indicating that the culture is enriched in astrocytes.

3.3. Stimulation of Astrocytes

As a means for evaluating the effect of the modulation of the astrocytic microenvironment, stimulation of astrocytes was performed, both chemically and electrically. Chemical stimulation was done with the purpose of confirming that the isolated astrocyte cultures are capable of responding to external stimuli, being eligible for the proposed experiment design. Afterwards, electrical stimulation of astrocytes was performed using ThinMEA© chips, while monitoring Ca^{2+} signals through Ca^{2+} imaging.

Characterization of Ca^{2+} waves was done in function of the applied electrical stimuli, signal amplitude and rise and decay times and mean propagation velocity.

3.3.1. Chemical Stimulation of Astrocytes

Astrocytes were stimulated using two different neurotransmitters, ATP (figure 7A and 7B) and Glutamate (figure 7C and 7D), known to trigger the elevation of cytosolic Ca^{2+} levels.

Stimulation of astrocytes with ATP and Glutamate, as expected, lead to an increase in intracellular Ca^{2+} levels, which then generated a Ca^{2+} wave, propagating to neighboring astrocytes. These results confirm the ability of astrocytes to respond to external stimulation, being important for the validation of astrocytic cultures for further experiments.

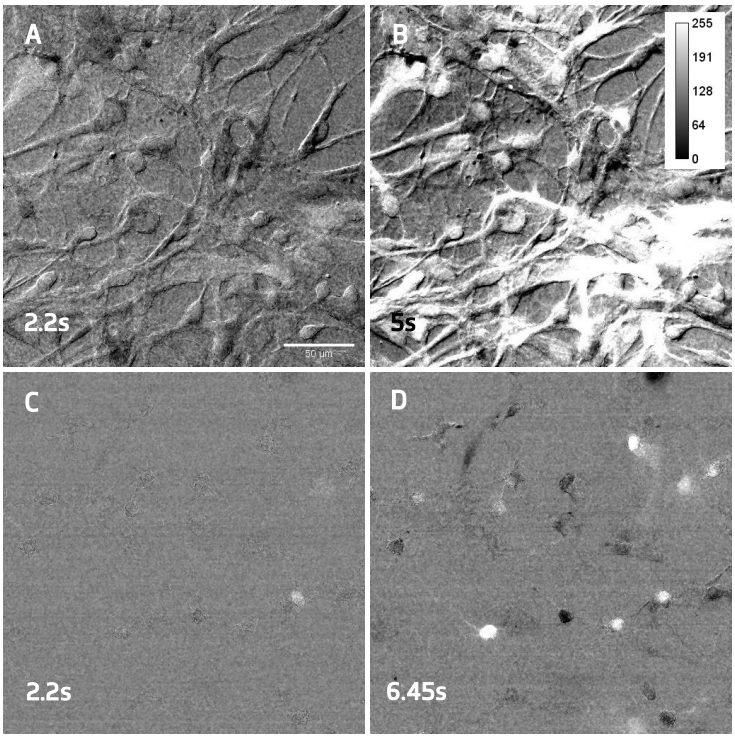

Figure 7 – Chemical stimulation of astrocytes elicited Ca^{2+} signaling in astrocytes. Stimulation was performed using ATP (A and B) and Glutamate (C and D) (40x). **A)** Astrocytes before the addiction of ATP to the medium, 2.2s after the beginning of the recording, where no detectable Ca^{2+} signals are seen. **B)** Astrocytes after addition of ATP, showing an increase in the Ca^{2+} levels, at 5s of recording. **C)** Astrocytes before addiction of Glutamate to the medium, which do not exhibit Ca^{2+}signals, 2.2s after the beginning of the recording. **D)** Ca^{2+} signals can be detected after Glutamate addition to astrocytes, 6.45s after the beginning of the recording.
The scale bar represents 50µm. All images were normalized (ΔF/F0).

3.4. Electrical Stimulation of Astrocytes

Electrical stimulation of FLUOFORTE® stained astrocytes, cultured in ThinMEA© chips, was achieved by using the MEA2100 system© (MultiChannel Systems©). A square biphasic stimulus of ±800mV of amplitude was applied once after a 6s baseline recording. Results are presented in figure 8.

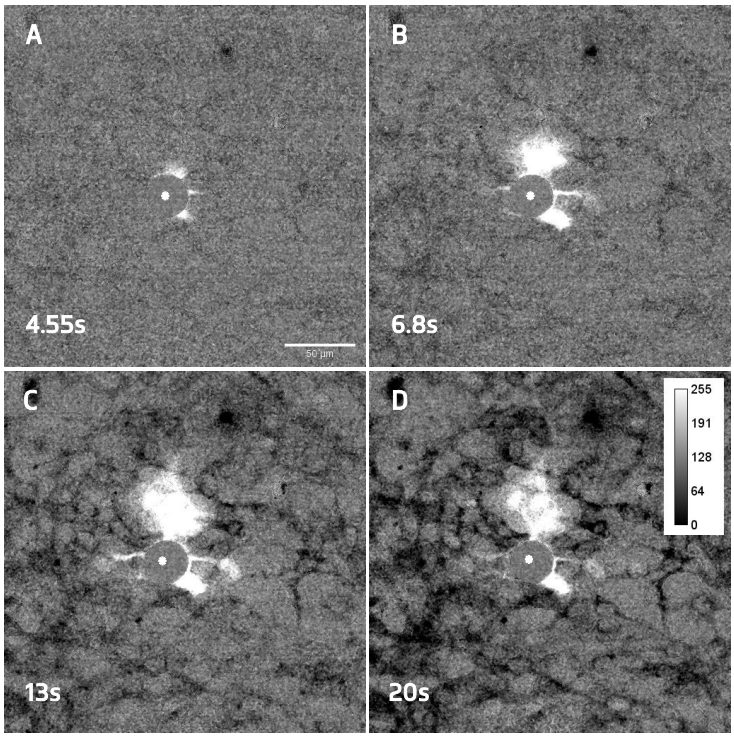

Figure 8 – Electrical stimulation of astrocytes. Astrocytes were electrically stimulated with a ±800mV biphasic stimulus using ThinMEAs© (40x). Elapsed time of the acquisition is displayed in the normalized image (ΔF/F0). **A)** Immediately after application of the electrical stimulus, astrocytes located around the microelectrode started to exhibit Ca^{2+} signals. **B-C)** Ca2+ waves propagated to neighboring cells, in a radial manner relatively to the microelectrode. **D) L**ast frame of the acquired stack image, showing a slight decay in the Ca2+ signals.
The scale bar represents 50µm. * represents the microelectrode.

Astrocytes exhibited a marked response upon electrical stimulation. After stimulus delivery, it was possible to observe an increase in Ca^{2+} levels in astrocytes adjacent to the microelectrode (figure 8A). Then, Ca^{2+} signals propagated throughout neighboring cells, in a radial manner relatively to the microelectrode (figure 8B and 8C). 15.45s after stimulation, Ca^{2+} levels of astrocytes around the microelectrode were slowly decaying, yet they still had not return to the baseline levels (figure 8D).

3.4.1. Delivery of Consecutive Stimuli to Astrocytes

Two consecutive square biphasic stimuli of ±800mV of amplitude were applied in a given microelectrode (after a 6s baseline recording) with a 10s interval between stimuli, in order to understand if astrocytes respond independently to two consecutive stimuli. Figure 9 presents an example of the Z-axis profile of a Ca^{2+} signal, measured in a representative ROI after calculating the ΔF/F0.

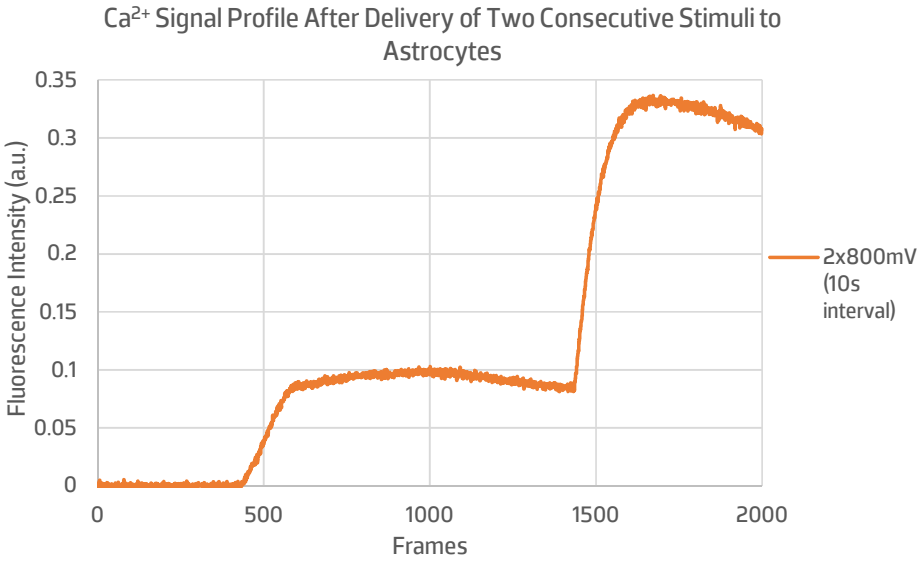

Figure 9 –Effect of the stimulation of astrocytes with two stimuli of the same amplitude , separated by 10s. Stimulation with two consecutive ±800mV stimuli resulted in two distinct Ca^{2+} increases separated by roughly 10s.

When stimulating for the second time with the two consecutive stimuli, after the first stimulation there was an increase in Ca^{2+} signals that soon stabilized (after approximately 1s), starting to decay when, 8.17s later a second ±800mV stimulus was delivered to astrocytes, resulting in an substantial increase in the Ca^{2+} levels. This experiment was repeated at least three times, generating consistent results (data not shown).

3.4.2. Simultaneous Stimulation on Neighboring Microelectrodes

Ca^{2+} signals originated upon electrical stimulation were observed only in astrocytes located around the microelectrode. To evaluate if the co-activation of two neighboring microelectrodes would favor the activation of astrocytic cells enclosed by those microelectrodes, the stimulation of two neighboring microelectrodes was performed simultaneously by applying a square biphasic ±800mV of amplitude to each microelectrode, after a 6s baseline recording and after the application of a single stimulus in each of the electrodes independently. Figure 10 represents the average of the three Ca^{2+}

profiles obtained upon stimulation. To consult the profile of the Ca^{2+} signals observed in the three experiments please refer to Appendix C.

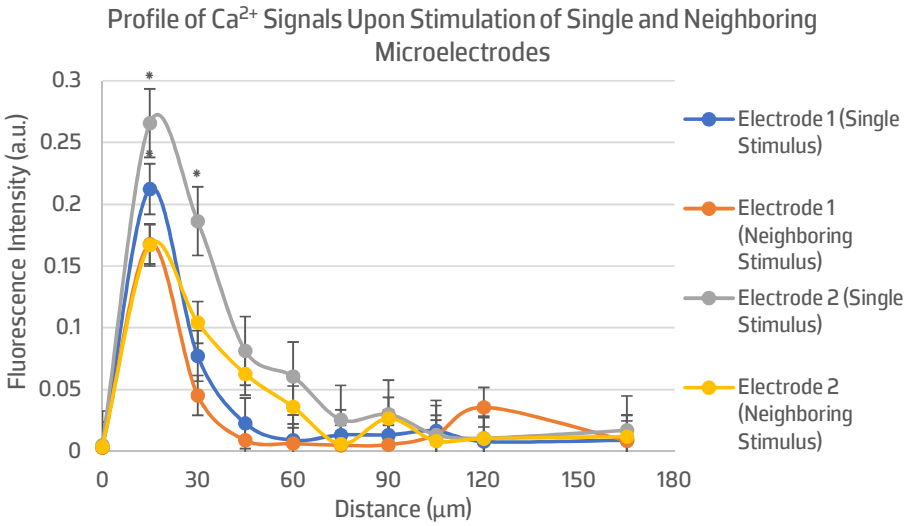

Figure 10 – Average Ca^{2+} signals' profiles from three different experiments, generated by the single and simultaneous stimulation of neighboring microelectrodes. The stimulation of two neighboring microelectrodes resulted in Ca^{2+} waves of similar amplitudes, however lower than the first and single stimulation performed on each microelectrode. * indicates $p \leq 0.05$.

Simultaneous stimulation of astrocytes located on neighboring microelectrodes lead to an increase in Ca^{2+} levels, but as seen in our previous results, only cells located around the microelectrode responded. Moreover, the second, simultaneous stimulus resulted in decreased Ca^{2+} wave amplitudes in astrocytes located around both stimulated microelectrodes when compared to the first, single stimulation, performed on the same microelectrodes.

3.4.3. Stimulation of Astrocytes with Stimuli of Different Amplitudes

Aiming at understanding the effect of the stimulus amplitude, different stimuli, of ±400mV, ±600mV and ±800m, were delivered independently to astrocytes, through a given microelectrode. Figure 11 represents the average amplitude of the Ca^{2+} signals of the five different stimulated microelectrodes. To see the profile of the Ca^{2+} signals observed in each microelectrode independently please refer to Appendix D.

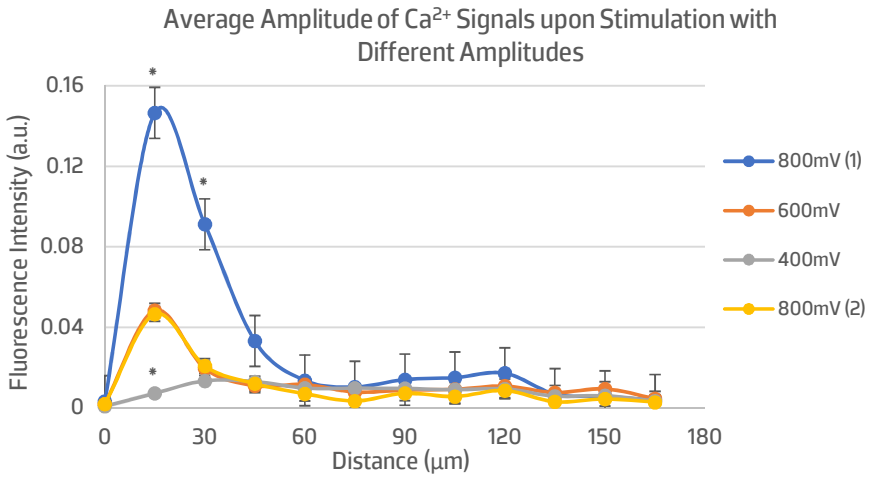

Figure 11 – Average profile of the Ca2+ waves resultant from stimuli with different amplitudes. Astrocytes did not respond to a ±400mV stimulus, yet they were able to respond to stimulus of ±800mV and ±600mV of amplitude; however, the first stimulus of ±800mV produced higher response amplitudes. * indicates p≤0.05.

As observed in figure 11, astrocytes stimulated with a ±800mV stimulus generated Ca^{2+}signals of higher amplitudes, when compared to stimulus of ±600mV of amplitude. However, it is worth noting that upon application of the first ±800mV stimulus, astrocytes displayed Ca^{2+} signals with a constantly higher amplitude than the second and last ±800mV stimulus. When stimulated with a ±400mV stimulus or below (data not shown), astrocytes did not present optically detectable Ca^{2+} signals in response to the stimulation.

Furthermore, by calculating the maximum intensity values of the images and plotting their average in function of the distance to the electrode, it is possible to gauge the travelled distance of Ca^{2+} signals. The fluorescence intensity reaches its peak within 15µm of distance from the microelectrode, in all tested amplitudes, decaying afterwards as the distance from the electrode increases. At 45µm of distance from the microelectrode, fluorescence levels are close to zero, indicating the absence of Ca^{2+} signals at and further from that distance to the microelectrode. Interestingly, when using a stimulus amplitude of ±600mV, it was observed that the travelled distance of Ca^{2+} signals was shorter, comparatively to a ±800mV stimulus. That said, signals are capable of reaching a distance of around 15µm with a ±600mV stimulus, whereas with a ±800mV stimulus signals are more likely to reach 30µm of distance.

3.4.4. Characterization of Astrocytic Ca^{2+} Signals

Ca^{2+} waves generated upon electrical stimulation were characterized by measuring their amplitudes, the rise and decay times and their mean velocity propagation.

3.4.4.1 Measurement of the Amplitude of Ca^{2+} Signals

The amplitude of Ca^{2+} signals was addressed by measuring the height of the maximum intensity fluorescence from five different microelectrodes upon application of a stimulus of either ±600mV or ±800mV of amplitude (figure 12).

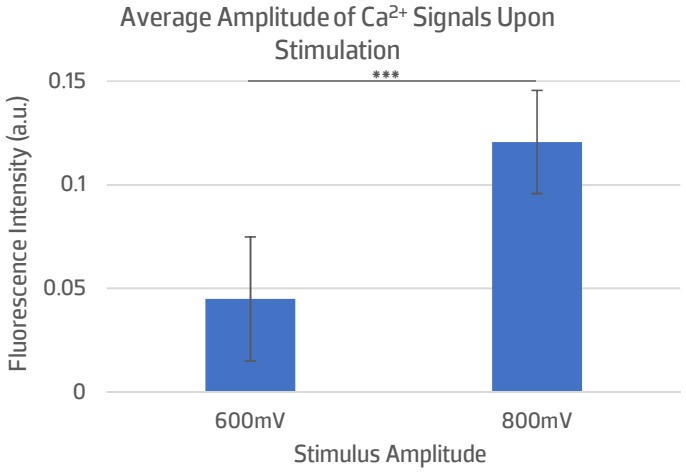

Figure 12 – Astrocytic response to different electrical stimuli. Stimulation of astrocytes with a ±800mV stimulus resulted in Ca^{2+} waves of higher amplitudes than stimulation with a ±600mV stimulus. *** indicates p≤0.001.

Stimulation of astrocytes with a ±600mV stimulus resulted in an average signal amplitude of 0,045±0,03a.u., whereas the application of a ±800mV stimulus resulted in a higher average Ca^{2+} signal amplitudes, of 0,121±0,025a.u.

3.4.4.2 Measurement of the Rise and Decay Times of Ca^{2+} Signals

Ca^{2+} signal kinetics were characterized as rise time, calculated from 20% to 80% of peak amplitude (T_{20-80}) and decay time, calculated from 80% to 20% of peak amplitude (T_{80-20}).

When stimulated with an amplitude of ±600mV, the T_{20-80} of astrocytic Ca^{2+} signals was of 1.65±0.53s, in contrast with a T_{20-80} of 2.71±1.46s when applied stimulus was of ±800mV (figure 13).

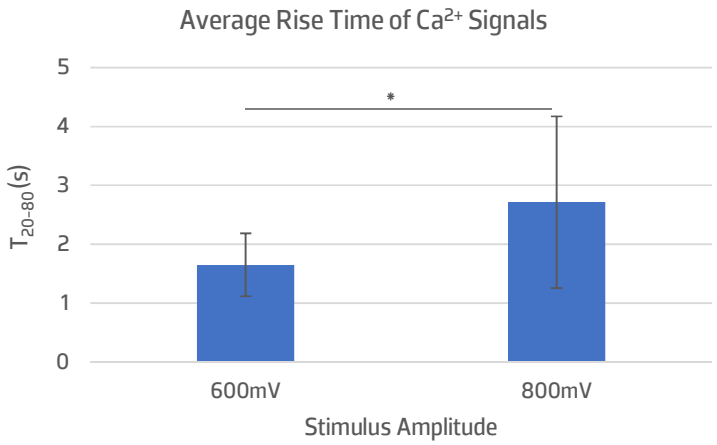

Figure 13 – Rise time of Ca^{2+} waves when stimulated with different amplitudes. Astrocytic Ca^{2+} waves showed an increased rise time (T_{20-80}) when stimulated with a ±800mV stimulus, when compared to the stimulation with a ±600mV stimulus. * indicates p≤0.05.

On the other hand, as for the T_{80-20} of Ca^{2+} signals it was not possible to obtain an accurate result, since the 20s of image acquisition were not enough for the signal to return to 20% of peak amplitude. This was the case for both ±600mV and ±800mV stimuli, where several ROIs could not be measured (table 1).

Table 1 – Decay time of Ca^{2+} waves when stimulated with both ±800mV and ±600mV stimulus.

Stimulus	ROI	Electrode				
		A6	B8	G11	B16	D12
600mV	1	5.4	5.1	-	5.8	7.3
	2	7	-	-	4	-
	3	-	4.5	-	4	-
	4	-	4.8	-	-	-
	5	2.9	4.7	-	-	7.4
Average		5.1	4.8	-	4.6	7.4
800mV	1	-	-	-	-	-
	2	-	-	-	-	-
	3	-	6.2	-	-	-
	4	-	7.6	-	-	-
	5	-	-	-	8.9	-
Average		-	6.9	-	8.9	-

Although it is not possible to precisely calculate the T_{80-20}, data presented in table 1 shows that Ca^{2+} signals resultant from a ±800mV stimulus tend to have a higher T_{80-20} when compared to a ±600mV stimulus, thus taking longer to recover to 20% amplitude peak.

3.4.4.3 Measurement of the Mean Velocity Propagation of Ca $^{2+}$ Waves

The mean propagation velocity of Ca^{2+} waves upon stimulation with both ±800mV and ±600mV was measured as a means for better characterizing Ca^{2+} waves. To do so, linear ROIs representative of the Ca^{2+} waves of five different videos were drawn, and the distance of the fluorescent signal was measured in six different frames. After plotting the results, the obtained regression line was computed in order to obtain the mean propagation velocity of Ca^{2+} waves, which are compared in figure 14.

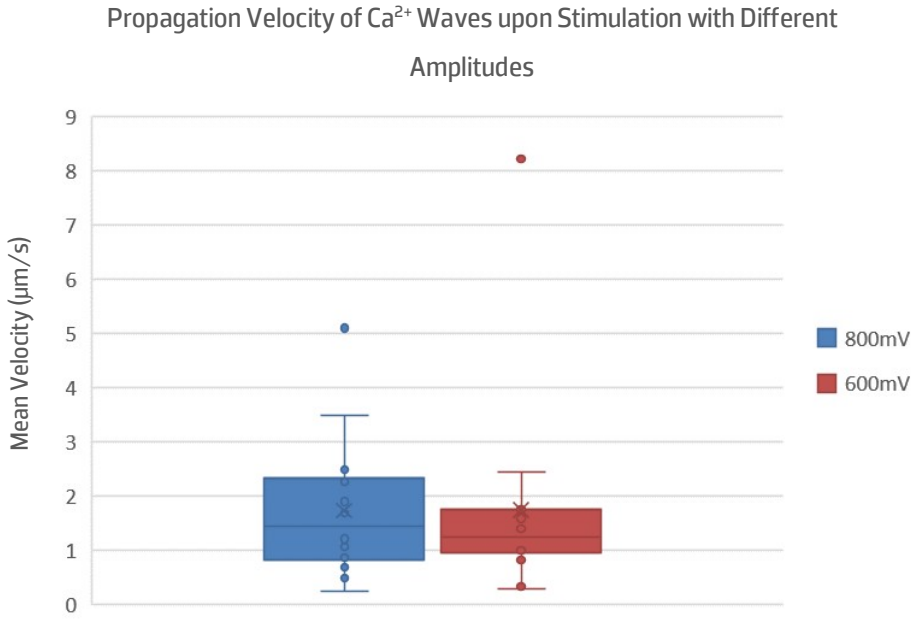

Figure 14 – Comparison of the mean propagation velocity of Ca $^{2+}$ waves after stimulation with both ±800mV and ±600mV. The distribution of the mean propagation velocity of five different experiments indicated that the stimulus with higher amplitude presented more variability, being able to reach slightly faster propagation velocities.

Figure 14 represents a comparison between the mean velocity propagation of Ca^{2+} waves resultant from the electrical stimulation with a ±800mV and ±600mV stimulus. It is possible to observe that although the average and median of mean velocities for both stimuli were not very different, the distribution of the values was slightly different. The average of the velocities was of approximately 1.73±1.31µm/s with a ±800mV stimulus and a 1.74±1.95µm/s with a ±600mV stimulus, whereas the obtained median values were of approximately 1.45µm/s in the ±800mV stimulus and of 1.24µm/s in the ±600mV stimulus.

However, a ±800mV stimulus resulted in a higher distance among values, ranging from 0.24µm/s to 3.5µm/s, than a ±600mV stimulus, with values situated between 0.29 and 2.5µm/s. Therefore, considering that the maximum values obtained were outliers, a ±800mV stimulus exhibit more variability between observations, being able to achieve slightly faster propagation velocities.

4. Discussion

The purpose of this work was to assess the effect of the modulation of the astrocytic electrophysiological microenvironment by Ca^{2+} imaging. For Ca^{2+} imaging, two organic dye Ca^{2+} indicators were used, CAL-520© AM and FLUOFORTE©. Final CAL-520© AM working concentration was optimized in the laboratory, being that several concentrations of this Ca^{2+} indicator dye have been used in the literature, ranging from 5μM(94) to 200μM(133,134). Nonetheless, it is recommended the use of the minimum concentration of dye as possible, in order to obtain an adequate signal while avoiding overloading artifacts and potential dye toxicity(100). After testing several conditions, incubation of astrocytes with 20μM of dye for 90 minutes at 37ºC plus 30 minutes at RT presented a significantly higher fluorescence intensity in comparison to all other conditions (figure 5), being selected for further Ca^{2+} imaging experiments. Overall, both Ca^{2+} indicators allowed the detection of small changes in Ca^{2+} levels while presenting a high SNR, being a good option for the study astrocytic Ca^{2+} activity.

In order to confirm if other cell types were present in isolated cultures, an immunocytochemistry with GFAP was performed, where the majority of cells in the field of view were found to express this astrocyte specific marker (figure 6)(52,82). Due to the character of the isolation and culture protocols, the amount of cells that did not present GFAP staining were unlikely to be neurons, since neurons do not survive long enough in the used astrocytic isolation protocol and culture medium. Later, astrocytes were chemically stimulated using ATP and Glutamate while performing Ca^{2+} imaging, with the purpose of confirming whether astrocytes were able to respond with Ca^{2+} elevations to external stimuli or not. As expected(39,48,49,135), an increase in the fluorescence upon addition of each neurotransmitter was detected, generating Ca^{2+} waves that propagated to neighboring astrocytes (figure 7), thus confirming that cultured astrocytes were responsive to stimulation. These two approaches were important to validate the isolated astrocytic cultures for further stimulation experiments.

Modulation of the astrocytic microenvironment was achieved by performing electrical stimulation of astrocytes cultured on ThinMEA© chips, suitable for imaging due to their reduced thickness, using the MEA2100 system© (MultiChannel© Systems). MEAs© are extracellular electrophysiology devices, which, contrarily to patch-clamp techniques, are non-invasive, maintaining cellular integrity and allowing their use in prolonged experiments(124). Nevertheless, despite their limitations, patch-clamp techniques have been widely used in the study of astrocytes, being responsible for the great majority of our knowledge on astrocytic electrophysiological properties. More recently, MEAs have been used for the electrophysiological recording of astrocytes. However, to our knowledge, only a few groups have successfully performed astrocytes' stimulation using MEAs, and just one has accomplished to monitor Ca^{2+} signals while stimulating mixed cultures of astrocytes and neurons.

Upon stimulation with a square biphasic stimulus of ±800mV, astrocytes displayed an increase in the Ca^{2+} signals in cells located immediately around the microelectrode, generating Ca^{2+} waves that then propagated to nearby astrocytes (figure 8). The stimulation protocol was based on Fleischer et al.(48), where they report the generation of Ca^{2+} dependent HFOs in astrocytes, triggered by VGCCs. However, by using Ca^{2+} imaging, and contrarily to what was reported by Bar El et al.(119), we did demonstrate the effect of the electrical stimulation in the increase of intracellular Ca^{2+} levels in astrocyte cultures; authors were only able to stimulate astrocytes in the presence of neurons, not obtaining any response when stimulating isolated astrocytic cultures(119). The increase in Ca^{2+} levels reported in this project is likely related to VGCCs: voltage causes channels to open, leading to the influx of Ca^{2+} ions in astrocytes, thus evoking Ca^{2+} signaling(35,39,48). VGCCs have been hypothesized to sensitize IP_3R for activation via CICR mechanism or by refilling luminal Ca^{2+} stores (41,71,136). Indeed, voltage-activated Ca^{2+} currents have been recorded in cultured astrocytes and the expression of numerous VGCCs has already been documented at a molecular level. Nevertheless, the presence of VGCCs in the living brain is still controversial, with few evidence for functional Ca^{2+} channels originating from in situ experiments.

In order to verify if astrocytes would respond to two independent but consecutive stimuli, a ±800mV was applied twice in the same microelectrode, with 10s of interval between stimuli. After the first stimulation, it was possible to observe an elevation in astrocytic Ca^{2+} levels, which soon stabilized until a new stimulus, 10s after, is delivered to astrocytes. Upon the second stimulation, astrocytic Ca^{2+} levels increase abruptly, indicating that astrocytes have the ability of responding independently to two consecutive stimulus, when separated by 10 seconds. Furthermore, since when the second stimulus was applied to astrocytes, Ca^{2+} signals were still not back to the baseline levels, it was observed a cumulative effect of Ca^{2+} levels.

ThinMEAs©' electrodes used on this experiment are separated by 200μm. Since we did not observe Ca^{2+} signals that could travel this distance, ideally ThinMEAs© with closer electrodes should be used, however they are not yet fabricated. Still, it was worthwhile to test if the co-activation of two neighboring microelectrodes would favor the activation of astrocytic cells that are enclosed by those electrodes, even though they were not activated by single microelectrode stimulation. However, our results suggest that there is no difference in the travelled distance of Ca^{2+} waves after stimulation, whether it is performed in a single microelectrode independently or simultaneously in two neighboring microelectrodes (figure 10).

Delivery of ±800mV, ±600mV and ±400mV stimuli was performed in order to determine if astrocytes responded with Ca^{2+} elevations of different amplitudes to diverse stimuli (figure 11). In all experiments, delivery of a ±400mV stimulus or below (data not shown) did not result in optically detectable Ca^{2+} signals. Moreover, it was observed that the first stimulus of ±800mV produced always Ca^{2+} signals with higher amplitudes, followed by the second ±800mV stimulus and then ±600mV

stimulus, which in two of the five experiments showed similar signal amplitudes. Noteworthy, the order by which the stimulation was performed was not always the same: although the first (to confirm if astrocytes were responsive to the stimulus) and last stimuli were always of ±800mV, the ±400mV and ±600mV stimuli were alternated. This allowed us to exclude the possibility of the differences in generated Ca^{2+} signals being related to the order by which the stimulation was performed, producing consistent results between experiments.

This was also observed when stimulating two neighboring microelectrodes, where the first stimulus, delivered in a given microelectrode originated higher Ca^{2+} signals' amplitudes, in average, than the second stimulus of the same amplitude; and when stimulating with two consecutive ±800mV stimuli, where the first, single stimulus produces a constantly increasing Ca^{2+} wave, whereas the second stimulus (2 times ±800mV with a 10s interval) showed a must faster decay after reaching the maximum amplitude.

It is unlikely that the decrease in the detectable fluorescence intensity between recordings is related to the photobleaching of the dye, since fluorescence values are normalized using the ΔF/F0 equation, resulting in a ratio comparing changes in fluorescence with the baseline fluorescence, thus eliminating factors like photobleaching of the dye(137). Normalization of fluorescence values is a very important step, since in this project the used Ca^{2+} indicator dyes were non-ratiometric, not allowing a quantitative analysis of the detected fluorescence(137). With this in mind, analysis of Ca^{2+} signals was qualitative, depending on the comparison of obtained ratios.

In this case, it is more likely that there is an astrocytic Ca^{2+} signalling mechanism involved in the generation of Ca^{2+} signals with lower amplitudes when stimulating twice with the same stimulus amplitude. Many conditionings are able to influence astrocytes' response to stimulation, namely the extracellular Ca^{2+} concentration. Notably, when studying HFOs, Fleischer et al. demonstrated that with lower extracellular Ca^{2+} concentrations some electrodes displayed longer oscillations, which were altered from stimulus to stimulus (with the same amplitude), thus indicating some kind of plasticity within the astrocyte layer that shapes the characteristics of responses(48). Therefore, there is a need for more experiments in order to better address this question and prove the existence of an astrocytic Ca^{2+} signaling mechanism underlying the generation of different amplitude responses to the same stimuli. Nevertheless, we can hypothesize that generated Ca^{2+} signals with different amplitudes in response to different stimuli (of ±600mV and ±800mV) is probably directly related to the amount, or a selectivity, of VGCCs that are activated upon stimulation(29,48). After activation, by sensitizing IP_3R via CICR mechanism(56), the detection and conversion of a local response above a given threshold is then turned into a propagating wave of local Ca^{2+} release events. We hypothesize that different stimulus thus originates different propagating waves or astrocytes respond differently to various electrical stimulus. Moreover, stimulation with ±400mV or below either does not activate VGCCs, or most likely does not reach the minimum threshold required for generating detectable Ca^{2+} waves or signals. The average travelled distance of Ca^{2+}

signals was also addressed relatively to the amplitude of the stimulus (figure 11). Ca^{2+} waves have been shown to be able to propagate within large distances, up to 400μm, when spontaneously generated or upon chemical stimulation(8,58). Our results, on the other hand, demonstrated that when astrocytes were electrically stimulated, Ca^{2+} elevations occurred mainly in astrocytes juxtaposed to the microelectrode, for both ±800mV and ±600mV stimulation amplitudes. However, the travelled distance of Ca^{2+} waves was in average higher upon delivery of the first ±800mV stimulus, propagating further (within around 30μm of distance from the microelectrode) than Ca^{2+} waves generated by 600mV stimulation (reaching a maximum distance of approximately 15μm). These results are in accordance with our previous results where higher Ca^{2+} waves' amplitudes were obtained when using a higher stimulus. Considering that an astrocyte's soma measures around 10μm to 20μm(8,9,52) and that we are mainly able to discern somas in our images, a ±800mV stimulus generates a Ca^{2+} wave that might have the ability of propagating intercellularly between two to three cells, whereas the Ca^{2+} wave generated by a ±600mV only has the ability of propagating intracellularly, or between two cells. Our results are in agreement with the results obtained by Fleischer et al., where they describe astrocytic HFOs restricted to the stimulation microelectrode, meaning that the signals do not have the ability of propagating to neighboring electrodes(48), which stand 200μm apart; however, they were not able to calculate the travelled distance of the signals. The authors verified that upon blockage of vesicular gliotransmission the oscillation power of HFOs was reduced to 75%, whereas the blockage of gap junctions and hemichannels with carbenoxolone lead to a reduction of the oscillation power to 63%(48). It is important to note that the specificity of carbenoxolone has been questioned (48,138), so we cannot completely exclude the possibility of gap junctions and hemichannels being involved in the generation of HFOs, and probably also in the propagation of Ca^{2+} waves. Propagation of Ca^{2+} waves is dependent on IP_3, which has to reach a minimum threshold concentration to trigger CICR events in neighboring cells by the diffusion through gap junctions(75). Whenever IP_3 does not reach the minimum threshold, propagation is ceased(75,139). PLCδ-mediated IP_3 production (75,140–142) has been proposed as a mechanism responsible for at least partial regeneration of IP_3 levels, inducing local concentrations large enough to trigger CICR(75,143). Therefore, the propagated distance of Ca^{2+} waves might be related to the concentration of IP_3,: a ±600mV stimulus might be sufficient to achieve the required concentration to induce CICR events in neighboring cells but soon ceases propagation, while a ±800mV stimulus is able to sustain the CICR mechanism for a longer period, probably due to a higher concentration of IP_3. Whether this is strictly related to the concentration of IP_3 or if the PLCδ-mediated IP_3 production(75) is activated in the ±800mV stimulus, it is not known.

Besides the intracellular fast IP_3 diffusion through gap junctions(55,56,75,144), vesicular release of gliotransmitters, namely ATP, have been shown to trigger metabotropic receptor-mediated Ca^{2+} release in neighboring cells regulating, in its turn, IP_3 (56,75,145,146), thus being relevant for the

propagation of Ca^{2+}. In this way, we can only hypothesize that both mechanisms might play a role in the propagation of Ca^{2+} signals; however, more experiments are needed to clarify this question.

To further investigate the properties of Ca^{2+} waves, a comparison between the amplitude (figure 12), the rise (figure 13) and decay times and the propagation velocity of Ca^{2+} signals (figure 14) upon stimulation with both ±800mV and ±600mV was done. Obtained data confirmed that, in average, the delivery of a stimulus of ±800mV of amplitude resulted in Ca^{2+} signals of higher amplitude when compared to a ±600mV stimulus. It was observed that the former took longer to reach its peak amplitude, tending to take even longer to decay back to the baseline level, most of the times not even reaching 20% of the peak amplitude during the whole recording (table 1).

When addressing the mean velocity of Ca^{2+} waves it was observed that although the average and median values obtained upon stimulation with both ±800mV and ±600mV stimulus amplitude were similar, the distribution of the mean velocities was slightly different. While the delivery of a ±800mV stimulus to astrocytes exhibited more variability among observations, it also had the ability of originating Ca+ waves that could propagate slightly faster than stimulating with a ±600mV stimulus.

Noteworthy, overall obtained velocities were lower than expected, ranging from 0.24μm/s to 3.5μm/s upon stimulation with a ±800mV stimulus, and ranging from 0.29 to 2.5μm/s upon stimulation with a ±600mV stimulus. It has been described that the fast propagation of persistent Ca^{2+} increases in the proximal region travelled at approximately 20μm/s(56,147), whereas the slow propagation of transient Ca^{2+} increases in the distal region was of approximately 13.9 μm/s(56,148). These values are related to the mechanisms involved in the propagation of Ca^{2+} signals, which is much faster when involving gap junctions, when compared to the propagation dependent on vesicular release of gliotransmitters. Our results, on the other hand, suggest the much slower propagation of Ca^{2+} waves, requiring further confirmation. However, it is important to note that the measured Ca^{2+} signals referred by Fujii et al. were not resultant of electrically stimulated astrocytes, but mechanically stimulated astrocytes(56,147). In fact, to our knowledge, the characterization of Ca^{2+} waves, with respect to their amplitude, rise and decay times and mean propagation velocity in electrically stimulated astrocytes has never been addressed before.

In summary, astrocytes are capable of sensing voltage alterations in their electrophysiological microenvironment, exhibiting characteristic Ca^{2+} activity in response to them. Stimulation with a higher stimulus amplitude (±800mV), resulted in Ca^{2+} waves of higher amplitudes as well, although taking longer to reach their peak amplitude and even longer to return to the baseline levels. Propagation of Ca^{2+} waves also takes longer, although they are able to reach longer distances than Ca^{2+} waves resultant from stimulation with a lower stimulus amplitude (±600mV). Taken together, data presented here constitutes piece of evidence that adds to the theory of astrocytes being electrically excitable cells.

5. Conclusion

Erstwhile neglected by many due to their inability of generating action potentials(3,149), astrocytes are involved in numerous physiological and pathological processes in the brain(52,82). Of those, the understanding that these glial cells are active partners in neuronal synapses(13,80,92) has been a game-changer for astrocytes, being increasingly studied since then. Today, it is known that astrocytes are capable of sensing and responding to the synaptic transmission, consequently modulating neuronal activity(19,85,150). Moreover, by increasing cytosolic Ca^{2+} levels astrocytes are able to generate intracellular Ca^{2+} waves, which may then propagate to neighboring astrocytes in the astrocytic syncytium(56). However, it is still not consensual whether astrocytes are electrically excitable cells, with various authors defending different points of view(14–18,151). For these reasons, comprehending the complex Ca^{2+} dynamics of astrocytes is not only a puzzling but necessary subject. Indeed, the development of Ca^{2+} imaging tools and new generation Ca^{2+} indicators allowed the study and understanding of many aspects of astrocytic Ca^{2+} activity, however there is still a lot left to unravel.

The main goal of this project was to assess the effect of the modulation of the electrophysiological microenvironment of astrocytes. To accomplish our goal, stimulation of primary astrocytes cultured on ThinMEA© chips was performed, while monitoring intracellular Ca^{2+} levels by Ca^{2+} imaging. These methodologies have revealed themselves as extremely useful in our quest for the understanding of astrocytic activity.

Using square biphasic stimuli of ±800mV(48) and ±600mV of amplitude, we were able to optically record the generation of Ca^{2+} waves in response to electrical stimulation. We also observed that: (1) the amplitude of the Ca^{2+} waves were higher when the stimulus of higher amplitude was applied; (2) stimuli of ±400mV or below did not generate detectable Ca^{2+} signals; (3) the response of astrocytes to the same stimulus applied twice was variable, being that the second stimulus always lead to the generation of Ca^{2+} waves of lower amplitudes than the first stimulus of the same amplitude; (4) stimulation with a higher stimulus amplitude generated Ca^{2+} waves that propagated further away from the microelectrode; (5) the rise time of Ca^{2+} waves was higher upon stimulation with a higher amplitude stimulus; (6) the velocity propagation of Ca^{2+} waves exhibited more variability with the application of the higher stimulus amplitude, being able to reach slightly higher propagation velocities. Taken our observations into account, we propose the following mechanism for the electrical stimulation of astrocytes: Ca^{2+} waves are most likely originated in the ER via sensitization of IP_3 and RyR by the increase in intracellular Ca^{2+} levels through VGCCs(29,48). We hypothesize that different stimuli originate different responses in astrocytes, probably due to a selectively of the ion channels or the amount of VGCCs the applied voltage is able to activate. Observed differences in the propagation distance and velocity of Ca^{2+} waves with respect to the amplitude of the stimulus might be related to the concentration of IP_3, which diffuses through gap junctions, or the

PLCδ-mediated IP_3 production mechanism, being more difficult for a lower amplitude stimulus to achieve the required concentration to induce CICR events in neighboring cells. However, it is known that vesicular gliotransmission release also play a role in the propagation of Ca^{2+} waves, and it also could be the case here.

Nevertheless, although data presented in this project is very premature and a lot more experiments are required to address all unanswered questions, our results are indeed promising and might shed a light into the electrophysiology of astrocytes as electrically excitable cells. Although stimulation amplitudes used here are not physiological, they are within the range of stimuli used for the stimulation of neuronal cultures using MEAs. Therefore, besides being able to sense the neuronal activity chemically, astrocytes might be able to sense it also electrically. However, further studies are needed to address this matter.

Moreover, since astrocytes are deeply involved in many pathologies, e.g. Alzheimer's disease, epilepsy or the generation of brain tumors, understanding exactly their role in the CNS is fundamental in order to give insights for future therapies, for instance using deep brain stimulation.

5.1. Future Perspectives

In order to better understand how calcium waves, generated by electrical stimulation of astrocytes, propagates through neighboring cells, inhibitors of gap junctions and gliotransmission should be used independently. These experiments might also shed some light on the propagation wave velocity, since the dynamics of the calcium propagation are different for both mechanisms (135,147).

When performing electrical stimulation of astrocytes, besides acquiring images from fluorescent Ca^{2+} signals, electrophysiological recordings were also acquired. The next step would be to analyze those recordings and correlate them with what has been observed from optical data described in this project. It would be extremely interesting if, as reported by Fleischer et al.(48), HFOs were detected in our astrocytic cultures.

The most propelling factor for the vision of astrocytes as a fundamental element in the CNS was the discovery of their role in shaping synaptic transmission(92). Since astrocytes are able to detect and respond to neuronal inputs, modulating their activity through Ca^{2+} signaling, it seems reasonable that our experiments should be repeated in a nearby future using astrocyte-neuron co-cultures. However, to investigate the astrocytic activity that might result specifically from neuronal electrical activity will be a challenging project, since electrical activity and neurotransmitter release are intimately connected in neurons(14).

Whatever comes next, one thing is certain: we should continue reaching for the stars… within.

References

1. Bassett DS, Gazzaniga MS. Understanding complexity in the human brain. Vol. 15, Trends in Cognitive Sciences. 2011. p. 200–9.
2. Verkhratsky A, Nedergaard M. Physiology of astroglia. Physiol Rev. 2018;98(1):239–389.
3. Fan X, Agid Y. At the Origin of the History of Glia. Neuroscience [Internet]. 2018;385:255–71. Available from: https://doi.org/10.1016/j.neuroscience.2018.05.050
4. Hubbard JA, Binder DK. History of Astrocytes [Internet]. Astrocytes and Epilepsy. 2016. 1–38 p. Available from: http://linkinghub.elsevier.com/retrieve/pii/B9780128024010000016
5. Baxter P. Astrocytes: more than just glue. Dev Med Child Neurol. 2012;291.
6. Vasile F, Dossi E, Rouach N. Human astrocytes: structure and functions in the healthy brain. Brain Struct Funct. 2017;222(5):2017–29.
7. Farmer WT, Murai K. Resolving astrocyte heterogeneity in the CNS. Front Cell Neurosci. 2017;11(September):1–7.
8. Verkhratsky A, Butt A. Glial Neurobiology: A Textbook. Glial Neurobiology: A Textbook. 2007. 1–215 p.
9. Hubbard JA, Binder DK, Hubbard JA, Binder DK. Chapter 2 – Astrocytes in the Mammalian Brain. Astrocytes and Epilepsy. 2016;39–51.
10. Tabata H. Diverse subtypes of astrocytes and their development during corticogenesis. Front Neurosci. 2015;9(APR):1–7.
11. Wu YW, Tang X, Arizono M, Bannai H, Shih PY, Dembitskaya Y, et al. Spatiotemporal calcium dynamics in single astrocytes and its modulation by neuronal activity. Cell Calcium [Internet]. 2014;55(2):119–29. Available from: http://dx.doi.org/10.1016/j.ceca.2013.12.006
12. Durkee CA, Araque A. Diversity and Specificity of Astrocyte–neuron Communication. Neuroscience. 2019;396:73–8.
13. Perea G, Navarrete M, Araque A. Tripartite Synapses: Astrocytes Process and Control Synaptic Information. Trends Neurosci. 2009;32(8):421–31.
14. Dallérac G, Chever O, Rouach N. How do astrocytes shape synaptic transmission? Insights from electrophysiology. Front Cell Neurosci [Internet]. 2013;7(October):1–19. Available from: http://journal.frontiersin.org/article/10.3389/fncel.2013.00159/abstract
15. Phillips CG. Intracelliular Records From Betz Cells In the Cat. Q J Exp Physiol Cogn Med Sci. 1956 Jan 22;41(1):58–69.
16. Sugaya E, Goldring S, O'Leary JL. Intracellular potentials associated with direct cortical response and seizure discharge in cat. Electroencephalogr Clin Neurophysiol. 1964;17(6):661–9.
17. Ransom BR, Goldring S. Slow hyperpolarization in cells presumed to be glia in cerebral cortex of cat. J Neurophysiol [Internet]. 1973 Sep [cited 2019 Sep 30];36(5):879–92. Available from: https://www.physiology.org/doi/10.1152/jn.1973.36.5.879

18. Karahashi Y, Goldring S. Intracellular potentials from "idle" cells in cerebral cortex of cat. Electroencephalogr Clin Neurophysiol. 1966;20(6):600–7.
19. Semyanov A. Spatiotemporal pattern of calcium activity in astrocytic network. Cell Calcium. 2019;78(December 2018):15–25.
20. Kang M, Othmer HG. Spatiotemporal characteristics of calcium dynamics in astrocytes. Chaos. 2009;19(3):1–21.
21. Shigetomi E, Patel S, Khakh BS. Probing the Complexities of Astrocyte Calcium Signaling. Trends Cell Biol [Internet]. 2016;26(4):300–12. Available from: http://dx.doi.org/10.1016/j.tcb.2016.01.003
22. Khakh BS, McCarthy KD. Astrocyte calcium signaling: From observations to functions and the challenges therein. Cold Spring Harb Perspect Biol. 2015;7(4):1–17.
23. Dossi E, Vasile F, Rouach N. Human astrocytes in the diseased brain. Brain Res Bull [Internet]. 2018;136:139–56. Available from: https://doi.org/10.1016/j.brainresbull.2017.02.001
24. Parpura V, Heneka MT, Montana V, Oliet SHR, Schousboe A, Haydon PG, et al. Glial cells in (patho)physiology. J Neurochem. 2012;121(1):4–27.
25. Li Q, Li QQ, Jia JN, Liu ZQ, Zhou HH, Mao XY. Targeting gap junction in epilepsy: Perspectives and challenges. Biomed Pharmacother. 2019;109(October 2018):57–65.
26. Patel DC, Tewari BP, Chaunsali L, Sontheimer H. Neuron–glia interactions in the pathophysiology of epilepsy. Nat Rev Neurosci [Internet]. 2019;20(5):282–97. Available from: http://dx.doi.org/10.1038/s41583-019-0126-4
27. Garwood CJ, Ratcliffe LE, Simpson JE, Heath PR, Ince PG, Wharton SB. Review: Astrocytes in Alzheimer's disease and other age-associated dementias: a supporting player with a central role. Neuropathol Appl Neurobiol. 2017;43(4):281–98.
28. Rodríguez-Arellano JJ, Parpura V, Zorec R, Verkhratsky A. Astrocytes in physiological aging and Alzheimer's disease. Neuroscience [Internet]. 2016;323(January):170–82. Available from: http://dx.doi.org/10.1016/j.neuroscience.2015.01.007
29. Sontheimer H. Voltage-dependent ion channels in glial cells. Glia. 1994;11(2):156–72.
30. Verma V. Innervation and membrane specialization at neuromuscular junctions in submaxillaris muscle of the frog. J Ultrasructure Res. 1984;87(2):136–48.
31. Kuffler SW, Nicholls JG. The physiology of neuroglial cells. Ergeb Physiol [Internet]. 1966 [cited 2019 Sep 30];57:1–90. Available from: http://www.ncbi.nlm.nih.gov/pubmed/5330861
32. Verkhratsky A, Steinhäuser C. Ion channels in glial cells. Vol. 32, Brain Research Reviews. 2000. p. 380–412.
33. Jones HC, Keep RF. The control of potassium concentration in the cerebrospinal fluid and brain interstitial fluid of developing rats. J Physiol [Internet]. 1987 Feb [cited 2019 Sep 30];383:441–53. Available from: http://www.ncbi.nlm.nih.gov/pubmed/3656129
34. Rose CR, Verkhratsky A. Principles of sodium homeostasis and sodium signalling in astroglia. Glia [Internet]. 2016 [cited 2019 Sep 30];64(10):1611–27. Available from:

http://www.ncbi.nlm.nih.gov/pubmed/26919326

35. Olsen ML, Khakh BS, Skatchkov SN, Zhou M, Lee CJ, Rouach N. New Insights on Astrocyte Ion Channels: Critical for Homeostasis and Neuron-Glia Signaling. J Neurosci [Internet]. 2015;35(41):13827–35. Available from: http://www.jneurosci.org/cgi/doi/10.1523/JNEUROSCI.2603-15.2015
36. Haydon PG, Nedergaard M. How do astrocytes participate in neural plasticity? Cold Spring Harb Perspect Biol. 2015;7(3):1–16.
37. Seifert G, Henneberger C, Steinhäuser C. Diversity of astrocyte potassium channels: An update. Brain Res Bull [Internet]. 2018;136:26–36. Available from: http://dx.doi.org/10.1016/j.brainresbull.2016.12.002
38. Alexander S, Mathie A, Peters J. Ion Channels. Br J Pharmacol. 2011;164(supplement s1):S137–74.
39. Ciappelloni S, Murphy-Royal C, Dupuis JP, Oliet SHR, Groc L. Dynamics of surface neurotransmitter receptors and transporters in glial cells: Single molecule insights. Cell Calcium [Internet]. 2017;67(July):46–52. Available from: http://dx.doi.org/10.1016/j.ceca.2017.08.009
40. Parpura V, Basarsky TA, Liu F, Jeftinija K, Jeftinija S, Haydon PG. Glutamate-mediated Astrocyte-Neuron Signalling. Nature. 1994;369:744–7.
41. Fiacco TA, McCarthy KD. Astrocyte calcium elevations: properties, propagation, and effects on brain signaling. Glia [Internet]. 2006 Nov 15 [cited 2019 Sep 30];54(7):676–90. Available from: http://www.ncbi.nlm.nih.gov/pubmed/17006896
42. Meier SD, Kafitz KW, Rose CR. Developmental profile and mechanisms of GABA-induced calcium signaling in hippocampal astrocytes. Glia [Internet]. 2008 Aug 1 [cited 2019 Sep 30];56(10):1127–37. Available from: http://www.ncbi.nlm.nih.gov/pubmed/18442094
43. Fraser D, Duffy S, Angelides K, Perez-Velazquez J, Kettenmann H, MacVicar B. GABAA/benzodiazepine receptors in acutely isolated hippocampal astrocytes. J Neurosci [Internet]. 1995 Apr 1 [cited 2019 Sep 30];15(4):2720–32. Available from: http://www.jneurosci.org/lookup/doi/10.1523/JNEUROSCI.15-04-02720.1995
44. Charles KJ, Calver AR, Jourdain S, Pangalos MN. Distribution of a GABAB-like receptor protein in the rat central nervous system. Brain Res. 2003 Nov 7;989(2):135–46.
45. Kang J, Jiang L, Goldman SA, Nedergaard M. Astrocyte-mediated potentiation of inhibitory synaptic transmission. Nat Neurosci. 1998;1(8):683–92.
46. Vélez-Fort M, Audinat E, Angulo MC. Central role of GABA in neuron–glia interactions. Neuroscientist [Internet]. 2012 Jun [cited 2019 Sep 30];18(3):237–50. Available from: http://www.ncbi.nlm.nih.gov/pubmed/21609943
47. O'Hare Doig RL, Bartlett CA, Smith NM, Hodgetts SI, Dunlop SA, Hool L, et al. Specific combinations of ion channel inhibitors reduce excessive Ca2+influx as a consequence of oxidative stress and increase neuronal and glial cell viability in vitro. Neuroscience [Internet]. 2016;339(October):450–62. Available from: http://dx.doi.org/10.1016/j.neuroscience.2016.10.005
48. Fleischer W, Theiss S, Slotta J, Holland C, Schnitzler A. High-frequency voltage oscillations in cultured

astrocytes. Physiol Rep. 2015;3(5):1–20.

49. Perea G. Properties of Synaptically Evoked Astrocyte Calcium Signal Reveal Synaptic Information Processing by Astrocytes. J Neurosci [Internet]. 2005;25(9):2192–203. Available from: http://www.jneurosci.org/cgi/doi/10.1523/JNEUROSCI.3965-04.2005
50. Morais TP, Coelho D, Vaz SH, Sebastião AM, Valente CA. Glycine Receptor Activation Impairs ATP-Induced Calcium Transients in Cultured Cortical Astrocytes. Front Mol Neurosci [Internet]. 2018;10(January):1–13. Available from: http://journal.frontiersin.org/article/10.3389/fnmol.2017.00444/full
51. Adermark L, Lovinger DM. Electrophysiological properties and gap junction coupling of striatal astrocytes. Neurochem Int. 2008 Jun;52(7):1365–72.
52. Verkhratsky A, Zorec R. Astroglial signalling in health and disease. Neurosci Lett [Internet]. 2018; Available from: https://doi.org/10.1016/j.neulet.2018.07.026
53. Retamal MA, Froger N, Palacios-Prado N, Ezan P, Sáez PJ, Sáez JC, et al. Cx43 hemichannels and gap junction channels in astrocytes are regulated oppositely by proinflammatory cytokines released from activated microglia. J Neurosci [Internet]. 2007 Dec 12 [cited 2019 Sep 30];27(50):13781–92. Available from: http://www.ncbi.nlm.nih.gov/pubmed/18077690
54. Contreras JE, SáezJuan C., Bukauskas FF, Bennett MVL. Gating and regulation of connexin 43 (Cx43) hemichannels. PNAS. 2003;
55. Giaume C, Venance L. Intercellular calcium signaling and gap junctional communication in astrocytes. Glia [Internet]. 1998 Sep [cited 2019 Sep 30];24(1):50–64. Available from: http://www.ncbi.nlm.nih.gov/pubmed/9700489
56. Fujii Y, Maekawa S, Morita M. Astrocyte calcium waves propagate proximally by gap junction and distally by extracellular diffusion of ATP released from volume-regulated anion channels. Sci Rep [Internet]. 2017;7(1):1–15. Available from: http://dx.doi.org/10.1038/s41598-017-13243-0
57. Borrachero-Conejo AI, Saracino E, Natali M, Prescimone F, Karges S, Bonetti S, et al. Electrical Stimulation by an Organic Transistor Architecture Induces Calcium Signaling in Nonexcitable Brain Cells. Adv Healthc Mater. 2019;8(3):1–12.
58. Zorec R, Araque A, Carmignoto G, Haydon PG, Verkhratsky A, Parpura V. Astroglial excitability and gliotransmission: An appraisal of Ca2+ as a signalling route. ASN Neuro. 2012;4(2):103–19.
59. Shigetomi E, Patel S, Khakh BS. Probing the complexities of astrocyte calcium imaging. Trends Cell Biol. 2016;26(4):300–12.
60. Chai H, Diaz-Castro B, Shigetomi E, Monte E, Octeau JC, Yu X, et al. Neural Circuit-Specialized Astrocytes: Transcriptomic, Proteomic, Morphological, and Functional Evidence. Neuron [Internet]. 2017;95(3):531-549.e9. Available from: http://dx.doi.org/10.1016/j.neuron.2017.06.029
61. Bezprozvanny I. The inositol 1,4,5-trisphosphate receptors. Cell Calcium [Internet]. [cited 2019 Sep 30];38(3–4):261–72. Available from: http://www.ncbi.nlm.nih.gov/pubmed/16102823
62. Brazhe AR, Postnov DE, Sosnovtseva O. Astrocyte calcium signaling: Interplay between structural and

dynamical patterns. Chaos. 2018;28(10).

63. Blaustein MP, Golovina VA. Structural complexity and functional diversity of endoplasmic reticulum Ca2+ stores. Trends Neurosci. 2001;24(10):602–8.

64. Verkhratsky A. Physiology and pathophysiology of the calcium store in the endoplasmic reticulum of neurons. Physiol Rev [Internet]. 2005 Jan [cited 2019 Sep 30];85(1):201–79. Available from: http://www.ncbi.nlm.nih.gov/pubmed/15618481

65. Berridge MJ, Bootman MD, Roderick HL. Calcium signalling: Dynamics, homeostasis and remodelling. Nat Rev Mol Cell Biol. 2003;4(7):517–29.

66. Srinivasan R, Huang BS, Venugopal S, Johnston AD, Chai H. Calcium signalling in astrocytes from IP3R2-/- mice in brain slices and during startle responses in vivo. Nat Neurosci. 2015;18(5):708–17.

67. Rungta RL, Bernier LP, Dissing-Olesen L, Groten CJ, LeDue JM, Ko R, et al. Ca2+ transients in astrocyte fine processes occur via Ca2+ influx in the adult mouse hippocampus. Glia. 2016;64(12):2093–103.

68. Otsu Y, Couchman K, Lyons DG, Collot M, Agarwal A, Mallet J-M, et al. Calcium dynamics in astrocyte processes during neurovascular coupling. Nat Neurosci [Internet]. 2015 Feb [cited 2019 Sep 30];18(2):210–8. Available from: http://www.ncbi.nlm.nih.gov/pubmed/25531572

69. Agarwal A, Wu PH, Hughes EG, Fukaya M, Tischfield MA, Langseth AJ, et al. Transient Opening of the Mitochondrial Permeability Transition Pore Induces Microdomain Calcium Transients in Astrocyte Processes. Neuron [Internet]. 2017;93(3):587-605.e7. Available from: http://dx.doi.org/10.1016/j.neuron.2016.12.034

70. MacVicar BA, Ko RWY. Mitochondrial Calcium Sparkles Light Up Astrocytes. Dev Cell. 2017;40(4):327–8.

71. Okubo Y, Kanemaru K, Suzuki J, Kobayashi K, Hirose K, Iino M. Inositol 1,4,5-trisphosphate receptor type 2-independent Ca 2+ release from the endoplasmic reticulum in astrocytes. Glia. 2019;67(1):113–24.

72. MacVicar BA, Ko RWY. Mitochondrial Calcium Sparkles Light Up Astrocytes. Dev Cell Previews. 2017;

73. Verkhratsky A, Parpura V. Store-operated calcium entry in neuroglia. Neurosci Bull. 2014;30(1):125–33.

74. Parpura V, Zorec R. Gliotransmission: Exocytotic release from astrocytes. Vol. 63, Brain Research Reviews. 2010. p. 83–92.

75. Goldberg M, de Pittà M, Volman V, Berry H, Ben-Jacob E. Nonlinear gap junctions enable long-distance propagation of pulsating calcium waves in astrocyte networks. PLoS Comput Biol. 2010;6(8).

76. Ashhad S, Narayanan R. Stores, Channels, Glue, and Trees: Active Glial and Active Dendritic Physiology. Mol Neurobiol. 2018;1–22.

77. Langer J, Stephan J, Theis M, Rose CR. Gap junctions mediate intercellular spread of sodium between hippocampal astrocytes in situ. Glia. 2012;60(2):239–52.

78. Harada K, Kamiya T, Tsuboi T. Gliotransmitter release from astrocytes: Functional, developmental, and pathological implications in the brain. Front Neurosci. 2016;9(JAN):1–9.

79. Papouin T, Dunphy J, Tolman M, Foley JC, Haydon PG. Astrocytic control of synaptic function. Philos Trans R Soc B Biol Sci. 2017;372(1715).
80. Hussaini SMQ, Jang MH. New roles for old glue: Astrocyte function in synaptic plasticity and neurological disorders. Int Neurourol J. 2018;22:S106–14.
81. Plata A, Lebedeva A, Denisov P, Nosova O, Postnikova TY, Pimashkin A, et al. Astrocytic Atrophy Following Status Epilepticus Parallels Reduced Ca2+ Activity and Impaired Synaptic Plasticity in the Rat Hippocampus. Front Mol Neurosci [Internet]. 2018;11(June):1–17. Available from: https://www.frontiersin.org/article/10.3389/fnmol.2018.00215/full
82. Garwood CJ, Ratcliffe LE, Simpson JE, Heath PR, Ince PG, Wharton SB. Review: Astrocytes in Alzheimer's disease and other age-associated dementias: a supporting player with a central role. Neuropathol Appl Neurobiol. 2017;43(4):281–98.
83. Bezzi P, Volterra A. A Neuron-glia Signalling Network in the Active Brain. Curr Opin Neurobiol. 2001;11(3):387–94.
84. Farhy-Tselnicker I, Allen NJ. Astrocytes, neurons, synapses: A tripartite view on cortical circuit development. Neural Dev. 2018;13(1):1–12.
85. Nadkarni S, Jung P, Levine H. Astrocytes Optimize the Synaptic Transmission of Information. PLoS Comput Biol. 2008;4(5).
86. Porto-Pazos AB, Veiguela N, Mesejo P, Navarrete M, Alvarellos A, Ibáñez O, et al. Artificial Astrocytes Improve Neural Network Performance. PLoS One. 2011;6(4):1–8.
87. Amiri M, Hosseinmardi N, Bahrami F, Janahmadi M. Astrocyte-neuron Interaction as a Mechanism Responsible for Generation of Neural Synchrony: a Study based on Modeling and Experiments. J Comput Neurosci. 2013;34(3):489–504.
88. Wade JJ, McDaid LJ, Harkin J, Crunelli V, Kelso JAS. Bidirectional Coupling between Astrocytes and Neurons Mediates Learning and Dynamic Coordination in the Brain: A Multiple Modeling Approach. PLoS One. 2011;6(12):1–24.
89. Nedegaard M. Direct Signaling from Astrocytes to Neurons in Cultures of Mammalian Brain Cells. Science (80-). 1994;263:1768–71.
90. Zur Nieden R, Deitmer JW. The role of metabotropic glutamate receptors for the generation of calcium oscillations in rat hippocampal astrocytes in situ. Cereb Cortex. 2006;16(5):676–87.
91. De Bock M, Decrock E, Wang N, Bol M, Vinken M, Bultynck G, et al. The dual face of connexin-based astroglial Ca2+ communication: A key player in brain physiology and a prime target in pathology. Biochim Biophys Acta - Mol Cell Res [Internet]. 2014;1843(10):2211–32. Available from: http://dx.doi.org/10.1016/j.bbamcr.2014.04.016
92. Halassa MM, Fellin T, Haydon PG. The Tripartite Synapse: Roles for Gliotransmission in Health and Disease. Trends Mol Med. 2007;13(2):54–63.
93. Hubbard JA, Binder DK. Gliotransmitters. Astrocytes and Epilepsy [Internet]. 2016;(1):53–73. Available from: https://linkinghub.elsevier.com/retrieve/pii/B978012802401000003X

94. Lock JT, Parker I, Smith IF. A comparison of fluorescent Ca2+indicators for imaging local Ca2+signals in cultured cells. Cell Calcium [Internet]. 2015;58(6):638–48. Available from: http://dx.doi.org/10.1016/j.ceca.2015.10.003
95. Losi G, Mariotti L, Sessolo M, Carmignoto G. New Tools to Study Astrocyte Ca2+ Signal Dynamics in Brain Networks In Vivo. Front Cell Neurosci [Internet]. 2017;11(May):1–7. Available from: http://journal.frontiersin.org/article/10.3389/fncel.2017.00134/full
96. van Lith R, Ameer GA. Antioxidant Polymers as Biomaterial. In: Oxidative Stress and Biomaterials. Elsevier; 2016. p. 251–96.
97. Photometrics. Non-Ratiometric Ca 2+ Indicator Dyes. :1–6. Available from: https://www.photometrics.com/applications/pdfs/Calcium-Imaging-AppNote.pdf
98. AAT Bioquest. Cal-520®, AM [Internet]. 2019 [cited 2019 Sep 21]. Available from: https://www.aatbio.com/products/cal-520-am
99. AAT Bioquest. Novel improved Ca2+ indicator dyes on the market-a comparative study of novel Ca2+ indicators with fluo-4 | AAT Bioquest [Internet]. 2019 [cited 2019 Sep 1]. Available from: https://www.aatbio.com/blog/1496965686/novel_improved_ca2_indicator_dyes_on_the_market_a_comparative_study_of_novel_ca2_indicators_with_fluo_4
100. AAT Bioquest. What's A Ratiometric Indicator [Internet]. 2019 [cited 2019 Sep 21]. Available from: https://www.aatbio.com/blog/1507935186/whats_a_ratiometric_indicator
101. LifeSciences E. CELLestial Dyes & Kits [Internet]. 2019 [cited 2019 Sep 1]. Available from: http://www.axxora.com/support/dyes-cellular-analysis/cellestial-dyes-kits-faqs/
102. Tian L, Andrew Hires S, Looger LL. Imaging neuronal activity with genetically encoded calcium indicators. Cold Spring Harb Protoc. 2012;7(6):647–56.
103. Nave KA, Winchenbach J, Düking T, Berghoff SA, Stumpf SK, Hülsmann S, et al. Inducible targeting of CNS astrocytes in Aldh1l1-CreERT2 BAC transgenic mice. F1000Research. 2016;5(1):1–14.
104. Shulyatnikova T, Verkhratsky A. Astroglia in Sepsis Associated Encephalopathy. Neurochem Res [Internet]. 2019;0(0):0. Available from: http://dx.doi.org/10.1007/s11064-019-02743-2
105. Srinivasan R, Lu T-Y, Chai H, Xu J, Huang BS, Golshani P, et al. New Transgenic Mouse Lines for Selectively Targeting Astrocytes and Studying Calcium Signals in Astrocyte Processes In Situ and In Vivo. Neuron [Internet]. 2016 Dec 21 [cited 2019 Sep 30];92(6):1181–95. Available from: http://www.ncbi.nlm.nih.gov/pubmed/27939582
106. Chen TW, Wardill TJ, Sun Y, Pulver SR, Renninger SL, Baohan A, et al. Ultrasensitive fluorescent proteins for imaging neuronal activity. Nature. 2013;499(7458):295–300.
107. Wang Y, Shi G, Miller DJ, Wang Y, Wang C, Broussard G, et al. Automated Functional Analysis of Astrocytes from Chronic Time-Lapse Calcium Imaging Data. Front Neuroinform [Internet]. 2017;11(July). Available from: http://journal.frontiersin.org/article/10.3389/fninf.2017.00048/full
108. Russell JT. Imaging calcium signals in vivo: A powerful tool in physiology and pharmacology. Br J Pharmacol. 2011;163(8):1605–25.

109. Savtchouk I, Carriero G, Volterra A. Studying Axon-Astrocyte Functional Interactions by 3D Two-Photon Ca2+ Imaging: A Practical Guide to Experiments and "Big Data" Analysis. Front Cell Neurosci [Internet]. 2018;12(April):1–14. Available from: http://journal.frontiersin.org/article/10.3389/fncel.2018.00098/full

110. Romano SA, Pérez-schuster V, Jouary A, Boulanger-Weill J, Candeo A, Pietri T, et al. An integrated calcium imaging processing toolbox for the analysis of neuronal population dynamics. PLoS Comput Biol. 2017;

111. Romano SA, Pérez-schuster V, Jouary A, Candeo A. A computational toolbox and step-by-step tutorial for the analysis of neuronal population dynamics in calcium imaging data. PLoS Comput Biol. 2017;

112. Lu J, Li C, Singh-alvarado J, Zhou ZC, Fro F, Mooney R, et al. MIN1PIPE : A Miniscope 1-Photon-Based Calcium Resource MIN1PIPE : A Miniscope 1-Photon-Based Calcium Imaging Signal Extraction Pipeline. 2018;3673–84.

113. Shen SP, Tseng H, Hansen KR, Wu R, Gritton HJ, Si J. Automatic Cell Segmentation by Adaptive Thresholding (ACSAT) for Large-Scale Calcium Imaging Datasets. 2018;5(October):1–15.

114. Clark JH, Engineering B, Ca S. Automated analysis of cellular signals from large-scale calcium imaging data. Neuron. 2012;63(6):747–60.

115. Giovannucci A, Friedrich J, Gunn P, Kalfon J, Koay A, Taxidis J, et al. CaImAn : An open source tool for scalable Calcium Imaging data Analysis. 2018;1–40.

116. Artimovich E, Jackson RK, Kilander MBC, Lin YC, Nestor MW. PeakCaller : an automated graphical interface for the quantification of intracellular calcium obtained by high - content screening. BMC Neurosci. 2017;1–15.

117. Mestre ALG, Inácio PMC, Elamine Y, Asgarifar S, Lourenço AS, Cristiano MLS, et al. Extracellular Electrophysiological Measurements of Cooperative Signals in Astrocytes Populations. Front Neural Circuits [Internet]. 2017;11(October):1–9. Available from: http://journal.frontiersin.org/article/10.3389/fncir.2017.00080/full

118. Spira ME, Hai A. Multi-electrode array technologies for neuroscience and cardiology. Nat Nanotechnol [Internet]. 2013;8(2):83–94. Available from: http://dx.doi.org/10.1038/nnano.2012.265

119. El YB, Kanner S, Barzilai A, Hanein Y. Activity changes in neuron-Astrocyte networks in culture under the effect of norepinephrine. PLoS One. 2018;13(10):1–20.

120. Henneberger C, Rusakov DA. Monitoring local synaptic activity with astrocytic patch pipettes. Nat Protoc. 2012;7(12):2171–9.

121. Sakmann B, Neher E. Patch Clamp Techniques for Studying Ionic Channels in Excitable Membranes. Annu Rev Physiol [Internet]. 1984 Oct [cited 2019 Sep 30];46(1):455–72. Available from: http://www.annualreviews.org/doi/10.1146/annurev.ph.46.030184.002323

122. Hai A, Shappir J, Spira ME. Long-term, multisite, parallel, in-cell recording and stimulation by an array of extracellular microelectrodes. J Neurophysiol. 2010;104(1):559–68.

123. Unsworth CP, Delivopoulos E, Gillespie T, Murray AF. Isolating single primary rat hippocampal neurons

and astrocytes on ultra-thin patterned parylene-C/silicon dioxide substrates. Biomaterials [Internet]. 2011;32(10):2566–74. Available from: http://dx.doi.org/10.1016/j.biomaterials.2010.12.017

124. Ness T V., Chintaluri C, Potworowski J, Łęski S, Głąbska H, Wójcik DK, et al. Modelling and Analysis of Electrical Potentials Recorded in Microelectrode Arrays (MEAs). Neuroinformatics. 2015;13(4):403–26.

125. Mestre ALG, Cerquido M, Inácio PMC, Asgarifar S, Lourenço AS, Cristiano MLS, et al. Ultrasensitive gold micro-structured electrodes enabling the detection of extra-cellular long-lasting potentials in astrocytes populations. Sci Rep. 2017;7(1):1–11.

126. Geissler M, Faissner A. A new indirect co-culture set up of mouse hippocampal neurons and cortical astrocytes on microelectrode arrays. J Neurosci Methods [Internet]. 2012;204(2):262–72. Available from: http://dx.doi.org/10.1016/j.jneumeth.2011.11.030

127. Rocha PRF, Medeiros MCR, Kintzel U, Vogt J, Araújo IM, Mestre ALG, et al. Extracellular electrical recording of pH-triggered bursts in C6 glioma cell populations. Sci Adv. 2016;2(12):1–8.

128. Medeiros MCR, Mestre A, Inácio P, Asgarif S, Araújo IM, Hubbard PC, et al. An electrical method to measure low-frequency collective and synchronized cell activity using extracellular electrodes. Sens Bio-Sensing Res [Internet]. 2016;10:1–8. Available from: https://doi.org/10.1016/j.sbsr.2016.06.002

129. Kuga N, Sasaki T, Takahara Y, Matsuki N, Ikegaya Y. Large-Scale Calcium Waves Traveling through Astrocytic Networks In Vivo. J Neurosci [Internet]. 2011;31(7):2607–14. Available from: http://www.jneurosci.org/cgi/doi/10.1523/JNEUROSCI.5319-10.2011

130. Schildge S, Bohrer C, Beck K, Schachtrup C. Isolation and Culture of Mouse Cortical Astrocytes. J Vis Exp [Internet]. 2013;(71):1–7. Available from: http://www.jove.com/video/50079/isolation-and-culture-of-mouse-cortical-astrocytes

131. BASF. Kolliphor® P 407 [Internet]. 2019 [cited 2019 Aug 18]. Available from: https://pharmaceutical.basf.com/en/Drug-Formulation/Kolliphor-P407.html

132. Hatton G, Parpua V. Glial ⇔ Neuronal Signaling [Internet]. 2004 [cited 2019 Aug 15]. p. 387–8. Available from: https://books.google.pt/books?id=FmvjBwAAQBAJ&pg=PA388&lpg=PA388&dq=glutamate+100um+astrocytes&source=bl&ots=OriBfYJ7AY&sig=ACfU3U3dmUoceYhIBAdwdowpdrU61w2kOg&hl=pt-PT&sa=X&ved=2ahUKEwiBgYH-lfjkAhVH1hoKHZzmDIwQ6AEwBnoECAkQAQ#v=onepage&q=glutamate%2520100um%25

133. Tsutsumi S, Yamazaki M, Miyazaki T, Watanabe M, Sakimura K, Kano M, et al. Structure–function relationships between aldolase C/Zebrin II expression and complex spike synchrony in the cerebellum. J Neurosci. 2015 Jan 14;35(2):843–52.

134. Tada M, Takeuchi A, Hashizume M, Kitamura K, Kano M. A highly sensitive fluorescent indicator dye for calcium imaging of neural activity in vitro and in vivo. Eur J Neurosci. 2014;39(11):1720–8.

135. Fujii Y, Maekawa S, Morita M. Astrocyte calcium waves propagate proximally by gap junction and distally by extracellular diffusion of ATP released from volume-regulated anion channels. Sci Rep

[Internet]. 2017;7(1):1–15. Available from: http://dx.doi.org/10.1038/s41598-017-13243-0

136. Pirttimaki TM, Sims RE, Saunders G, Antonio SA, Codadu NK, Parri HR. Astrocyte mediated neuronal synchronisation properties revealed by false gliotransmitter release. J Neurosci [Internet]. 2017;37(41):2761–16. Available from: http://www.jneurosci.org/lookup/doi/10.1523/JNEUROSCI.2761-16.2017
137. Macleod GT. Imaging and analysis of nonratiometric calcium indicators at the Drosophila larval neuromuscular junction. Cold Spring Harb Protoc [Internet]. 2012 Jul 1 [cited 2019 Sep 30];2012(7):802–9. Available from: http://www.ncbi.nlm.nih.gov/pubmed/22753596
138. Beaumont M, Maccaferri G. Is connexin36 critical for GABAergic hypersynchronization in the hippocampus? J Physiol. 2011 Apr;589(7):1663–80.
139. Venance L, Stella N, Glowinski J, Giaume C. Mechanism involved in initiation and propagation of receptor-induced intercellular calcium signaling in cultured rat astrocytes. J Neurosci [Internet]. 1997 Mar 15 [cited 2019 Sep 30];17(6):1981–92. Available from: http://www.ncbi.nlm.nih.gov/pubmed/9045727
140. Sneyd J, Wetton BT, Charles AC, Sanderson MJ. Intercellular calcium waves mediated by diffusion of inositol trisphosphate: a two-dimensional model. Am J Physiol [Internet]. 1995 Jun [cited 2019 Sep 30];268(6 Pt 1):C1537-45. Available from: http://www.ncbi.nlm.nih.gov/pubmed/7611375
141. Harootunian AT, Kao JP, Paranjape S, Tsien RY. Generation of calcium oscillations in fibroblasts by positive feedback between calcium and IP3. Science [Internet]. 1991 Jan 4 [cited 2019 Sep 30];251(4989):75–8. Available from: http://www.ncbi.nlm.nih.gov/pubmed/1986413
142. Höfer T, Venance L, Giaume C. Control and plasticity of intercellular calcium waves in astrocytes: a modeling approach. J Neurosci [Internet]. 2002 Jun 15 [cited 2019 Sep 30];22(12):4850–9. Available from: http://www.ncbi.nlm.nih.gov/pubmed/12077182
143. Falcke M. Reading the patterns in living cells —the physics of ca2+ signaling. Adv Phys. 2004;53(3):255–440.
144. Kettenmann H, Schipke CG. Calcium signaling in glia. In: Glial ⇔ Neuronal Signaling. Springer US; 2004. p. 297–321.
145. Newman EA, Zahs KR. Calcium waves in retinal glial cells. Science [Internet]. 1997 Feb 7 [cited 2019 Sep 30];275(5301):844–7. Available from: http://www.ncbi.nlm.nih.gov/pubmed/9012354
146. Guthrie PB, Knappenberger J, Segal M, Bennett M V, Charles AC, Kater SB. ATP released from astrocytes mediates glial calcium waves. J Neurosci [Internet]. 1999 Jan 15 [cited 2019 Sep 30];19(2):520–8. Available from: http://www.ncbi.nlm.nih.gov/pubmed/9880572
147. Charles AC, Merrill JE, Dirksen ER, Sanderson MJ. Intercellular signaling in glial cells: calcium waves and oscillations in response to mechanical stimulation and glutamate. Neuron [Internet]. 1991 Jun [cited 2019 Sep 30];6(6):983–92. Available from: http://www.ncbi.nlm.nih.gov/pubmed/1675864
148. Wang Z, Tymianski M, Jones OT, Nedergaard M. Impact of cytoplasmic calcium buffering on the spatial and temporal characteristics of intercellular calcium signals in astrocytes. J Neurosci [Internet]. 1997

Oct 1 [cited 2019 Sep 30];17(19):7359–71. Available from: http://www.ncbi.nlm.nih.gov/pubmed/9295382

149. Robertson JM. The gliocentric brain. Int J Mol Sci. 2018;19(10).

150. Perea G, Sur M, Araque A. Neuron-glia networks: integral gear of brain function. Front Cell Neurosci [Internet]. 2014;8(November):1–8. Available from: http://journal.frontiersin.org/article/10.3389/fncel.2014.00378/abstract

151. Castellucci VF, Goldring S. Contribution to steady potential shifts of slow depolarization in cells presumed to be glia. Electroencephalogr Clin Neurophysiol. 1970;28(2):109–18.

Appendix

Appendix A

The custom-written Fiji/ImageJ macro for the preprocessment of images and the assessment of Ca^{2+} wave amplitude and rise and decay times is presented here.

```
//Pre-Processment
image_Orig = getTitle();
//Select Image
run("Duplicate...", "duplicate range=1-2000");
imageT_F = getTitle();
selectWindow(imageT_F);

//Filtering
run("Median...", "radius=1 stack");
imageT_F_Filtered = getTitle();

//Duplicate Image
run("Duplicate...", "duplicate range=1-300");
imageT_F_Filtered_Dup = getTitle();

//Calculate F0
selectWindow(imageT_F_Filtered_Dup);
run("Z Project...", "projection=Median");
imageT_F0 = getTitle();

//Calculate F - F0
imageCalculator("Subtract create 32-bit stack", imageT_F_Filtered, imageT_F0);
imageT_F_minus_F0 = getTitle();

//Calculate (F - F0)/F0
imageCalculator("Divide create 32-bit stack", imageT_F_minus_F0, imageT_F0);
imageT_DF_over_F0 = getTitle();
waitForUser("Observe DFoF0", "Click ok when done")
selectWindow(imageT_DF_over_F0);
```

```
//Close Images
close(imageT_F0)
close(imageT_F_minus_F0)
close(imageT_F_Filtered)
close(imageT_F_Filtered_Dup)

//Median Intensity Projection
run("Z Project...", "projection=Median");
image_MedianDFoF0 = getTitle();

//Maximum Intensity Projection of Normalized Image
selectWindow(imageT_DF_over_F0);
run("Z Project...", "projection=[Max Intensity]");

//Calibrate Image
run("Set Scale...", "distance=1 known=0.4996 pixel=1 unit=µm");


//Calculate Aamplitude and Time20-80 and Time80-20

nr_ROIs = getNumber("Please insert number of ROIs", 5);

//path = getDirectory(image_Orig);
dir = getDirectory("Choose a Directory for SAVING");
for (counter = 1; counter <= nr_ROIs; counter++) {

        selectWindow(image_MedianDFoF0);
        setTool("oval");
        makeOval(224, 214, 10, 10);
        waitForUser("ROI Definition", "Please place ROI and click OK.");
        roiManager("Add");
        roiManager("Select", counter-1);
        roiManager("Rename", "ROI "+counter);
        roiManager("Show All with labels");
```

```
        selectWindow(imageT_DF_over_F0);
        run("Restore Selection");
        run("Plot Z-axis Profile");
        Plot_ZProfile = getTitle()
        Title = counter;

        saveAs("Results", "C:/Users/sccs_/Desktop/1.csv");

        setTool("rectangle");
        waitForUser("Amplitude", "Please draw rectangule selecting the maximum and baseline
of the wave and click OK.");
        run("Set Measurements...", "bounding redirect=None decimal=3");
        run("Measure");
        run("Colors...", "foreground=blue background=black selection=blue");
        run("Draw", "slice");
        run("16_colors");
        saveAs("TIFF");
        close();
        selectWindow("Plot Values")
        saveAS("CSV");
    }
```

Appendix B

The custom-written Fiji/ImageJ macro for the semi-automated definition of radial ROIs, used in the detection of different astrocytic responses to different stimuli and inferring the travelled distance of Ca^{2+} waves is presented here.

```
// Radial ROIs
//Duplicate Image
run("Duplicate...");
image_Med_Dup = getTitle();
selectWindow(image_Med_Dup);

//Definition of Radius and number of ROIs
inc_radius = getNumber("Please insert ROI radius", 30);

nr_circles = getNumber("Please insert ROI number", 12);

//Convert Scale to Pixels
run("Set Scale...", "distance=1 known=1 pixel=1 unit=pixel");

toScaled(inc_radius);

//Definition of Electrode
setTool("oval");
waitForUser("ROI Definition", "Please draw ROI and click OK.");

//Electrode's Coordinates
run("Set Measurements...", "centroid bounding redirect=None decimal=3");
run("Measure");
xc = getResult("BX", nResults-1);
yc = getResult("BY", nResults-1);
diameter = getResult("Width", nResults-1);
run("Close");

//ROI Definition
```

```
for (counter = 0; counter < nr_circles; counter++) {
                        if (counter == 0) {
                                makeOval(xc, yc, diameter, diameter);
                                roiManager("Add");
                                roiManager("Select", 0);
                                roiManager("Rename", "Electrode");
                        }
                        else {
                                run("Enlarge...", "enlarge="+inc_radius);
                                roiManager("Add");
                                roiManager("Select", counter);
                                roiManager("Rename", "ROI "+counter);
}}

//Remove Radial ROIs Within ROIs
for (n = 0; n < nr_circles-1; n++) {
        roiManager("Select", newArray(n+1,n));
        roiManager("XOR");
        roiManager("Add");

        //Rename New ROIs
        if (n == 0) {
                roiManager("Select", nr_circles);
                roiManager("Rename", "ROI "+n+1 + " XOR Electrode");
        }

        else {
                roiManager("Select", n+nr_circles);
                roiManager("Rename", "ROI "+n+1 +" XOR "+n);
        }
}

//Get ROI Measures
run("Set Measurements...", "area mean standard min redirect=None decimal=3");
```

```
for (i=0; i < nr_circles + nr_circles-1; i++) {
        roiManager("Select", i);
        roiManager("multi-measure append");
        }
```

Appendix C

Experiments performed to address the Ca^{2+} signals amplitudes of astrocytes in response to simultaneous stimulation of neighboring microelectrodes is presented in this appendix.

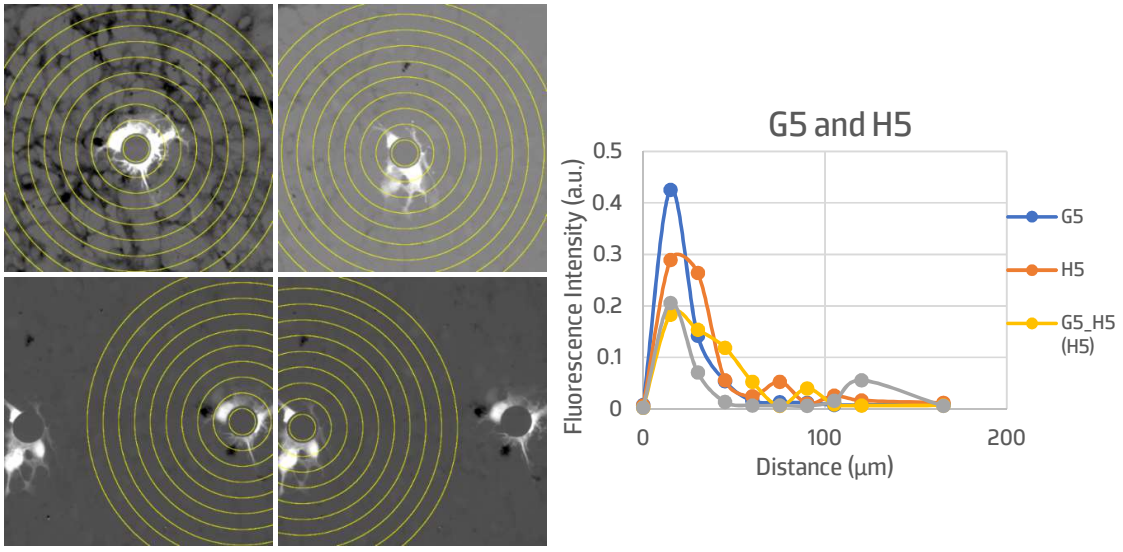

Figure 1 – Simultaneous stimulation of the neighboring electrodes G5 and H5. Images were normalized and the median intensity Z-projection was computed. The custom-written Fiji/ImageJ macro was used in order to evaluate the response of astrocytes to the stimulation (40x). **Upper left)** Single stimulation on the microelectrode G5. **Upper right)** Single stimulation on the microelectrode H5. **Lower left and Lower right)** Simultaneous stimulation of microelectrodes G5 and H5. **Graphic)** Ca^{2+} wave profiles for each stimulus, where it is seen that waves do not propagate further away from the microelectrode. Response amplitudes are higher when the stimulus is applied for the first time.

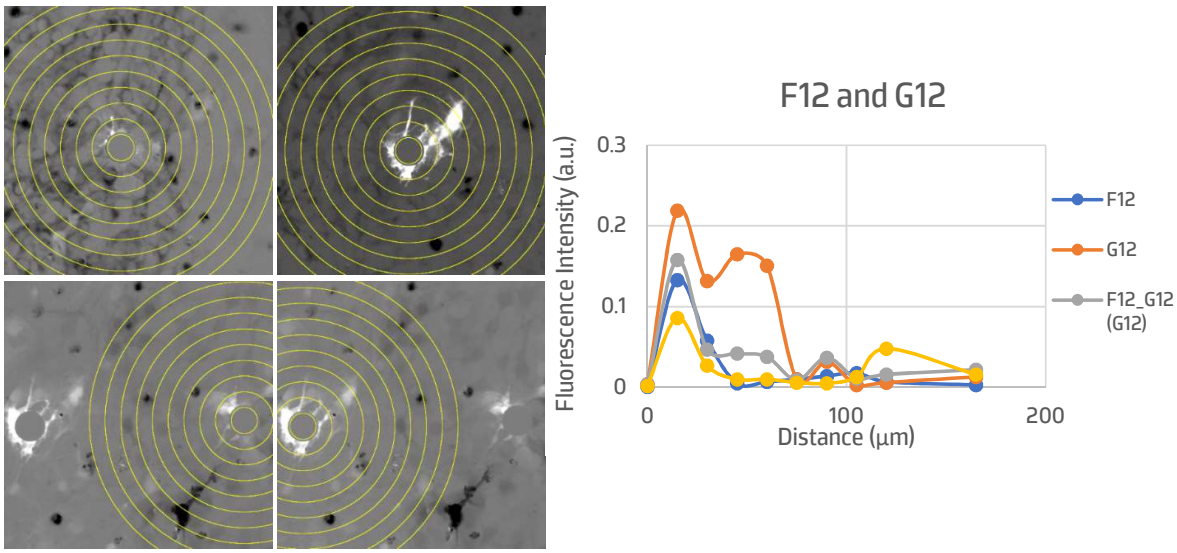

Figure 2 – Simultaneous stimulation of the neighboring electrodes F12 and G12. Images were normalized and the median intensity Z-projection was computed. The custom-written Fiji/ImageJ macro was used in order to evaluate the response of astrocytes to the stimulation (40x). **Upper left)** Single stimulation on the microelectrode F12. **Upper right)** Single stimulation on the microelectrode G12. **Lower left and Lower right)** Simultaneous stimulation of microelectrodes F12 and G12. **Graphic)** Ca^{2+} wave profiles for each stimulus, where it is seen that waves do not propagate further away from the microelectrode. Response amplitudes are higher when the stimulus is applied for the first time.

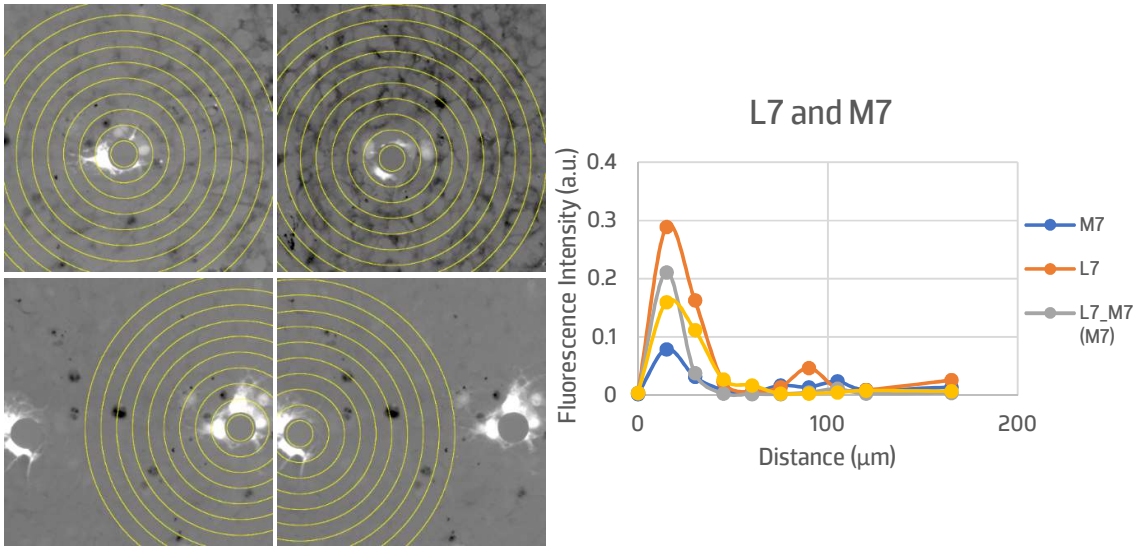

Figure 3 – Simultaneous stimulation of the neighboring electrodes L7 and M7. Images were normalized and the median intensity Z-projection was computed. The custom-written Fiji/ImageJ macro was used in order to evaluate the response of astrocytes to the stimulation (40x). **Upper left)** Single stimulation on the microelectrode L7. **Upper right)** Single stimulation on the microelectrode M7. **Lower left and Lower right)** Simultaneous stimulation of microelectrodes L7 and M7. **Graphic)** Ca^{2+} wave profiles for each stimulus, where it is seen that waves do not propagate further away from the microelectrode. Response amplitudes are higher when the stimulus is applied for the first time.

Appendix D

Experiments performed to address the Ca^{2+} signals amplitudes of astrocytes in response to different stimulus' amplitude is presented in this appendix.

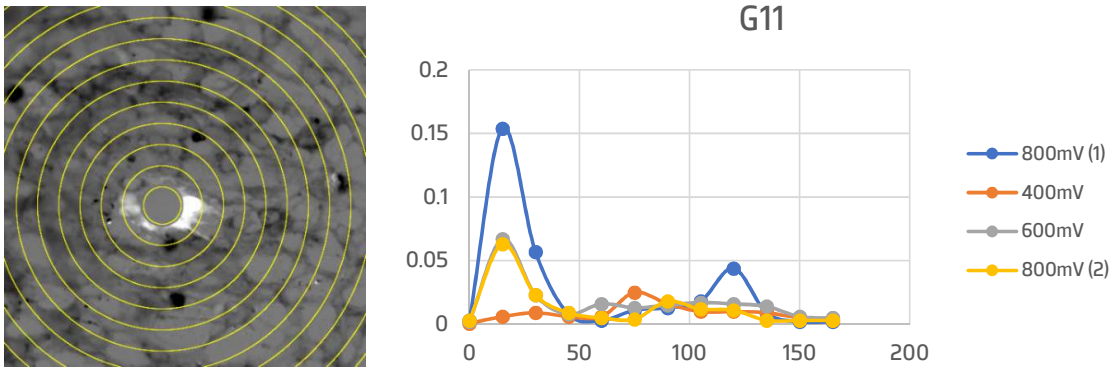

Figure 4 – Stimulation of the electrodes with different stimuli. Images were normalized and the median intensity Z-projection was computed. The custom-written Fiji/ImageJ macro was used in order to evaluate the response of astrocytes to the stimulation (40x). **Left)** Single stimulation on the microelectrode G11. **Graphic)** Ca^{2+} wave profiles for each stimulus, where it is seen that waves do not propagate further away from the microelectrode. Response amplitudes are higher when the stimulus is applied for the first time.

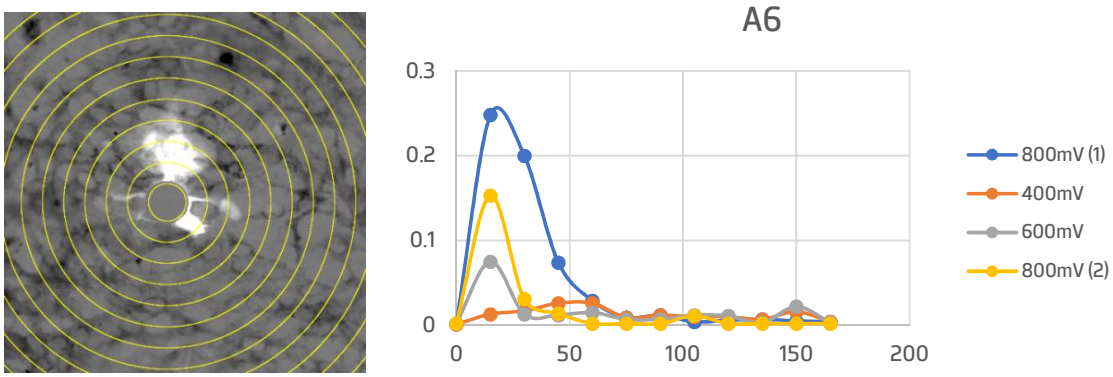

Figure 5 – Stimulation of the electrodes with different stimuli. Images were normalized and the median intensity Z-projection was computed. The custom-written Fiji/ImageJ macro was used in order to evaluate the response of astrocytes to the stimulation (40x). **Left)** Single stimulation on the microelectrode A6. **Graphic)** Ca^{2+} wave profiles for each stimulus, where it is seen that waves do not propagate further away from the microelectrode. Response amplitudes are higher when the stimulus is applied for the first time.

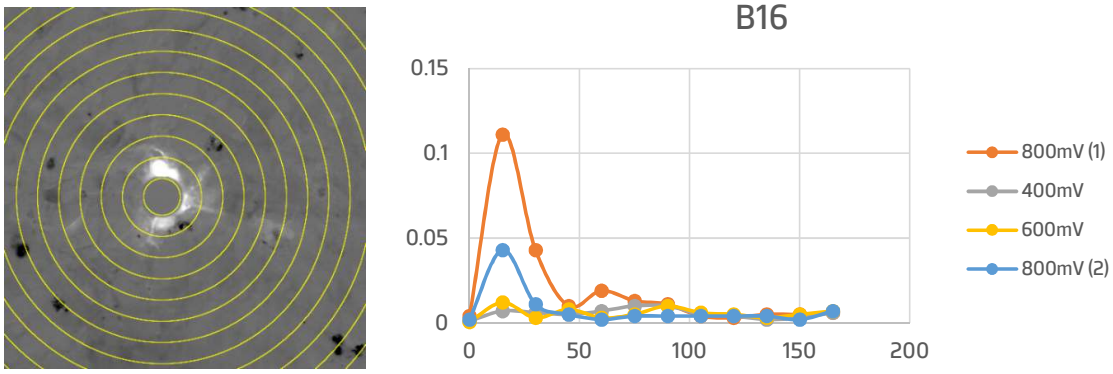

Figure 6 – Stimulation of the electrodes with different stimuli. Images were normalized and the median intensity Z-projection was computed. The custom-written Fiji/ImageJ macro was used in order to evaluate the response of astrocytes to the stimulation (40x). **Left)** Single stimulation on the microelectrode B16. **Graphic)** Ca^{2+} wave profiles for each stimulus, where it is seen that waves do not propagate further away from the microelectrode. Response amplitudes are higher when the stimulus is applied for the first time.

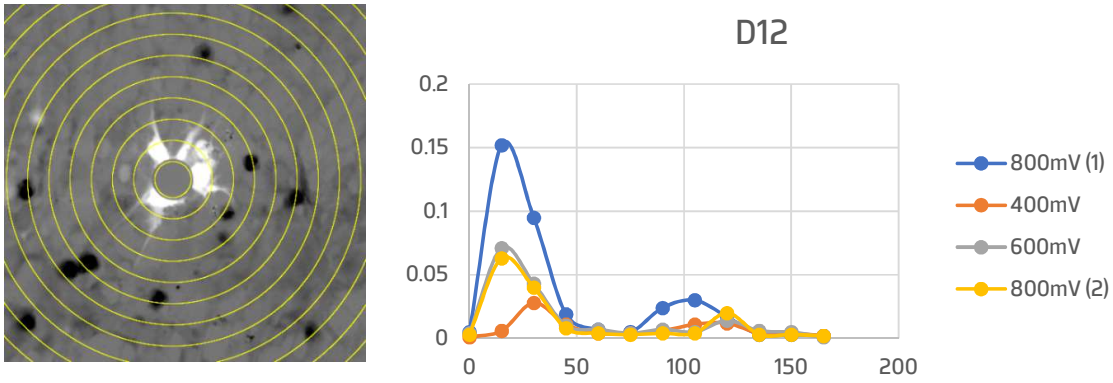

Figure 7 – Stimulation of the electrodes with different stimuli. Images were normalized and the median intensity Z-projection was computed. The custom-written Fiji/ImageJ macro was used in order to evaluate the response of astrocytes to the stimulation (40x). **Left)** Single stimulation on the microelectrode D12. **Graphic)** Ca^{2+} wave profiles for each stimulus, where it is seen that waves do not propagate further away from the microelectrode. Response amplitudes are higher when the stimulus is applied for the first time.

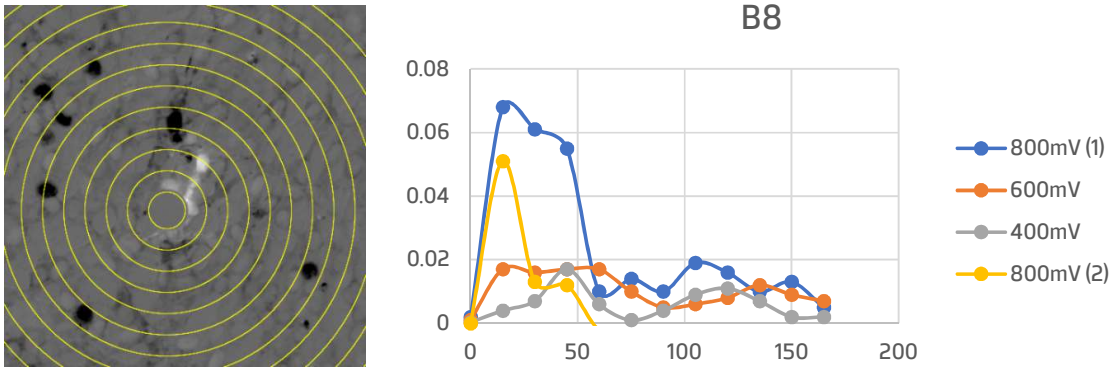

Figure 8 – Stimulation of the electrodes with different stimuli. Images were normalized and the median intensity Z-projection was computed. The custom-written Fiji/ImageJ macro was used in order to evaluate the response of astrocytes to the stimulation (40x). **Left)** Single stimulation on the microelectrode B8. **Graphic)** Ca^{2+} wave profiles for each stimulus, where it is seen that waves do not propagate further away from the microelectrode. Response amplitudes are higher when the stimulus is applied for the first time.